

ACKNOWLEDGEMENTS

I would like to thank my advisor, Kristen Billiar for guiding and supporting me over the years. You have set an example of excellence as a researcher, mentor, instructor, and role model.

I would like to thank my thesis committee members for all of their guidance through this process; your discussion, ideas, and feedback have been absolutely invaluable.

I'd like to thank my fellow graduate students, research technicians, collaborators, and the multitude of undergraduates who contributed to this research. I am very grateful to all of you.

I would like to thank my undergraduate research advisors, Dr. Surya Mallapragada and Dr. Richard Seagrave for their constant enthusiasm and encouragement.

I would especially like to thank my amazing family for the love, support, and constant encouragement I have gotten over the years. In particular, I would like to thank my parents, my brother, and my aunt Cathy. You are the salt of the earth, and I undoubtedly could not have done this without you.

I would also like to thank my 'greater Worcester family': Christian Grove, Chiara Silvestri, William Johnson, Vladimir Floroff, Sudepta Shanbhag, Becca Munro, Abe Shultz, Nick Perry, Kae Collins, Maria Pappas, Victoria Leeds, Nicole Belanger, Cha Cha Connor, Paul Sheprow, Caramia Phillips, Paolo Piselli, Billy Roberts, Angelina Bernadini, Zoe Reidinger, Anna O'Connor, Celine Nader, Nate Marini, and Sara Duran. Your love, laughter and music have kept me smiling and inspired. You are and always will be my family.

Finally, I would like to thank and dedicate this thesis to my grandfather, Dr. Silvio Balestrini. It was you who originally generated my love for science with visits to your laboratory and lessons on chemistry and physics. Although it has been years since you have passed, I still take your lessons with me, every day.

TABLE OF CONTENTS

	Page number
Chapter 1: Overview	1
1.1 Introduction	1
1.2 Objectives and Specific Aims	2
1.3 References	6
Chapter 2: Background	8
2.1 Introduction	8
2.1.1 Function and composition of connective tissues	8
2.1.2 Mechanoregulation in planar soft connective tissues	9
2.2 Adult healing in soft connective tissue: growth, repair and disease	11
2.2.1 Phases of wound healing	11
2.2.2 The formation of the provisional matrix and the role of fibrin	11
2.2.3 The formation of granulation tissue	12
2.2.4 Tissue remodeling, wound retraction, scar formation and the myofibroblast	13
2.2.5 Connective tissue pathology	15
2.2.6 Impact of mechanical loading during wound healing <i>in vivo</i>	16
2.2.7 The production of non-physiological stretch levels and fibrotic tissue propagation	17
2.2.8 Cyclic stretch regulates fibroblast behavior in 2D systems	18
2.3 Current 3D <i>in vitro</i> models of wound healing	20
2.3.1 3D <i>in vitro</i> systems for use in mechanobiology	20
2.3.2 3D models for use in tissue engineering and regenerative medicine	21
2.4 Mechanoregulation of fibroblasts in three dimensional models	22
2.4.1 Mechanobiology in 3D systems	22
2.4.2 Determining optimal loading conditions for the creation of tissue equivalents for use in load bearing applications	24
2.4.3 Creating accurate models of planar tissue with non-uniform strain distribution	25
2.5 Conclusions	25
2.6 References	26
Chapter 3: Equibiaxial cyclic stretch stimulates fibroblasts to rapidly remodel fibrin	35
3.1 Introduction	37
3.2 Materials and methods	
3.2.1 Fabrication of fibrin gels	37
3.2.2 Application of stretch	37
3.2.3 Validation of strain field	38
3.2.4 Mechanical characterization	38
3.2.5 Histological analysis	39
3.2.6 Transmission electron microscopy	39

3.2.7	Matrix alignment analysis	40
3.2.8	Density, cell number and viability, and collagen content determination	40
3.2.9	Inhibition of crosslinking	40
3.2.10	Statistical analysis	41
3.3	Results	41
3.3.1	Cyclic stretch increases tissue compaction and matrix density	42
3.3.2	Cyclic stretch increases tissue strength relative to static controls	43
3.3.3	Cyclic stretch regulates cell morphology	43
3.3.4	Collagen crosslinking impacts tissue compaction, UTS, and extensibility	44
3.4	Discussion	44
3.4.1	Cyclic stretch increases cell-mediated and passive compaction	44
3.4.2	Stretch does not modify cell number or viability	45
3.4.3	Cyclic stretch induces cell-mediated strengthening of fibrin gels	46
3.4.4	Conclusions	46
3.4.5	Acknowledgements	46
3.4.6	References	47
Chapter 4: Magnitude and duration of stretch modulate fibroblast remodeling		50
4.1	Introduction	50
4.2	Materials and methods	52
4.2.1	Fabrication of fibrin gels	52
4.2.2	Application of stretch	52
4.2.3	Determination of cell number and total collagen content	53
4.2.4	Determination of physical properties	54
4.2.5	Low-force biaxial mechanical characterization	54
4.2.6	Retraction assay	56
4.2.7	Histological analysis	57
4.2.8	Statistical and regression analysis	57
4.3	Results	58
4.3.1	Effect of stretch on compaction	58
4.3.2	Effect of stretch on mechanical properties	59
4.3.3	Effect of stretch on cell number and collagen density	60
4.3.4	Effect of stretch on matrix retraction	62
4.3.5	Effect of intermittent stretch on the matrix stiffness	63
4.4	Discussion	64
4.4.1	Cyclic stretch increases tissue strength in fibrin gels	64
4.4.2	UTS increases exponentially as a function of stretch magnitude	65
4.4.3	Tissue compaction is both a passive and an active response to stretch	65
4.4.4	Stretch-induced increases in failure tension are contingent on a rest period	66
4.4.5	Matrix stiffness increases with intermittent stretch magnitude	67
4.4.6	Tissue retraction is dependent on stretch magnitude	68

4.4.7	Conclusions and summary	68
4.5	Acknowledgments	68
4.6	References	69
Chapter 5: Applying controlled non-uniform deformation for in vitro studies of cell mechanobiology		73
5.1	Introduction	73
5.2	Materials and methods	75
5.2.1	Experimental Approach	75
5.2.2	Fabrication of the rigid inclusion model system	76
5.2.3	Ring inserts to limit strain	76
5.2.4	Strain field verification	77
5.2.5	Strain field verification for 3D model systems	78
5.2.6	Statistical analysis and modeling	79
5.2.7	Demonstration of cell orientation to non-homogeneous strain field created by rigid inclusion in 2D and 3D	80
5.3	Results	82
5.3.1	Effect of the subimage size on the resolution of strain distribution	83
5.3.2	Effect of the rigid inclusion on strain distribution in 2D	85
5.3.3	Results of regression analysis and modeling	87
5.3.4	Effect of ring inserts on global strain distribution	90
5.3.5	Effect of the rigid inclusion on strain distribution in 3D	91
5.3.6	Effect of non-homogeneous strain field created by rigid inclusion on cell orientation in 2D	92
5.3.7	Effect of non-homogeneous strain field created by rigid inclusion on fiber orientation in 3D	94
5.4	Discussion	96
5.4.1	Gradients of strain can be ‘tuned’ by altering applied strain or the inclusion size	96
5.4.2	Benefit of a 2D gradient system	97
5.4.3	Isolating anisotropy, gradient and magnitude effects	98
5.4.4	Optimization of effective resolution	100
5.4.5	Our findings of symmetric strain gradients support the predictions of Moore and colleagues	101
5.4.6	Restrictions to utilizing the proposed system	102
5.4.7	Conclusions and summary	102
5.4.8	Acknowledgements	103
5.4.9	References	103
Chapter 6: Conclusions and future work		106
6.1	Overview	106
6.2	Isolating the effects of mechanical loading on cell-mediated matrix remodeling during fibroplasia	106
6.2.1	Minimizing fiber alignment to isolate stretch effects	106

6.2.2	Establishing the relationship between stretch magnitude and duration and matrix remodeling	107
6.2.3	Determining passive and active stretch effects	109
6.3	Developing relevant mechanobiological models of wound healing in planar connective tissues	110
6.3.1	Fibrin gels as models of early wound healing	110
6.3.2	Modeling the complex mechanical environment of connective tissue	113
6.4	Mechanical conditioning for use in regenerative medicine	115
6.5	Future work	115
6.6	Final Conclusions	119
6.7	References	120
Appendices		i
Appendix A:		i
Appendix B:		iv
Appendix C:		vii
Appendix D:		ix
Appendix E:		xx

TABLE OF FIGURES

	Page number
Figure 2.1 Connective tissue underlying the epithelium	8
Figure 2.2. Internal and external force transmission in the dermis	10
Figure 2.3. The three phases of wound healing in connective tissues	11
Figure 2.4. The provisional matrix during fibroplasia and remodeling as seen in pulmonary wound healing	13
Figure 2.5. Regeneration versus pathological healing, the outcomes of wound repair	15
Figure 2.6. Methods of mechanical stimulation	19
Figure 2.7. Photo depicting Apligraf, a dermal tissue equivalent	22
Figure 3.1. Schematic of the method of stretching the fibroblast-populated fibrin gels	37
Figure 3.2. Brightfield images of hematoxylin and eosin stained sections of fibrin gels	41
Figure 3.3. TEM images of fibroblasts and extracellular matrix in static and stretched fibrin gels	43
Figure 4.1. Schematics representing a fibrin gel with foam anchor attached prior to after loading onto the biaxial device	55
Figure 4.2. Representative brightfield images of hematoxylin and eosin stained sections of fibrin gels	58
Figure 4.3. Tissue thickness, UTS, collagen density, extensibility, failure tension, stiffness, active retraction, passive retraction and cell number of CS (24 hr/day), and IS (6 hr/day) fibrin gels cycled at 2, 4, 8, and 16% stretch	59
Figure 4.4. Representative fibroblast-populated fibrin gel at 40 seconds and 7 minutes post release from its substrate	63
Figure 4.5. Representative engineering stress-strain plot of equibiaxial loading along orthogonal '1' and '2' directions	63
Figure 5.1 Schematics of the of the rigid inclusion system with a ring insert	83
Figure 5.2 Representative radial stretch ratio, λ_r versus radius for a 10mm inclusion system cycled to '6%' applied strain	84
Figure 5.3 Effect of increasing inclusion size and applied strain on the deformation of the membrane.	86
Figure 5.4 Strain gradients for '6%' applied strain for different inclusion sizes (5mm, 10mm, and 15mm) and for b) 10mm inclusion at '2%', '4%', and '6%' applied strain	86
Figure 5.5 Radial and circumferential stretch ratio data	89
Figure 5.6 Stretch anisotropy for '6%' applied strain as a function of radial distance from center for each inclusion size	89
Figure 5.7 Comparison of '6%' applied strain data for radial and circumferential directions from this study and scaled data from Mori et al., 2005	90
Figure 5.8 Relationship between the height of the Delrin inserts and the	91

	resulting applied strain for a mechanically loaded silicone membrane.	
Figure 5.9	Effect of deformation of the 5mm inclusion system with and without a fibroblast-populated fibrin gel	92
Figure 5.10	Representative images of human dermal fibroblasts cultured on membranes with 5mm diameter inclusions for two days at 0.2Hz at '2%' applied strain	93
Figure 5.11	Representative confocal and histological H&E images of human dermal fibroblasts cultured in fibrin gels with 5mm diameter inclusions for eight days at 0.2Hz at '6%' applied strain	95
Figure 5.12	Representative thickness of fibrin gels taken from histological H&E images of human dermal fibroblasts cultured in fibrin gels	97

TABLE OF TABLES

	Page number
Table 2.1. Mechanobiological responses of cells to various applications of mechanical conditioning	23
Table 3.1. Physical and biochemical properties of fibroblast-populated fibrin gels statically cultured or cyclically stretched for 8 days of culture	42
Table 3.2. Effect of BAPN on the mechanical and biochemical properties of statically-cultured and cyclically-stretched fibroblast-populated fibrin gels	44
Table. 4.1. Regression analysis for normalized remodeling metrics as a function of stretch magnitude (M), the length per day of stretch (CS vs. IS), and an interaction term (I)	60
Table. 4.2. Raw mechanical, biochemical, and physiological data for continuously stretched gels cycled at 0, 2, 4, 8, and 16% stretch magnitudes for 8 days at 0.2 Hz.	61
Table 4.3. Raw mechanical, biochemical, and physiological data for intermittently stretched gels cycled at 0, 2, 4, 8, and 16% stretch magnitudes for 8 days at 0.2 Hz.	61
Table 5.1. Optimal parameter values for stretch ratio vs. radius curves and interpolated parameters for '2%' and '4%' curves based on optimal parameters for '6%' curves.	87

ABSTRACT

Mechanical loads play a pivotal role in the growth, maintenance, remodeling, and disease onset in connective tissues. Harnessing the relationship between mechanical signals and how cells remodel their surrounding extracellular matrix would provide new insights into the fundamental processes of wound healing and fibrosis and also assist in the creation of custom-tailored tissue equivalents for use in regenerative medicine. In 3D tissue models, uniaxial cyclic stretch has been shown to stimulate the synthesis and crosslinking of collagen while increasing the matrix density, fiber alignment, stiffness, and tensile strength in the direction of principal stretch. Unfortunately, the profound fiber realignment in these systems render it difficult to differentiate between passive effects and cell-mediated remodeling. Further, these previous studies generally focus on a single level of stretch magnitude and duration, and they also investigate matrix remodeling under homogeneous strain conditions. Therefore, these studies are not sufficient to establish key information regarding stretch-dependent remodeling for use in tissue engineering and also do not simulate the complex mechanical environment of connective tissue.

We first developed a novel *in vitro* model system using equibiaxial stretch on fibrin gels (early models of wound healing) that enabled the isolation of mechanical effects on cell-mediated matrix remodeling. Using this system we demonstrated that in the absence of in-plane alignment, stretch stimulates fibroblasts to produce a stronger tissue by synthesizing collagen and condensing their surrounding matrix. We then developed dose-response curves for multiple aspects of tissue remodeling as a function of stretch magnitude and duration (intermittent versus continuous stretch). Our results indicate that both the magnitude of stretch and the duration per day are important factors in mechanically induced cell activity, as evidenced by dose-dependent responses of several remodeling metrics (UTS, matrix stiffness, collagen content, cell number) in response to these two parameters. In addition, we found that cellularity, collagen content, and resistance to tension increased when the tissues were mechanically loaded intermittently as opposed to continuously. Finally, we developed a novel model system that produces a non-homogeneous strain distribution, allowing for the simultaneous study of strain gradients, strain anisotropy, and strain magnitude in planar and three-dimensional culture conditions. Establishing a system that produces complex strain distributions provides a more accurate model of the mechanical conditions found in connective tissue, and also allows for the investigation of cellular adaptations to a changing mechanical environment.

CHAPTER 1

A brief overview of this thesis work

1.1. Introduction

Virtually all connective tissues are exposed to complex biaxial mechanical loads *in vivo*, and these loads play a pivotal role in the development, maintenance and remodeling, and pathogenesis of these tissues [1]. During wound healing, mechanical cues modulate fibroblast synthetic and contractile capacity and are responsible for, in part, driving the wound healing response toward a positive or negative outcome (e.g., wound closure vs. excessive contracture) [2]. Other classic examples of mechanical regulation of tissue include bone growth and remodeling due to loading, arterial wall thickening due to hypertension, or wound contracture due to fibroblast tractional forces [3].

Clinicians and researchers have long sought to understand the relationship between mechanical loading and cell response, in order to assist in the creation of wound healing therapies (e.g., splint usage in dermal healing) [4], determine what role tissue mechanics plays in disease onset and persistence (e.g., fibrotic tissue propagation)[3], and to enable the manipulation of cell behavior to build custom tailored tissue equivalents [5]. The overall research goal of this thesis is to better understand cell-mediated matrix remodeling in planar tissues subjected to complex biaxial loading, and, in particular, the role mechanical of loads during the process of wound healing.

1.2. Objectives and specific aims

Objective I: Establish a model system to isolate mechanical effects of stretch on cell-mediated matrix remodeling.

To investigate how mechanical cues guide cell activity in a controlled mechano-chemical environment, *in vitro* 3D tissue models such as cell-populated collagen and fibrin gels have been utilized extensively [5-23]. In these systems, uniaxial cyclic stretch has been shown to stimulate the synthesis and crosslinking of collagen while increasing the matrix density, fiber alignment, stiffness, and tensile strength in the direction of stretch.

Although these studies provide valuable information of stretch-induced matrix remodeling in uniaxially loaded tissue (e.g., tendons), it remains unclear if the changes in tissue architecture are primarily cell-mediated, or if they are predominantly derived from fiber alignment. Further, these studies do not simulate the mechanical conditions during growth, healing, or pathology in planar tissue (e.g, skin, heart valves, lung tissue, etc.).

The first aim of this thesis work is to develop a model system to isolate mechanical effects on cell-mediated matrix remodeling and to determine if stretch stimulates dermal fibroblasts to reorganize and remodel their surrounding matrix into a stronger tissue without the addition of in-plane tissue alignment.

In Chapter 3, I discuss the development of a novel method to isolate the impact of mechanical stretch on the mechanical, morphological, and biochemical properties of fibroblast-populated fibrin gels in *in vitro* models of early wound healing. Equibiaxial stretch is used instead of uniaxial stretch in order to limit the confounding effects of fibril alignment on the mechanics of the matrix, thus enabling the investigation of more subtle remodeling mechanisms. We applied continuous cyclic equibiaxial stretch (16% stretch at 0.2 Hz) to fibroblast-populated fibrin gels to *in vitro* wound models for eight days. Compaction, density, tensile strength, and collagen content were quantified as functional measures of tissue remodeling. Evaluation of the stretched samples revealed that they

were approximately ten times stronger, eight-fold more collagen-dense, and eight times thinner than statically cultured samples. These changes were not accompanied by differences in cell number or viability. These findings increase our understanding of how mechanical forces guide the healing response in connective tissue. Further, the methods employed in this study may also prove to be valuable tools for investigating stretch-induced remodeling of other planar connective tissues and for creating mechanically-robust engineered tissues.

Objective 2: Establish dose-response curves of matrix remodeling in terms of stretch magnitude and duration.

Quantitatively establishing the relationships between mechanical simulation and extracellular matrix remodeling would be an important step towards the rational design of manual therapies for wound healing and also for the use of mechanical conditioning as a means to custom tailor tissue analogs with specific requirements such as strength, stiffness, and contractility. Although much has been learned about the mechanisms of strain-dependent remodeling in 3D models of connective tissue, the appropriate combinations of strain levels, ranges, and durations utilized in previous experiments are not sufficient to characterize the complex relationships between parameters of mechanical conditioning (magnitude, duration, etc.) and metrics of matrix remodeling (strength, stiffness, alignment, etc.).

The second aim of this thesis is to establish dose-response relationships between stretch parameters (2, 4, 8, and 16% magnitude and either 6 or 24 hour durations per day) and functional matrix remodeling metrics (compaction, strength, extensibility, collagen content, contraction and cellularity).

In Chapter 4, I present the development of these dose-response curves and determine the significance of each stretch parameter. Cyclic equibiaxial stretch of 2 to 16 % was applied to fibroblast-populated fibrin gels for either 6 or 24 hours per day for 8 days. Trends in matrix remodeling metrics as a function of stretch magnitude and duration were

Chapter 1 - Overview

analyzed using regression analysis. The compaction and ultimate tensile strength of the tissues increased in a dose-dependent manner with increasing stretch magnitude, yet remained unaffected by the duration in which they were cycled (6 versus 24 hours/day). Within the range of magnitudes tested within this study, collagen density increased exponentially as a function of both the magnitude and duration of stretch. Interestingly, samples that were stretched for the reduced duration per day had the highest levels of collagen accumulation. Cell number and failure tension were also dependent on both the magnitude and duration of stretch, although stretch-induced increases in these metrics were only present in the samples loaded for 6 hours/day. Our results indicate that both the magnitude and the duration per day of stretch are critical parameters in modulating fibroblast remodeling of the extracellular matrix, yet these two stretch parameters regulate different aspects of this remodeling. These findings move us one step closer to fully characterizing culture conditions for tissue equivalents, developing improved wound healing treatments, and understanding tissue responses to changes in mechanical environments during growth, repair, and disease states.

Objective 3: Determine how regional increases in local strain result in heightened remodeling and lead to global changes in tissue architecture.

Cells within connective tissues routinely experience a wide range of non-uniform mechanical loads that are required for normal health and homeostasis. These strains are often anisotropic, inhomogeneous, and have local gradients of strain magnitude [24, 25]. These non-uniformities in strain direction and magnitude are especially pronounced near local areas of increased stiffness (in tissues undergoing clinical intervention with the addition of stents, prosthetics, etc.) or during disease onset such as the formation of stiff fibrotic foci [26, 27]. Strain anisotropy and magnitude are known to be important regulators of cellular activity (e.g., collagen production, cell proliferation, cellular retraction capacity); however, previous studies have been limited to either extremely anisotropic or equibiaxial strain conditions, and have therefore ignored more subtle responses to alternative biaxial states of strain found *in vivo*. In addition, understanding tissue responses and cellular adaptations to changing mechanical conditions will assist in

minimizing adverse effects of clinical intervention and also help understand the propagation of self-sustaining fibrosis.

The third aim of this thesis work is to develop a model system with an inhomogeneous strain distribution as seen in connective tissue, and to also determine if stiff inclusions alter the distribution of strain magnitudes in tissues, ultimately leading to changes in global tissue architecture.

In Chapter 5, we present the development of an experimental system to produce complex strain patterns for the study of strain magnitude, anisotropy, and gradient effects on cells and cell-populated tissue in culture. An equibiaxial cell stretching system was modified by affixing glass coverslips of various sizes (5, 10, or 15mm diameter) to the center of 35mm diameter flexible-bottomed culture wells. Ring inserts were utilized to limit applied strain to different levels in each individual well, thus enabling parallel experiments at different strain levels. The addition of the glass coverslip creates strong circumferential and radial strain gradients, with a continuous range of stretch anisotropy ranging from strip biaxial to equibiaxial stretch. Dermal fibroblasts seeded within our 2D system (5mm inclusions and cycled to '2%' applied strain for 2 days) demonstrated the characteristic orientation perpendicular to the direction of principal strain. Similarly, dermal fibroblasts seeded within a 3D system (5mm inclusions and cycled to '6%' applied strain for 8 days) also oriented themselves perpendicular to the direction of principle strain, and compacted their matrix in accordance with strain magnitude resulting in differential thickness across the tissue. This study verifies how inhomogeneous strain fields can be produced in a tunable and simply constructed system, and demonstrates the potential utility for studying gradients with a continuous spectrum of strain magnitudes and anisotropies.

This thesis describes an investigation of how the complex non-uniform mechanical loads seen in planar connective tissue regulates cell-mediated matrix remodeling and changes in tissue architecture. Harnessing the relationship between stretch and cell behavior will

assist in creating tissue-engineered constructs with custom tailored properties and provide new insights into the fundamental processes of wound healing, hyperplasia, and fibrosis.

1.3. References

- [1] Lunden, K., 2006, "Effect of mechanical loading on soft connective tissues," Functional soft tissue examination and treatment by manual methods, W. Hammer, ed., Jones and Bartlett, Sudbury, MA, pp. 13-120.
- [2] Silver, F. H., Siperko, L. M., and Seehra, G. P., 2003, "Mechanobiology of force transduction in dermal tissue," *Skin Res Technol*, 9(1), pp. 3-23.
- [3] Mori, D., David, G., Humphrey, J. D., and Moore, J. E., Jr., 2005, "Stress distribution in a circular membrane with a central fixation," *J Biomech Eng*, 127(3), pp. 549-553.
- [4] Sanders, J. E., Goldstein, B. S., and Leotta, D. F., 1995, "Skin response to mechanical stress: adaptation rather than breakdown--a review of the literature," *J Rehabil Res Dev*, 32(3), pp. 214-226.
- [5] Isenberg, B. C., and Tranquillo, R. T., 2003, "Long-term cyclic distention enhances the mechanical properties of collagen-based media-equivalents," *Annals of Biomedical Engineering*, 31(8), pp. 937-949.
- [6] Butcher, J. T., Barrett, B. C., and Nerem, R. M., 2006, "Equibiaxial strain stimulates fibroblastic phenotype shift in smooth muscle cells in an engineered tissue model of the aortic wall," *Biomaterials*, 27(30), pp. 5252-5258. Epub 2006 Jun 5227.
- [7] Carver, W., Nagpal, M. L., Nachtigal, M., Borg, T. K., and Terracio, L., 1991, "Collagen expression in mechanically stimulated cardiac fibroblasts," *Circ Res*, 69(1), pp. 116-122.
- [8] Cummings, C. L., Gawlitta, D., Nerem, R. M., and Stegemann, J. P., 2004, "Properties of engineered vascular constructs made from collagen, fibrin, and collagen-fibrin mixtures," *Biomaterials*, 25(17), pp. 3699-3706.
- [9] Dartsch, P. C., Hammerle, H., and Betz, E., 1986, "Orientation of cultured arterial smooth muscle cells growing on cyclically stretched substrates," *Acta Anat (Basel)*, 125(2), pp. 108-113.
- [10] Girton, T. S., Barocas, V. H., and Tranquillo, R. T., 2002, "Confined compression of a tissue-equivalent: collagen fibril and cell alignment in response to anisotropic strain," *J Biomech Eng*, 124(5), pp. 568-575.
- [11] Husse, B., Briest, W., Homagk, L., Isenberg, G., and Gekle, M., 2007, "Cyclical mechanical stretch modulates expression of collagen I and collagen III by PKC and tyrosine kinase in cardiac fibroblasts," *Am J Physiol Regul Integr Comp Physiol*, 293(5), pp. R1898-1907.
- [12] Kanda, K., and Matsuda, T., 1994, "Mechanical stress-induced orientation and ultrastructural change of smooth muscle cells cultured in three-dimensional collagen lattices," *Cell Transplant*, 3(6), pp. 481-492.

- [13] Kim, B. S., Nikolovski, J., Bonadio, J., and Mooney, D. J., 1999, "Cyclic mechanical strain regulates the development of engineered smooth muscle tissue," *Nat Biotechnol*, 17(10), pp. 979-983.
- [14] Kratz, C., Tollback, A., and Kratz, G., 2001, "Effects of continuous stretching on cell proliferation and collagen synthesis in human burn scars," *Scand J Plast Reconstr Surg Hand Surg*, 35(1), pp. 57-63.
- [15] Langelier, E., Rancourt, D., Bouchard, S., Lord, C., Stevens, P. P., Germain, L., and Auger, F. A., 1999, "Cyclic traction machine for long-term culture of fibroblast-populated collagen gels," *Ann Biomed Eng*, 27(1), pp. 67-72.
- [16] Prajapati, R. T., Eastwood, M., and Brown, R. A., 2000, "Duration and orientation of mechanical loads determine fibroblast cyto-mechanical activation: monitored by protease release," *Wound Repair and Regeneration*, 8(3), pp. 238-246.
- [17] Seliktar, D., Nerem, R. M., and Galis, Z. S., 2003, "Mechanical strain-stimulated remodeling of tissue-engineered blood vessel constructs," *Tissue Eng*, 9(4), pp. 657-666.
- [18] Syedain, Z. H., Weinberg, J. S., and Tranquillo, R. T., 2008, "Cyclic distension of fibrin-based tissue constructs: evidence of adaptation during growth of engineered connective tissue," *Proc Natl Acad Sci U S A*, 105(18), pp. 6537-6542.
- [19] Tower, T. T., Neidert, M. R., and Tranquillo, R. T., 2002, "Fiber alignment imaging during mechanical testing of soft tissues," *Ann Biomed Eng*, 30(10), pp. 1221-1233.
- [20] Tranquillo, R. T., 2002, "The tissue-engineered small-diameter artery," *Ann N Y Acad Sci*, 961, pp. 251-254.
- [21] Wille, J. J., Elson, E. L., and Okamoto, R. J., 2006, "Cellular and matrix mechanics of bioartificial tissues during continuous cyclic stretch," *Ann Biomed Eng*, 34(11), pp. 1678-1690.
- [22] Yao, L., Swartz, D. D., Gugino, S. F., Russell, J. A., and Andreadis, S. T., 2005, "Fibrin-based tissue-engineered blood vessels: differential effects of biomaterial and culture parameters on mechanical strength and vascular reactivity," *Tissue Eng*, 11(7-8), pp. 991-1003.
- [23] Ye, Q., Zund, G., Benedikt, P., Jockenhoevel, S., Hoerstrup, S. P., Sakyama, S., Hubbell, J. A., and Turina, M., 2000, "Fibrin gel as a three dimensional matrix in cardiovascular tissue engineering," *Eur J Cardiothorac Surg*, 17(5), pp. 587-591.
- [24] Hashima, A. R., Young, A. A., McCulloch, A. D., and Waldman, L. K., 1993, "Nonhomogeneous analysis of epicardial strain distributions during acute myocardial ischemia in the dog," *J Biomech*, 26(1), pp. 19-35.
- [25] Oomens, C. W., van Ratingen, M. R., Janssen, J. D., Kok, J. J., and Hendriks, M. A., 1993, "A numerical-experimental method for a mechanical characterization of biological materials," *J Biomech*, 26(4-5), pp. 617-621.
- [26] Giannone, G., and Sheetz, M. P., 2006, "Substrate rigidity and force define form through tyrosine phosphatase and kinase pathways," *Trends Cell Biol*, 16(4), pp. 213-223.
- [27] Ingber, D. E., 1997, "Tensegrity: the architectural basis of cellular mechanotransduction," *Annu Rev Physiol*, 59, pp. 575-599.

CHAPTER 2

Background and Significance

2.1. Introduction

2.1.1. *Function and composition of connective tissues*

Soft connective tissues provide the structural framework, elasticity, and durability to withstand internal and external forces imparted on the body. Soft connective tissue proper includes dense connective tissues (e.g., the dermis) and also loose interstitial connective tissues that separate and connect muscles and surround all organs, nerves, and blood vessels [6, 7]. These tissues create a stroma that is distinct from, but inextricably related to, the functioning parenchyma of the viscera.

The connective tissue system is primarily composed of resident fibroblasts, extracellular matrix, and interstitial fluid, although there is also a small population of resident immune cells such as mast cells and macrophages [6]. Figure 2.1 illustrates the constituents of connective tissue proper.

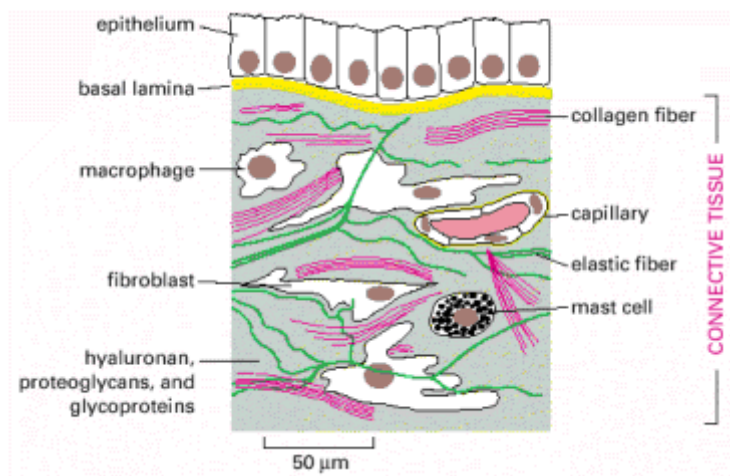


Fig. 2.1. Connective tissue underlying the epithelium. Connective tissue contains a variety of cells and extracellular matrix components. The predominant cell type is the fibroblast, which secretes abundant extracellular matrix including elastin, collagen, and components of the ground substance (e.g., hyaluronan, proteoglycans, etc). (From Alberts et. al., *Molecular Biology of the Cell*, 2002) [1]

Chapter 2: Background and Significance

Fibroblasts are the characteristic cell type of differentiated connective tissue, and the predominant cell type in these tissues. The principal functions of these cells are the synthesis, secretion and modulation of fibrous and non-fibrous connective tissue proteins that constitute the extracellular matrix (ECM), a highly organized arrangement of proteoglycans, collagenous proteins, loose reticular fibers, and elastin [9, 10]. It is through the molecules that compose the ECM that the essential physical attributes and biological properties of connective tissues are produced [6]. Collagenous proteins, primarily collagen type I, form the largest part of the non-aqueous extracellular matrix and have a very high tensile strength and stiffness that provides the necessary tissue scaffolding and a reinforcing meshwork for cells. It is the composition and architecture of collagenous fibers (e.g., content, crosslinks, and orientation) that primarily contribute to the tensile strength, load-bearing capacity and creep resistance of these tissues [11].

2.1.2. Mechanoregulation in planar soft connective tissues

Soft connective tissues define the shape of the body, and cells within these load bearing tissues are continuously subjected to a range of internal and external mechanical forces including gravity, movement, breathing, and heart beat [12, 13]. Soft connective tissues that are planar in nature (e.g., fascia, dermis, loose connective tissue) are generally loaded multiaxially [14]; the distribution of these loads is often anisotropic (different magnitudes along different directions), heterogeneous, and have local gradients of strain magnitude [15, 16]. Connective tissues must therefore be able to withstand a diverse range of mechanical forces and respond robustly and reversibly to the deformations caused by these forces.

The internal and external forces imparted on these tissues are generated passively by components in the matrix, and actively by cells to create a tension across the tissue. For example, the mechanical state of the dermis is such that internal forces create a passive tension across collagen fibers, and are directed along Langer's lines (lines of tension across the dermis) [17]. The active component of tension is produced via fibroblast

Chapter 2: Background and Significance

cytoskeletal tension and contraction of collagen fibers in the extracellular matrix [18]. External forces applied to connective tissues also change the mechanical state of the tissue through several mechanisms including fibroblast-fibroblast interactions in the dermis, fibroblast-ECM interactions, and ECM-ECM interactions [12]. The mechanical state of the dermis is illustrated in Figure 2.2.

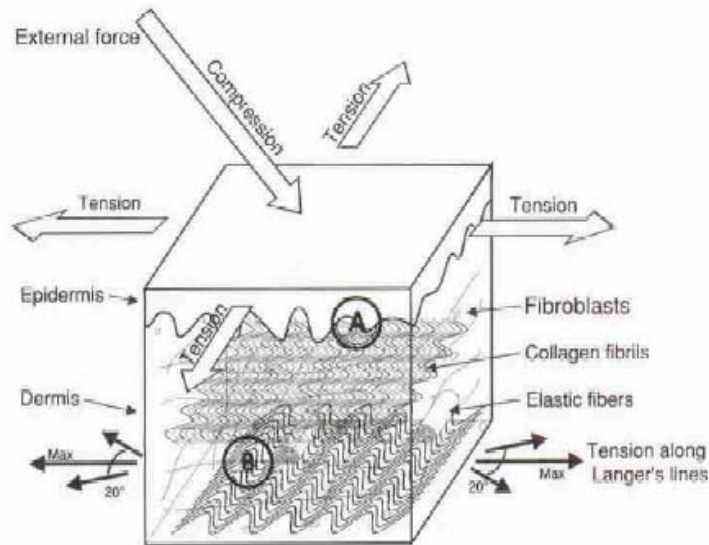


Fig. 2.2. Internal and external force transmission in the dermis. Tension in the dermis arises from deformation of collagen fibrils that are oriented virtually parallel to Langer's lines. Internal forces in the dermis are composed of passive tension distributed across collagen fiber networks, and active cellular tension that is produced by fibroblasts. (From Silver et al., *Skin Res Technol*, 2003) [2]

These deformations also act as mechanical cues that are essential for the physical maintenance and management of these tissues. In addition, mechanical loads also play a particularly important role in dictating the outcomes of wound healing and tissue repair [11]. It has been long known that mechanical tension generated during wound healing regulates fibroblast tractional forces and are responsible for, in part, driving the wound healing response towards either a positive or pathological outcome (e.g., wound closure vs. excessive contracture) [19]. These cues regulate cellular remodeling activity that ultimately guides the overall architecture of the tissue. In the case of dermal wound healing, the formation of scar tissue is characterized by the alignment of these collagen fibers in the direction of principal strain. This difference is distinct from the “basket woven” structure that enable tissues to withstand loads in multiple orientations in native dermis; the alignment of collagen fibrins seen in scar tissue reduces the capacity of these tissue to withstand the multiaxial loads seen *in vivo* [2].

2.2. Adult wound healing in connective tissue: growth, repair and disease

2.2.1. Phases of wound healing

When connective tissue architecture is disrupted due to injury, the body undergoes a fibroproliferative healing response that ultimately develops into scar tissue [20]. This repair process is a complex and interactive event that is orchestrated by soluble mediators, blood elements (e.g., platelets, proteins, etc.), extracellular matrix components, and parenchymal cells [21]. As illustrated in Figure 2.3, the wound repair process can be categorized chronologically into three overlapping major phases that create the continuum of healing: inflammation, fibroplasia and revascularization (granulation tissue formation, or the proliferation phase), and matrix remodeling (or maturation).

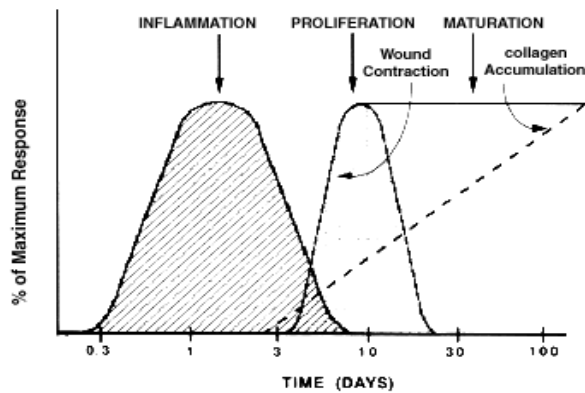


Fig 2.3. The three phases of wound healing in connective tissues. The process of wound healing is composed of three overlapping events that are categorized as inflammation, cell proliferation and matrix deposition, and matrix remodeling and maturation (From Clark R.A.F., Am J Med Sci, 1994) [3].

2.2.2. The formation of the provisional matrix and the role of fibrin

The inflammatory phase begins immediately following injury or surgical wounding, and typically subsides in 4 to 6 days [22]. One of the first events of inflammation is the infiltration of neutrophils to remove bacteria, microorganisms and foreign particles that have lodged in the wound site. Simultaneously, platelets begin to generate a fibrin-rich

Chapter 2: Background and Significance

clot that serves two purposes: it reestablishes homeostasis within severed blood vessels, and provides a temporary or “provisional matrix” within the wound space for cell migration to promote tissue repair and the reestablishment of tissue integrity [23]. The fibrin clot is formed by the combination of fibrinogen, a plasma protein secreted into circulation by the liver (at concentrations of approximately 3 mg/ml) and thrombin, a proteolytic enzyme that cleaves fibrinogen to create fibrin monomers [24, 25]. The creation of this fibrin clot typically occurs within 24 hours post wounding, marks the beginning of fibroplasia, and in conjunction with fibronectin and proteoglycans create what is referred to as the provisional matrix [22]. During inflammation the provisional matrix serves to provide chemoattractant agents and cytokines that attract immune cells such as neutrophils, leukocytes, and macrophages to promote the removal of necrotic tissue, bacteria, and debris [21]. In addition, the provisional matrix promotes new tissue formation by providing the scaffolding required for contact guidance of cells, a soft substrate that limits cell mobility, and also a reservoir of cytokines and mitogenic factors that simultaneously promote infiltration of blood vessels, macrophages, and fibroblasts into the wound bed [3, 26-28].

During fibroplasia, macrophages, previously quiescent fibroblasts, and blood vessels also provide separate yet critical roles [10]. Macrophages dispose of necrotic tissue in the wound and also secrete cytokines that stimulate fibroplasia and angiogenesis, blood vessels carry oxygen and vital nutrients necessary for cell survival and metabolism, and fibroblasts produce an amorphous ground substance composed of mucopolysaccharides and glycoproteins and begin to synthesize collagen to restore integrity to the tissue [3, 22].

2.2.3. *The formation of granulation tissue*

Approximately 4 days after injury (~3 days after fibrin clot formation), fibroblasts increase in their synthetic and proliferative activity, begin to transform into myofibroblasts, and initiate remodeling of the fibrin-rich provisional matrix by

synthesizing, organizing, and crosslinking collagen and other matrix components to form granulation tissue and replace the provisional matrix [21]. Figure 2.4 illustrates this process.



Fig 2.4. The provisional matrix during fibroplasia and remodeling as seen in pulmonary wound healing. The formation of a clot then serves as a temporary shield protecting the denuded wound tissues and provides a provisional matrix over and through which cells can migrate during the repair process. Fibroblasts (blue cells) migrate from the interstitial connective tissue, remodel the surrounding matrix and deposit a newly synthesized replacement tissue. (Adapted from White *et al.*, J Pathol. 2003) [5]

Each component of the granulation tissue serves a critical function during wound repair: myofibroblasts begin to contract the wound bed, collagen types I, II, and V provide nascent tensile strength for the wound, the presence of hyaluronic acid enables the penetration of infiltrating parenchymal cells, and proteoglycans increase wound resistance to deformation [20, 21, 23, 29]. Despite the number of fibroblasts in the wound bed remaining relatively constant during this phase of healing, the rate of collagen produced continues to increase dramatically (mainly collagen type I and III), resulting in more collagen accumulation than required to achieve sufficient formation of new stroma [22]. In addition, although it has been clearly demonstrated that fibroblasts are exposed to and generating a variety of mechanical signals during this phase, little is known about how these mechanical cues impact wound healing or the underlying mechanisms that regulate this process.

2.2.4. *Tissue remodeling, wound retraction, scar formation and the myofibroblast*

The final phase of wound healing, or tissue remodeling, is characterized by the transition from provisional matrix into collagenous scar. This transition includes extracellular

Chapter 2: Background and Significance

matrix remodeling, wound contraction, cell maturation, and cell apoptosis [21]. In response to mechanical and biochemical cues, the collagen fibers increase in size and number, align in the direction of tension, and are arranged into bundles [21]. The remodeling process results in a dramatic compaction of the matrix by resident cells (fibroblasts and myofibroblasts) and in an increase in the tensile strength and stiffness of the scar [20, 30]. During this time, fibrillar collagen has accumulated relatively rapidly and has been remodeling coordinately with myofibroblast-driven contraction. Despite this increase in collagen content, fully mature scar tissue is at maximum only 70% as strong as the native tissue it replaces [21].

Fibroblasts undergo several phenotypic shifts during granulation tissue formation and remodeling that continually modify their interactive relationship with the extracellular matrix. During the first phase of healing fibroblasts assume a migratory phenotype, and after 2-3 weeks, a proportion of these fibroblasts modulate into myofibroblasts, a profibrotic and contractile phenotype. Wound contraction is primarily thought to be ascribed to myofibroblasts, the most numerous cells in mature granulation tissue. Myofibroblasts are known to align within the wound along the lines of contraction. Interestingly, although fibroblast generated contractile forces are at equal levels in all wounds during this phase, the shape of the wound will dictate the resultant speed of contraction: linear wounds contract rapidly, rectangular wounds contract at a moderate pace, and circular wounds contract slowly [23].

The fibroblast-to-myofibroblast conversion is triggered by growth factors such as TGF- β and mechanical cues related to the forces resisting contraction [31, 32]. Myofibroblasts produce abundant collagen types I and III and impart tractional forces on the surrounding tissue to reduce the size of the wound bed [33, 34]. The myofibroblast phenotype is characterized by the presence of stress fibers, bundles of F-actin thought to be the force generating element involved in wound contraction and retractile phenomena found in fibrotic disease, the expression the cytoskeletal marker α -SMA, and the initiation of novel cell-cell (gap junctions) and cell-matrix linkages (the fibronexus) not seen in quiescent fibroblasts *in vivo* [34-41]. The fibronexus (supermature focal adhesion) uses

transmembrane integrins to link intracellular actin with extracellular fibronectin domains. Functionally this provides a mechanotransduction system capable to transmitting the force that is generated by stress fibers in myofibroblasts to the surrounding extracellular matrix [42].

2.2.5. Connective tissue pathology

Myofibroblasts are essential for appropriate wound healing, but in excess are associated with a variety of connective tissue diseases. When normal wound healing repair mechanisms become deregulated, fibrosis or wound contracture can develop.

Pathological phenomena resulting in fibrosis are characterized by a more permanent presence of a connective tissue bearing features of granulation tissue, resulting in excessive extracellular matrix deposition (Figure 2.5).

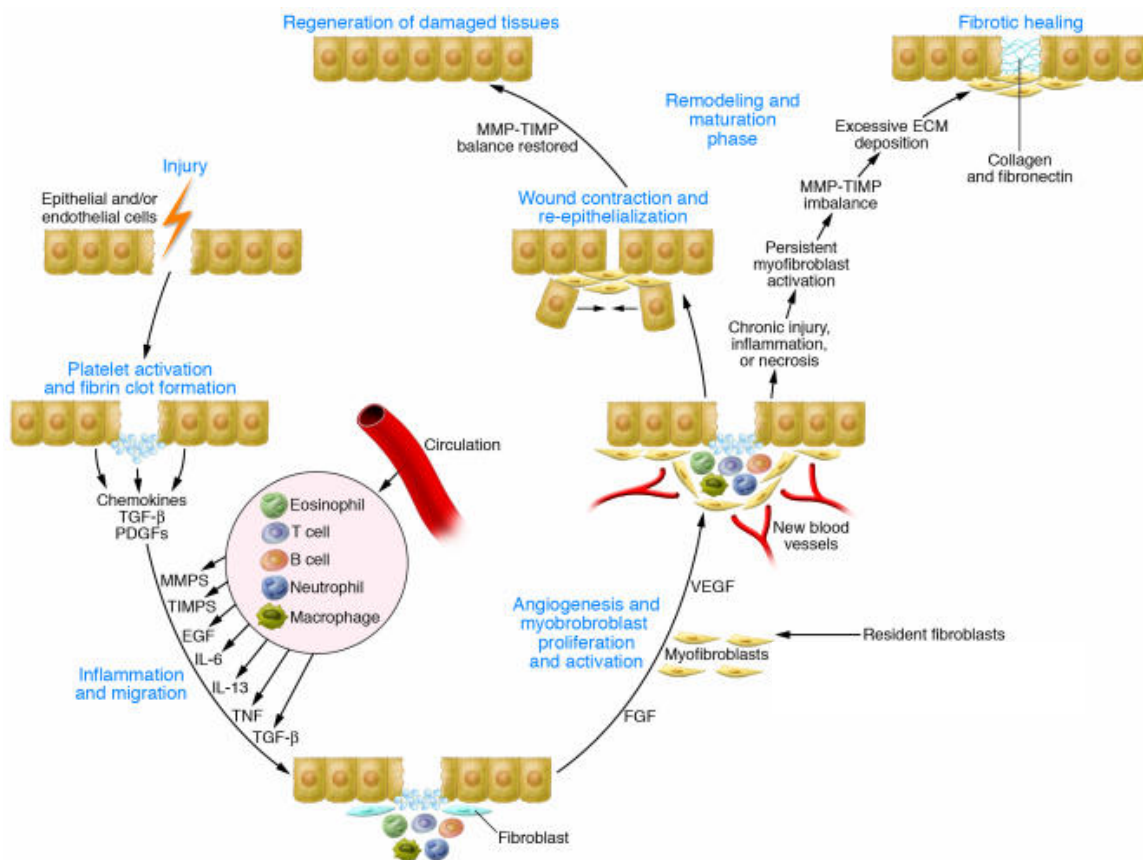


Fig 2.5. Regeneration versus pathological healing, the outcomes of wound repair. Fibro-contractive disorders in connective tissue differ from normal healing, and are defined as a dysregulated reparative response to chronic injury, inflammation, or necrosis that results in excessive collagen accumulation and tissue contracture (From Wynn T.A, et al, J Clin Invest, 2007) [4].

Chapter 2: Background and Significance

Fibrocontractive disorders in connective tissue are defined as a dysregulated reparative response to injury that results in excessive collagen accumulation and tissue contracture [4]. Fibrosis is defined as excessive collagen accumulation, developing from the imbalance of collagen deposition and catabolism. Contracture is the overcompensation of wound closure, associated with an increase in tissue stiffness, reduced range of motion, undesirable aesthetics, patient discomfort, and in some cases severe deformity [23].

These disorders can impact virtually every organ system and therefore present some of the most taxing clinical problems in medicine [43, 44]. Examples include tissue retraction, burn contracture, hypertrophic scarring, keloid formation, liver cirrhosis, kidney and pulmonary fibrosis, chronic asthma, heart disease, scleroderma, fibromatoses, atherosclerosis, and fibrosing alveolitis [45-47]. These diseases can be inherited or acquired, and come from a variety of sources including reactions to surgical materials, mechanical or thermal trauma, abnormal mechanical loading conditions, chemical or electrical burns, autoimmune diseases or inflammatory disorders, sepsis, degenerative and congenital disease, or heritable disorders such as Dupuytren's disease [6, 11]. Abnormal loading conditions in connective tissue could result from material property mismatch (e.g., the addition of a stiff inclusion such as a prosthetic or fibrotic foci formation in soft tissue) [48], trauma [49], aging [50], or degradative diseases such as emphysema [51, 52]. Regardless of etiology, the end result of these diseases is loss of tissue function. It is our hope that a better understanding of fibroblast mechanobiology will lead to therapies to mitigate mechanically-induced fibrosis.

2.2.6. Impact of mechanical loading during wound healing in vivo

Clinicians and researchers have long recognized that applying external forces during connective tissue wound healing can enable the manipulation of healing rates and can alter the appearance, mechanical and biochemical properties of scar tissue [23]. Some examples of external loading (i.e., mechanical conditioning) include serial casting, VAC

Chapter 2: Background and Significance

pressure usage, massage, dynamic splints, deep tissue massage, serial casting, z-plasty, range of motion exercises, ambulation, and stretching techniques.

Several animal studies have also shown that mechanically loading healing wounds produces a thinner, stronger, more compliant scar with a reduced incidence of contracture [53-56]. In these studies that utilized uniaxial stretch, a marked increase in fiber alignment in the predominant direction of stretch is observed [57], paralleling a striking increase in the stiffness [58] and tensile strength of the tissue [59-61]. For tissues such as tendons, fiber alignment induced by uniaxial stretch is a potentially beneficial and desirable result [62]. In planar tissues however, a highly aligned matrix is undesirable as it reduces the capacity of tissue to withstand multiaxially loading present in connective tissues, and could result in an even greater reduction in range of motion for the patient. Alternatively, biaxial stretching more closely models mechanical environment of planar tissues and appears to result in a more uniform angular distribution of collagen fibers *in vivo* [54, 62, 63].

2.2.7. The production of non-physiological stretch levels and fibrotic tissue propagation

Abnormal mechanical loading conditions (e.g., hypertension) can alter cellular function and change the structure and composition of the ECM, eventually leading to organ pathologies such as fibrosis or contracture [11]. Clinically undesirable results have been attributed to the application of stretch including hypertrophic scarring, edema, and scar lengthening and widening [64, 65]. It has been hypothesized that the outcome of wound repair could be related to the method of mechanical loading such as the amount (i.e., magnitude), length of time (i.e., duration), and direction that the stretch stimulus is applied [11, 61]. Clearly, establishing optimal loading regimens that promote the desired aspects of healing without stimulating detrimental side effects would be beneficial in skin and other connective tissues.

Clinical interventions such as the inclusion of a catheter, a tissue biopsy, or the insertion of a rigid device also can dramatically alter the local environment of the tissue by producing non-physiological stress conditions across the wound bed [66]. As the mechanical environment of the connective tissue is dramatically altered during clinical intervention and disease states, the resulting changes in strain levels could play a critical role in disease progression. Even minimally invasive technologies such as stent deployment can produce large strain gradients upon global stretching of connective tissue. These large deformations could potentially lead to fibrotic remodeling surrounding the stiff inclusion, pathological alterations in tissue composition and architecture, and ultimately promote a progressive and self-sustaining fibrotic process as seen during intimal hyperplasia and idiopathic pulmonary fibrosis [48].

2.2.8. *Cyclic stretch regulates fibroblast behavior in 2D systems*

To investigate how these mechanical signals found *in vivo* regulate cell behavior in a simple and controlled environment, cells are often plated on an elastic membrane that is deformed as homogeneously as possible. *In vitro* stretching devices can generally be grouped into three classes: uniaxial [67-78], strip biaxial [79], or equibiaxial [72, 80, 81]. These devices are typically motor driven systems that apply stretch in either in one direction (uniaxial), held tight in one axis while deformed in the transverse axis (strip biaxial stretch, termed ‘pure uniaxial stretch), or stretched equally in all directions in the x-y plane (equibiaxial). Examples for each of these loading systems are included in Figure 2.6.

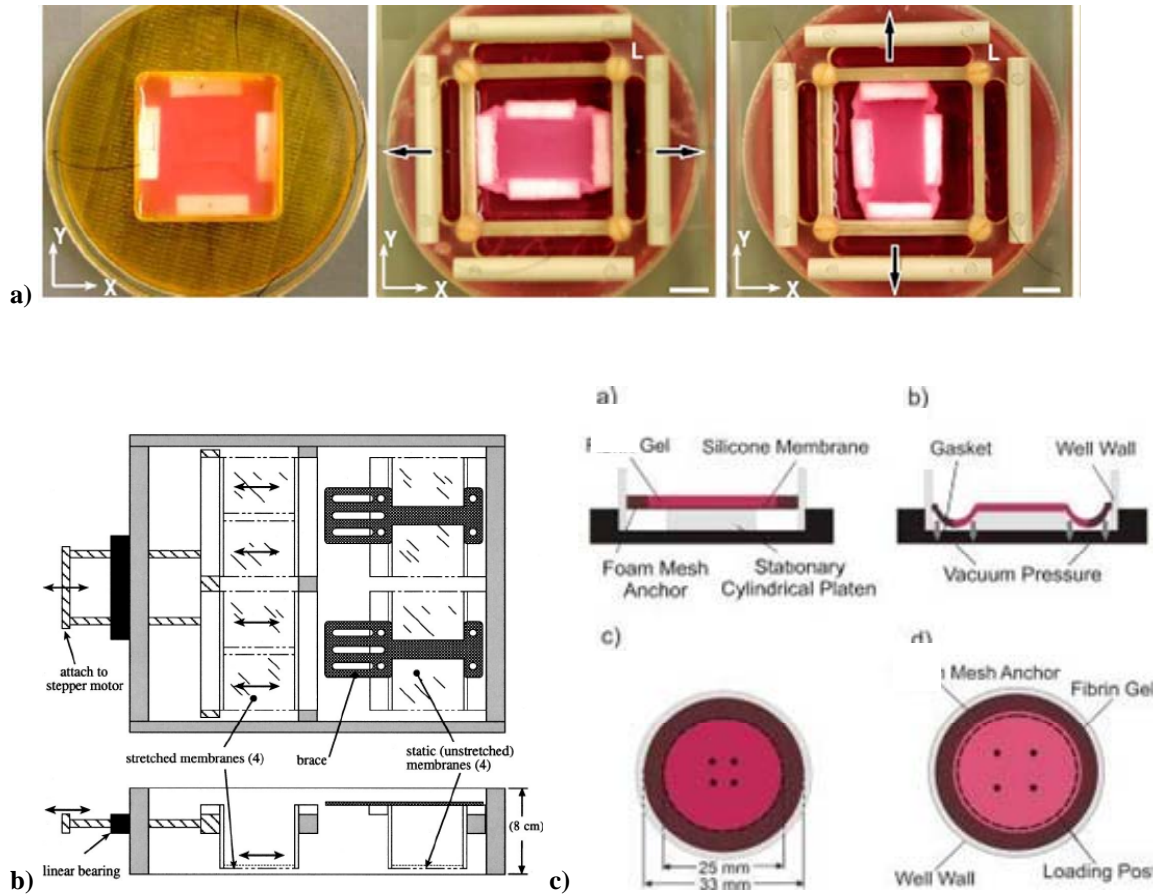


Fig. 2.6. Methods of mechanical stimulation. A) Strip biaxial: unidirected stretch with one axis held stationary [79] (From Lee, E. J. et al., *Ann Biomed Eng.* 2007), b) Uniaxial: one axis deformed while the alternative axis stretches inward due to Poisson effect (From Clark, C. B. *Rev of Scie Instr.* 2001)[70], and c) Equibiaxial: substrate is stretched uniformly (isotropically) in all directions [82] (From Balestrini et al., *J Biomech.* 2006).

These studies have demonstrated the profound impact of uniaxial stretch on cellular function including changes in ion transport [11], release of secondary messengers [11], cell shape [83], reorientation of fibroblasts and smooth muscles [84], increases in proliferation rates [85-87], alteration of migratory behavior [88], and changes in the expression and synthesis of a variety of contractile and regulatory proteins [86, 87, 89] including growth factor production [77, 85]. In addition, there is evidence to suggest that stretch-dependent cell behavior is dependent on the magnitude [68, 77, 80, 83, 84, 90, 91], duration [76, 84, 92], and frequency [68, 81, 93] of the mechanical conditioning.

Chapter 2: Background and Significance

Several cell types including fibroblasts and smooth muscle cells have been shown to align to the direction of minimum strain in 2D systems. In a uniaxially stretched system, the principal strains are along the stretch and perpendicular directions due to tensile and compressive forces; cell orientation in 2D is slightly off axis due to negative transverse strain produced by the Poisson effect [72, 88]. In strip biaxial systems minimum principal strain is perpendicular to the direction of pure uniaxial stretch [94], and cells orient themselves perpendicular to the direction of stretch. As there is no principal strain direction in a true equibiaxial stretch system, cells do not have any preferred orientation.

Although the above-mentioned research has provided much insight into the mechano-regulation of individual cells, these systems can not accurately mimic the governing biochemical and mechanical cues occurring between fibroblasts and their environment during cell-mediated extracellular matrix remodeling [95]. The mechanical environment of the connective tissue is composed not only of individual cell contributions but also contributions between cells and their surrounding extracellular matrix [95] and from the growth factor milieu in which they are bathed [96]. The relationship between fibroblasts and the extracellular matrix is a complex interaction involving feedback control between fibroblasts, cytokines, fibrinolysis enzymes, and the extracellular matrix; the fibroblasts are the primary effector cell responsible for the creation of the extracellular matrix, and the extracellular matrix itself regulates fibroblastic function, including fibroblast ability to synthesize, deposit, and remodel the extracellular matrix. Therefore, only a three-dimensional model can provide this complex and interactive relationship *in vitro*.

2.3. Current 3D *in vitro* models of wound healing

2.3.1. 3D in vitro systems for use in mechanobiology

To investigate cell-mediated remodeling and wound contraction in a controlled mechano-chemical environment, *in vitro* three-dimensional wound healing models such as cell-populated collagen and fibrin gels have been utilized extensively [25, 30, 97-100]. Type

Chapter 2: Background and Significance

I collagen gels, typically purified rat tail collagen, are commonly used in many standard *in vitro* 3D models such as fibroblast contraction and migration [97, 101], angiogenesis invasion [102, 103], vasculargenesis [104], and macrophage migration [105, 106].

Collagen gels are also a commonly used model of granulation tissue formation, and as collagen type I is the most abundant fibrous protein of interstitial tissue (e.g., dermis, pulmonary tissue, etc.) it is often utilized as a model of disease persistence within these tissues [107, 108]. The external and intrinsic tensile forces acting on and exerted by wound fibroblasts before, during, and after wound contraction have been studied in collagen gel model systems [96]. For example, potential signals that regulate wound contraction are analyzed by releasing mechanically stressed anchored gels from their substrate attachments to simulate the loss of resistance after a wound has closed [96, 108, 109].

As fibrin is the primary component in healing wounds during fibroplasia and is also involved in inflammation cascades, angiogenesis, and the abnormal growth of tissue (neoplasia), these matrices are most often utilized to model the early stages of wound healing and disease onset. Fibrin gels are typically composed of fibrinogen (2-4 mg/ml), thrombin, and a cellular solution [25, 110]. Studies utilizing these model systems include the investigation of cell migration, angiogenesis and gel contraction [24-26, 111-115].

2.3.2. *3D models for use in tissue engineering and regenerative medicine*

Cellularized collagen and fibrin gels are “living biomaterials” that not only provide a means for researching fundamental relationships in matrix mechanics and wound healing, but also potentially provide viable tissue analogs for regenerative medicine [116]. In order to completely restore functionality in diseased tissue, it is necessary to utilize tissue analogs that either intrinsically retain or can be manipulated to have comparable strength, density and ECM composition to native tissue.

Currently, collagen gels are the most commonly used biopolymers in tissue engineering; however, these tissue analogs lack sufficient mechanical integrity and composition for

most clinical usage [117]. One exception is a skin substitute that was developed by Organogenesis (Fig. 2.7), Apligraf®. Apligraf is currently approved by the Food and Drug Administration for use as a skin substitute and is comprised of a contracted collagen gel matrix and donated foreskin keratinocytes and dermal fibroblasts. The intrinsic strength of these tissue analogs is sufficient as they are used superficially (on the surface of the wound) and therefore do not undergo load-bearing *in vivo*.



Fig 2.7. Photo depicting Apligraf, a dermal tissue equivalent. Apligraf is a living, bilayered skin substitute composed of a contracted collagen matrix, keratinocytes, and dermal fibroblasts. (Petit-Zeman, S. Nat Biotechnol, 2001)[8]

In addition to collagen gels, fibrin gels have emerged for use in a variety of tissue replacement therapies, and have been met with some success [60, 114-119]. This success is in part due to fibroblasts seeded in fibrin gels exhibit substantially more ECM synthesis as compared to collagen gels [107, 118]. Some current applications include its use as a wound sealant or surgical glue [120], and for use in venous grafts to promote angiogenesis [121].

2.4. Mechanoregulation of fibroblasts in 3D models

2.4.1. Mechanobiology in 3D systems

Recently, the use of external mechanical conditioning (i.e., stretching devices) has been investigated as a means to produce tissue equivalents with superior mechanical properties and also as a means to determine how mechanical loading guides cells to synthesize and remodel their surrounding matrix during wound healing. Similar to 2D systems, mechanical loading of fibroblasts has been shown to alter cell proliferation, production and gene expression of ECM components in 3D matrices. In addition, these cellular responses, similar to cells in 2D stretched environments, appear to have been specifically adapted in response to loading conditions in terms of stretch orientation, magnitude, and duration (Table 2.1).

Table 2.1. Mechanobiological responses of cells to various applications of mechanical conditioning.

Cellular response	Loading regimen (load/level/duration/freq)	Model system	Reference
Increases in structural realignment created increases in UTS and matrix stiffness	Isotonically loaded under strip biaxial conditions, loaded with 200 mg weights, 72 hours	Dermal fibroblast-populated collagen cells	Lee et al. (2008)[79]
Increases in MMP-9, and MMP-2 expression	Cyclic uniaxial loading, 480 dynes/h , 2 days, 1 cycle per hour,	Dermal fibroblast-populated collagen cells	Prajapati et al. (2000)[122]
Fibroblasts align in the direction of principal strain	Cyclic uniaxial loading, 120 dyne force, 24 hours, graded frequency	Dermal fibroblast-populated collagen gels	Eastwood et al. (1998)[98]
Increases in TGF- β expression and MMP-2 activity	Cyclic uniaxial stretch, 10-16% strain, 96 hours, 1 Hz	Vascular SMC-populated collagen gel	O'Callaghan et al. (2000)[123]
Increases in UTS and material modulus after 8 days of conditioning. No changes present after 4 days.	Cyclic distention, 10% strain, 4 or 8 days, 1 Hz	SMC-populated collagen gel	Seliktar et al. (2000) [124]
Isotonically stretched samples displayed a synthetic phenotype. Cyclically stretched tissues displayed a contractile phenotype.	Either isotonic or cyclic "periodic stretching", 5% cyclic distention, 4 weeks, at 60 rpm	Arterial SMC-populated collagen gels,	Kanda et al. (1994)[125]
No effects after 2 weeks of stimulation. After 5 weeks, UTS, Elastic Modulus increased	Cyclic circumferential distension, 5% strain, 2 or 5 weeks, 0.5 Hz for either 12.5% duty cycle	Rat aortic SMC-populated collagen gels	Isenberg et al. (2003)[126]
Increase in cell number, collagen fiber alignment, and up-regulation of ligament fibroblast markers, including collagen types I and III and tenascin-C	Continuous uniaxial stretch, translational strain (10%) and rotational strain (25%),21 days, 0.0167 Hz	Mesenchymal progenitor cells-populated collagen gels	Altman et. al (2002)[57]
For constant strain, ultimate tensile strength (UTS) and tensile modulus increased. Stretching incrementally resulted in even greater increases in UTS, modulus, collagen production	Either constant or incremental strain, strain magnitudes ranged from 2.5% to 20%, 3 weeks of cyclic distension, graded frequency	Porcine VIC or dermal fibroblast-populated fibrin gels	Syedain et al. 2008 [127]
Increase in UTS, toughness, compaction and a decrease in cell proliferation	Continuous cyclic distension, 10% strain, 4 days, 1 Hz for a period of	Rat aortic SMC-populated collagen-fibrin gels	Cummings et al. (2004)[60]

Chapter 2: Background and Significance

The bulk of studies dedicated to investigating mechanical conditioning of tissue has been performed utilizing uniaxial cyclic stretching systems. Uniaxial stretch has been demonstrated to stimulate the synthesis and crosslinking of collagen while increasing the matrix density, fiber alignment, stiffness, and tensile strength in the direction of stretch [60, 124, 126, 128-130].

Although these results are promising for constructing mechanically competent tissue equivalents, it is understood that a substantial portion of the observed increase in mechanical properties is simply due to fiber alignment. It is therefore unclear if changes in tissue composition and mechanical properties are actually due to cell-mediated matrix remodeling or if they are simply artifact of passive fiber alignment. Therefore, in order to begin to understand how mechanical cues govern cell behavior during states of wound healing and repair, it is important to isolate the effect of mechanical stimulation on cell activity. In addition, although uniaxial-stretch induced fiber alignment may be highly beneficial for tissues that are uniaxially loaded or distended such as tendons and blood vessels, these systems do not accurately model the fiber architecture of planar connective tissues. One approach to isolating the impact of mechanical loading on cell matrix remodeling would be to utilize equibiaxial stretch. Equibiaxial stretch systems produce isotropic strain across the area of interest, and therefore would minimize or eliminate tissue alignment and simultaneously provide a multiaxially loaded model of planar tissue.

2.4.2. Determining optimal loading conditions for the creation of tissue equivalents for load bearing applications

Although there is a plethora of information that indicates that stretch is a powerful regulator of matrix remodeling [69, 119, 131], the bulk of previous research has narrowly focused on a single level of stretch when investigating stretch-dependent cell activity. Therefore, the combinations of strain magnitudes, ranges, and durations investigated thus far are not sufficient to characterize the complex relationships between mechanical conditioning parameters (magnitude, duration, etc.) and remodeling parameters (strength, stiffness, alignment, etc.). In addition, applying a single and

Chapter 2: Background and Significance

continuous level of strain does not assist in understanding tissue responses to changes in mechanical environments during growth, repair, and disease states. Quantitative dose-response curves between stretch parameters and alterations in matrix properties would assist in the development and rational design of therapies and would also aid in the understanding and prevention of scarring.

2.4.3. *Creating accurate models of planar tissue with non-uniform strain distribution*

Strain anisotropy has also been shown to be an important regulator in cell activity [72, 90, 132]. For example, there is substantial evidence to indicate differences in cell proliferation, shape, orientation, and synthetic activity between fibroblasts stretched biaxially and uniaxially [67, 94, 133]. In addition to strain orientation, there is evidence demonstrating that cell synthetic and proliferative activities in two dimensional studies are regulated by strain magnitude [68, 87, 90, 134]. Despite this knowledge, there is very little information regarding how cells will respond to gradients of strain as seen *in vivo*. Therefore, there is a need to develop a culture system that produces non-uniform strain patterns for studying the effects of strain magnitude, anisotropy, and gradients on cells culture.

2.5. Conclusions

Accurate mechanobiological models of planar tissue healing are desired to gain further insight into the effects of mechanical factors on scarring and the pathophysiology of diseases such as contracture, hypertrophic scarring, and keloid formation. Furthermore, these models offer a secondary role as tissue equivalent for use in regenerative medicine. Understanding tissue responses and cellular adaptations to changing mechanical stresses in planar tissue will allow for the manipulation of cell behavior within three-dimensional matrices for custom tailoring of tissue equivalents, assist in minimizing adverse effects of clinical intervention, and help understand the process of self-sustaining fibrosis (e.g., idiopathic pulmonary fibrosis, hypertrophic scarring).

2.6. References

- [1] Alberts, B., Johnson, A., Lewis, J., Raff, M., Roberts, K., and Walter, P., 2002, *Molecular Biology of the Cell*, Garland Science, New York.
- [2] Silver, F. H., Siperko, L. M., and Seehra, G. P., 2003, "Mechanobiology of force transduction in dermal tissue," *Skin Res Technol*, 9(1), pp. 3-23.
- [3] Clark, R. A., 1993, "Regulation of fibroplasia in cutaneous wound repair," *Am J Med Sci*, 306(1), pp. 42-48.
- [4] Wynn, T. A., 2007, "Common and unique mechanisms regulate fibrosis in various fibroproliferative diseases," *J Clin Invest*, 117(3), pp. 524-529.
- [5] White, E. S., Lazar, M. H., and Thannickal, V. J., 2003, "Pathogenetic mechanisms in usual interstitial pneumonia/idiopathic pulmonary fibrosis," *J Pathol*, 201(3), pp. 343-354.
- [6] Gardner, D. L., 1992, "Biology of connective tissue disease," *Pathological basis of connective tissue diseases*, D. L. Gardner, ed., Lea and Febiger, Philadelphia, PA, pp. 13-120.
- [7] Tortora, G. J., and Grabowski, S. R., 2003, "The tissue level of organization," *Principles of anatomy and physiology*, B. Roesch, ed., John Wiley and Sons, New York, pp. 118-136.
- [8] Petit-Zeman, S., 2001, "Regenerative medicine," *Nat Biotechnol*, 19(3), pp. 201-206.
- [9] Goodpaster, T., Legesse-Miller, A., Hameed, M. R., Aisner, S. C., Randolph-Habecker, J., and Collier, H. A., 2008, "An immunohistochemical method for identifying fibroblasts in formalin-fixed, paraffin-embedded tissue," *J Histochem Cytochem*, 56(4), pp. 347-358.
- [10] McClain, S. A., Simon, M., Jones, E., Nandi, A., Gailit, J. O., Tonnesen, M. G., Newman, D., and Clark, R. A., 1996, "Mesenchymal cell activation is the rate-limiting step of granulation tissue induction," *Am J Pathol*, 149(4), pp. 1257-1270.
- [11] Lundon, K., 2006, "Effect of mechanical loading on soft connective tissues," *Functional soft tissue examination and treatment by manual methods*, W. Hammer, ed., Jones and Bartlett, Sudbury, MA, pp. 13-120.
- [12] Silver, F. H., and Siperko, L. M., 2003, "Mechanosensing and mechanochemical transduction: how is mechanical energy sensed and converted into chemical energy in an extracellular matrix?," *Crit Rev Biomed Eng*, 31(4), pp. 255-331.
- [13] Wang, J. H., and Thampatty, B. P., 2006, "An introductory review of cell mechanobiology," *Biomech Model Mechanobiol*, 5(1), pp. 1-16.
- [14] Gilbert, J. A., Weinhold, P. S., Banes, A. J., Link, G. W., and Jones, G. L., 1994, "Strain profiles for circular cell culture plates containing flexible surfaces employed to mechanically deform cells in vitro," *J Biomech*, 27(9), pp. 1169-1177.
- [15] Hashima, A. R., Young, A. A., McCulloch, A. D., and Waldman, L. K., 1993, "Nonhomogeneous analysis of epicardial strain distributions during acute myocardial ischemia in the dog," *J Biomech*, 26(1), pp. 19-35.

Chapter 2: Background and Significance

- [16] Oomens, C. W., van Ratingen, M. R., Janssen, J. D., Kok, J. J., and Hendriks, M. A., 1993, "A numerical-experimental method for a mechanical characterization of biological materials," *J Biomech*, 26(4-5), pp. 617-621.
- [17] Chiquet, M., Renedo, A. S., Huber, F., and Fluck, M., 2003, "How do fibroblasts translate mechanical signals into changes in extracellular matrix production?," *Matrix Biol*, 22(1), pp. 73-80.
- [18] Grinnell, F., 2000, "Fibroblast-collagen-matrix contraction: growth-factor signalling and mechanical loading," *Trends in Cell Biology*, 10(9), pp. 362-365.
- [19] Gabbiani, G., 2003, "The myofibroblast in wound healing and fibrocontractive diseases," *J Pathol*, 200(4), pp. 500-503.
- [20] Linares, H. A., 1996, "From wound to scar," *Burns*, 22(5), pp. 339-352.
- [21] Clark, R. A. F., 1996, *The molecular and cellular biology of wound repair*, Plenum Press, New York.
- [22] Wilkins, R. B., and Kulwin, D. R., 1979, "Wendell L. Hughes Lecture. Wound healing," *Ophthalmology*, 86(4), pp. 507-510.
- [23] Hardy, M. A., 1989, "The biology of scar formation," *Physical Therapy*, 69(12), pp. 1014-1024.
- [24] Brown, L. F., Lanir, N., McDonagh, J., Tognazzi, K., Dvorak, A. M., and Dvorak, H. F., 1993, "Fibroblast migration in fibrin gel matrices," *Am J Pathol*, 142(1), pp. 273-283.
- [25] Tuan, T. L., Song, A., Chang, S., Younai, S., and Nimni, M. E., 1996, "In vitro fibroplasia: matrix contraction, cell growth, and collagen production of fibroblasts cultured in fibrin gels," *Exp Cell Res*, 223(1), pp. 127-134.
- [26] Dvorak, H. F., Harvey, V. S., Estrella, P., Brown, L. F., McDonagh, J., and Dvorak, A. M., 1987, "Fibrin containing gels induce angiogenesis. Implications for tumor stroma generation and wound healing," *Lab Invest*, 57(6), pp. 673-686.
- [27] Gailit, J., Clarke, C., Newman, D., Tonnesen, M. G., Mosesson, M. W., and Clark, R. A., 1997, "Human fibroblasts bind directly to fibrinogen at RGD sites through integrin alpha(v)beta3," *Exp Cell Res*, 232(1), pp. 118-126.
- [28] Stirk, C. M., Reid, A., Melvin, W. T., and Thompson, W. D., 2000, "Locating the active site for angiogenesis and cell proliferation due to fibrin fragment E with a phage epitope display library," *Gen Pharmacol*, 35(5), pp. 261-267.
- [29] Roche, W. R., 1990, "Myofibroblasts," *J Pathol*, 161(4), pp. 281-282.
- [30] Tomasek, J. J., Haaksma, C. J., Eddy, R. J., and Vaughan, M. B., 1992, "Fibroblast contraction occurs on release of tension in attached collagen lattices: dependency on an organized actin cytoskeleton and serum," *Anatomical Record*, 232(3), pp. 359-368.
- [31] Desmouliere, A., Geinoz, A., Gabbiani, F., and Gabbiani, G., 1993, "Transforming growth factor-beta 1 induces alpha-smooth muscle actin expression in granulation tissue myofibroblasts and in quiescent and growing cultured fibroblasts," *J Cell Biol*, 122(1), pp. 103-111.
- [32] Grinnell, F., 1994, "Fibroblasts, myofibroblasts, and wound contraction," *J Cell Biol*, 124(4), pp. 401-404.
- [33] Gabbiani, G., Chaponnier, C., and Huttner, I., 1978, "Cytoplasmic filaments and gap junctions in epithelial cells and myofibroblasts during wound healing," *J Cell Biol*, 76(3), pp. 561-568.

Chapter 2: Background and Significance

- [34] Welch, M. P., Odland, G. F., and Clark, R. A., 1990, "Temporal relationships of F-actin bundle formation, collagen and fibronectin matrix assembly, and fibronectin receptor expression to wound contraction," *J Cell Biol*, 110(1), pp. 133-145.
- [35] Darby, I., Skalli, O., and Gabbiani, G., 1990, "Alpha-smooth muscle actin is transiently expressed by myofibroblasts during experimental wound healing," *Lab Invest*, 63(1), pp. 21-29.
- [36] Hinz, B., and Gabbiani, G., 2003, "Cell-matrix and cell-cell contacts of myofibroblasts: role in connective tissue remodeling," *Thromb Haemost*, 90(6), pp. 993-1002.
- [37] Hinz, B., and Gabbiani, G., 2003, "Mechanisms of force generation and transmission by myofibroblasts," *Curr Opin Biotechnol*, 14(5), pp. 538-546.
- [38] Hinz, B., Mastrangelo, D., Iselin, C. E., Chaponnier, C., and Gabbiani, G., 2001, "Mechanical tension controls granulation tissue contractile activity and myofibroblast differentiation," *Am J Pathol*, 159(3), pp. 1009-1020.
- [39] Skalli, O., Pelte, M. F., Pecelet, M. C., Gabbiani, G., Gugliotta, P., Bussolati, G., Ravazzola, M., and Orci, L., 1989, "Alpha-smooth muscle actin, a differentiation marker of smooth muscle cells, is present in microfilamentous bundles of pericytes," *J Histochem Cytochem*, 37(3), pp. 315-321.
- [40] Skalli, O., Ropraz, P., Trzeciak, A., Benzonana, G., Gillessen, D., and Gabbiani, G., 1986, "A monoclonal antibody against alpha-smooth muscle actin: a new probe for smooth muscle differentiation," *J Cell Biol*, 103(6 Pt 2), pp. 2787-2796.
- [41] Skalli, O., Schurch, W., Seemayer, T., Lagace, R., Montandon, D., Pittet, B., and Gabbiani, G., 1989, "Myofibroblasts from diverse pathologic settings are heterogeneous in their content of actin isoforms and intermediate filament proteins," *Lab Invest*, 60(2), pp. 275-285.
- [42] Desmouliere, A., and Gabbiani, G., 1996, "The role of the myofibroblast in wound healing and fibrocontractive diseases," *The molecular and cellular biology of wound repair*, R. A. F. Clark, ed., Plenum Press, New York, pp. 391-423.
- [43] Desmouliere, A., 1995, "Factors influencing myofibroblast differentiation during wound healing and fibrosis," *Cell Biol Int*, 19(5), pp. 471-476.
- [44] Society, A. T., 2002, "American Thoracic Society/European Respiratory Society International Multidisciplinary Consensus Classification of the Idiopathic Interstitial Pneumonias. This joint statement of the American Thoracic Society (ATS), and the European Respiratory Society (ERS) was adopted by the ATS board of directors, June 2001 and by the ERS Executive Committee, June 2001," *Am J Respir Crit Care Med*, 165(2), pp. 277-304.
- [45] Adler, K. B., Low, R. B., Leslie, K. O., Mitchell, J., and Evans, J. N., 1989, "Contractile cells in normal and fibrotic lung," *Lab Invest*, 60(4), pp. 473-485.
- [46] Appleton, I., Tomlinson, A., Chander, C. L., and Willoughby, D. A., 1992, "Effect of endothelin-1 on croton oil-induced granulation tissue in the rat. A pharmacologic and immunohistochemical study," *Lab Invest*, 67(6), pp. 703-710.
- [47] Thiemermann, C., and Corder, R., 1992, "Is endothelin-1 the regulator of myofibroblast contraction during wound healing?," *Lab Invest*, 67(6), pp. 677-679.

Chapter 2: Background and Significance

- [48] Mori, D., David, G., Humphrey, J. D., and Moore, J. E., Jr., 2005, "Stress distribution in a circular membrane with a central fixation," *J Biomech Eng*, 127(3), pp. 549-553.
- [49] Sanders, J. E., Goldstein, B. S., and Leotta, D. F., 1995, "Skin response to mechanical stress: adaptation rather than breakdown--a review of the literature," *J Rehabil Res Dev*, 32(3), pp. 214-226.
- [50] Sugihara, T., Martin, C. J., and Hildebrandt, J., 1971, "Length-tension properties of alveolar wall in man," *J Appl Physiol*, 30(6), pp. 874-878.
- [51] Gefen, A., Elad, D., and Shiner, R. J., 1999, "Analysis of stress distribution in the alveolar septa of normal and simulated emphysematic lungs," *J Biomech*, 32(9), pp. 891-897.
- [52] Maksym, G. N., and Bates, J. H., 1997, "A distributed nonlinear model of lung tissue elasticity," *J Appl Physiol*, 82(1), pp. 32-41.
- [53] Brunius, U., Zederfeldt, B., and Ahren, C., 1967, "Healing of skin incisions closed by non-suture technique. A tensiometric and histologic study in the rat," *Acta Chir Scand*, 133(7), pp. 509-516.
- [54] Langrana, N. A., Alexander, H., Strauchler, I., Mehta, A., and Ricci, J., 1983, "Effect of mechanical load in wound healing," *Annals of Plastic Surgery*, 10(3), pp. 200-208.
- [55] Sussman, M. D., 1966, "Effect of increased tissue traction upon tensile strength of cutaneous incisions in rats," *Proceedings of the Society for Experimental Biology and Medicine*, 123(1), pp. 38-41.
- [56] Thorngate, S., and Ferguson, D. J., 1958, "Effect of tension on healing of aponeurotic wounds," *Surgery*, 44(4), pp. 619-624.
- [57] Altman, G. H., Horan, R. L., Martin, I., Farhadi, J., Stark, P. R., Volloch, V., Richmond, J. C., Vunjak-Novakovic, G., and Kaplan, D. L., 2002, "Cell differentiation by mechanical stress," *FASEB J*, 16(2), pp. 270-272. Epub 2001 Dec 2028.
- [58] Calve, S., Syed, F. N., Dennis, R. G., Grosh, K., Garikipati, K., and Arruda, E. M., 2005, "Mechanical Characterization of Growth in Fibrin-Based Tendon Constructs," Summer Bioengineering Conference, ASME, Vail, Colorado.
- [59] Grenier, G., Remy-Zolghadri, M., Larouche, D., Gauvin, R., Baker, K., Bergeron, F., Dupuis, D., Langelier, E., Rancourt, D., Auger, F. A., and Germain, L., 2005, "Tissue reorganization in response to mechanical load increases functionality," *Tissue Eng*, 11(1-2), pp. 90-100.
- [60] Cummings, C. L., Gawlitta, D., Nerem, R. M., and Stegemann, J. P., 2004, "Properties of engineered vascular constructs made from collagen, fibrin, and collagen-fibrin mixtures," *Biomaterials*, 25(17), pp. 3699-3706.
- [61] Seliktar, D., Black, R. A., Vito, R. P., and Nerem, R. M., 2000, "Dynamic mechanical conditioning of collagen-gel blood vessel constructs induces remodeling in vitro," *Ann Biomed Eng*, 28(4), pp. 351-362.
- [62] Timmenga, E. J., Schoorl, R., and Klopper, P. J., 1990, "Biomechanical and histomorphological changes in expanded rabbit skin," *Br J Plast Surg*, 43(1), pp. 101-106.

Chapter 2: Background and Significance

- [63] Timmenga, E. J., and Das, P. K., 1992, "Histomorphological observations on dermal repair in expanded rabbit skin: a preliminary report," *Br J Plast Surg*, 45(7), pp. 503-507.
- [64] Arem, A. J., and Madden, J. W., 1976, "Effects of stress on healing wounds: I. Intermittent noncyclical tension," *Journal of Surgical Research*, 20(2), pp. 93-102.
- [65] Sommerlad, B. C., and Creasey, J. M., 1978, "The stretched scar: a clinical and histological study," *British Journal of Plastic Surgery*, 31(1), pp. 34-45.
- [66] Junker, J. P., Kratz, C., Tollback, A., and Kratz, G., 2008 "Mechanical tension stimulates the transdifferentiation of fibroblasts into myofibroblasts in human burn scars," *Burns*, pp. 0305-4179.
- [67] Berry, C. C., Cacou, C., Lee, D. A., Bader, D. L., and Shelton, J. C., 2003, "Dermal fibroblasts respond to mechanical conditioning in a strain profile dependent manner," *Biorheology*, 40(1-3), pp. 337-345.
- [68] Boccafoschi, F., Bosetti, M., Gatti, S., and Cannas, M., 2007, "Dynamic fibroblast cultures: response to mechanical stretching," *Cell Adh Migr*, 1(3), pp. 124-128.
- [69] Boerboom, R. A., Rubbens, M. P., Driessen, N. J., Bouten, C. V., and Baaijens, F. P., 2008, "Effect of strain magnitude on the tissue properties of engineered cardiovascular constructs," *Ann Biomed Eng*, 36(2), pp. 244-253.
- [70] Clark, C. B., Burkholder, T. J., and Frangos, J. A., 2001, "Uniaxial strain system to investigate strain rate regulation in vitro," *Rev of Scie Instr*, 72(5), pp. 2415-2422.
- [71] Kaunas, R., Nguyen, P., Usami, S., and Chien, S., 2005, "Cooperative effects of Rho and mechanical stretch on stress fiber organization," *Proc Natl Acad Sci U S A*, 102(44), pp. 15895-15900.
- [72] Mudera, V. C., Pleass, R., Eastwood, M., Tarnuzzer, R., Schultz, G., Khaw, P., McGrouther, D. A., and Brown, R. A., 2000, "Molecular responses of human dermal fibroblasts to dual cues: contact guidance and mechanical load," *Cell Motil Cytoskeleton*, 45(1), pp. 1-9.
- [73] Prajapati, R. T., Eastwood, M., and Brown, R. A., 2000, "Duration and orientation of mechanical loads determine fibroblast cyto-mechanical activation: monitored by protease release," *Wound Repair and Regeneration*, 8(3), pp. 238-246.
- [74] Tower, T. T., Neidert, M. R., and Tranquillo, R. T., 2002, "Fiber alignment imaging during mechanical testing of soft tissues," *Ann Biomed Eng*, 30(10), pp. 1221-1233.
- [75] Wakatsuki, T., Kolodney, M. S., Zahalak, G. I., and Elson, E. L., 2000, "Cell mechanics studied by a reconstituted model tissue," *Biophys J*, 79(5), pp. 2353-2368.
- [76] Wang, J. G., Miyazu, M., Matsushita, E., Sokabe, M., and Naruse, K., 2001, "Uniaxial cyclic stretch induces focal adhesion kinase (FAK) tyrosine phosphorylation followed by mitogen-activated protein kinase (MAPK) activation," *Biochem Biophys Res Commun*, 288(2), pp. 356-361.
- [77] Yang, G., Crawford, R. C., and Wang, J. H., 2004, "Proliferation and collagen production of human patellar tendon fibroblasts in response to cyclic uniaxial stretching in serum-free conditions," *J Biomech*, 37(10), pp. 1543-1550.

Chapter 2: Background and Significance

- [78] Yost, M. J., Simpson, D., Wrona, K., Ridley, S., Ploehn, H. J., Borg, T. K., and Terracio, L., 2000, "Design and construction of a uniaxial cell stretcher," *Am J Physiol Heart Circ Physiol*, 279(6), pp. H3124-3130.
- [79] Lee, E. J., Holmes, J. W., and Costa, K. D., 2008, "Remodeling of engineered tissue anisotropy in response to altered loading conditions," *Ann Biomed Eng*, 36(8), pp. 1322-1334.
- [80] Lee, A. A., Delhaas, T., McCulloch, A. D., and Villarreal, F. J., 1999, "Differential responses of adult cardiac fibroblasts to in vitro biaxial strain patterns," *J Mol Cell Cardiol*, 31(10), pp. 1833-1843.
- [81] Nishimura, K., Blume, P., Ohgi, S., and Sumpio, B. E., 2007, "Effect of different frequencies of tensile strain on human dermal fibroblast proliferation and survival," *Wound Repair Regen*, 15(5), pp. 646-656.
- [82] Balestrini, J. L., and Billiar, K. L., 2006, "Equibiaxial cyclic stretch stimulates fibroblasts to rapidly remodel fibrin," *J Biomech*, 39(16), pp. 2983-2990.
- [83] Arold, S. P., Wong, J. Y., and Suki, B., 2007, "Design of a new stretching apparatus and the effects of cyclic strain and substratum on mouse lung epithelial-12 cells," *Ann Biomed Eng*, 35(7), pp. 1156-1164.
- [84] Loesberg, W. A., Walboomers, X. F., van Loon, J. J., and Jansen, J. A., 2005, "The effect of combined cyclic mechanical stretching and microgrooved surface topography on the behavior of fibroblasts," *J Biomed Mater Res A*, 75(3), pp. 723-732.
- [85] Bishop, J. E., Mitchell, J. J., Absher, P. M., Baldor, L., Geller, H. A., Woodcock-Mitchell, J., Hamblin, M. J., Vacek, P., and Low, R. B., 1993, "Cyclic mechanical deformation stimulates human lung fibroblast proliferation and autocrine growth factor activity," *Am J Respir Cell Mol Biol*, 9(2), pp. 126-133.
- [86] Breen, E. C., Fu, Z., and Normand, H., 1999, "Calcyclin gene expression is increased by mechanical strain in fibroblasts and lung," *Am J Respir Cell Mol Biol*, 21(6), pp. 746-752.
- [87] Wang, J. H., Yang, G., and Li, Z., 2005, "Controlling cell responses to cyclic mechanical stretching," *Ann Biomed Eng*, 33(3), pp. 337-342.
- [88] Raeber, G. P., Lutolf, M. P., and Hubbell, J. A., 2008, "Part II: Fibroblasts preferentially migrate in the direction of principal strain," *Biomech Model Mechanobiol*, 7(3), pp. 215-225.
- [89] Katsumi, A., Naoe, T., Matsushita, T., Kaibuchi, K., and Schwartz, M. A., 2005, "Integrin activation and matrix binding mediate cellular responses to mechanical stretch," *J Biol Chem*, 280(17), pp. 16546-16549..
- [90] Dartsch, P. C., Hammerle, H., and Betz, E., 1986, "Orientation of cultured arterial smooth muscle cells growing on cyclically stretched substrates," *Acta Anat (Basel)*, 125(2), pp. 108-113.
- [91] Husse, B., Briest, W., Homagk, L., Isenberg, G., and Gekle, M., 2007, "Cyclical mechanical stretch modulates expression of collagen I and collagen III by PKC and tyrosine kinase in cardiac fibroblasts," *Am J Physiol Regul Integr Comp Physiol*, 293(5), pp. R1898-1907.
- [92] Kratz, C., Tollback, A., and Kratz, G., 2001, "Effects of continuous stretching on cell proliferation and collagen synthesis in human burn scars," *Scand J Plast Reconstr Surg Hand Surg*, 35(1), pp. 57-63.

Chapter 2: Background and Significance

- [93] Winston, F. K., Macarak, E. J., Gorfien, S. F., and Thibault, L. E., 1989, "A system to reproduce and quantify the biomechanical environment of the cell," *J Appl Physiol*, 67(1), pp. 397-405.
- [94] Wang, J. H., Goldschmidt-Clermont, P., Moldovan, N., and Yin, F. C., 2000, "Leukotrienes and tyrosine phosphorylation mediate stretching-induced actin cytoskeletal remodeling in endothelial cells," *Cell Motil Cytoskeleton*, 46(2), pp. 137-145.
- [95] Grinnell, F., 2003, "Fibroblast biology in three-dimensional collagen matrices," *Trends Cell Biol*, 13(5), pp. 264-269.
- [96] Martin, P., 1997, "Wound healing--aiming for perfect skin regeneration," *Science*, 276(5309), pp. 75-81.
- [97] Bell, E., Ivarsson, B., and Merrill, C., 1979, "Production of a tissue-like structure by contraction of collagen lattices by human fibroblasts of different proliferative potential in vitro," *Proc Natl Acad Sci U S A*, 76(3), pp. 1274-1278.
- [98] Eastwood, M., McGrouther, D. A., and Brown, R. A., 1998, "Fibroblast responses to mechanical forces," *Proc Inst Mech Eng [H]*, 212(2), pp. 85-92.
- [99] Tranquillo, R. T., and Murray, J. D., 1993, "Mechanistic model of wound contraction," *J Surg Res*, 55(2), pp. 233-247.
- [100] Zhu, Y. K., Umino, T., Liu, X. D., Wang, H. J., Romberger, D., Spurzem, J. R., and Rennard, S. I., 2001, "Contraction of fibroblast-containing collagen gels: initial collagen concentration regulates the degree of contraction and cell survival," *In Vitro Cell. Dev. Biol.- Animal*, 37, pp. 10-16.
- [101] Brown, R. A., Prajapati, R., McGrouther, D. A., Yannas, I. V., and Eastwood, M., 1998, "Tensional homeostasis in dermal fibroblasts: mechanical responses to mechanical loading in three-dimensional substrates," *J Cell Physiol*, 175(3), pp. 323-332.
- [102] Montesano, R., and Orci, L., 1985, "Tumor-promoting phorbol esters induce angiogenesis in vitro," *Cell*, 42(2), pp. 469-477.
- [103] Yang, S., Graham, J., Kahn, J. W., Schwartz, E. A., and Gerritsen, M. E., 1999, "Functional roles for PECAM-1 (CD31) and VE-cadherin (CD144) in tube assembly and lumen formation in three-dimensional collagen gels," *Am J Pathol*, 155(3), pp. 887-895.
- [104] Ng, C. P., Helm, C. L., and Swartz, M. A., 2004, "Interstitial flow differentially stimulates blood and lymphatic endothelial cell morphogenesis in vitro," *Microvasc Res*, 68(3), pp. 258-264.
- [105] Brown, A. F., 1982, "Neutrophil granulocytes: adhesion and locomotion on collagen substrata and in collagen matrices," *J Cell Sci*, 58, pp. 455-467.
- [106] Entschladen, F., Niggemann, B., Zanker, K. S., and Friedl, P., 1997, "Differential requirement of protein tyrosine kinases and protein kinase C in the regulation of T cell locomotion in three-dimensional collagen matrices," *J Immunol*, 159(7), pp. 3203-3210.
- [107] Clark, R. A., Nielsen, L. D., Welch, M. P., and McPherson, J. M., 1995, "Collagen matrices attenuate the collagen-synthetic response of cultured fibroblasts to TGF-beta," *J Cell Sci*, 108(Pt 3), pp. 1251-1261.

Chapter 2: Background and Significance

- [108] Montesano, R., and Orci, L., 1988, "Transforming growth factor beta stimulates collagen-matrix contraction by fibroblasts: implications for wound healing," *Proc Natl Acad Sci U S A*, 85(13), pp. 4894-4897.
- [109] He, Y., and Grinnell, F., 1994, "Stress relaxation of fibroblasts activates a cyclic AMP signaling pathway," *J Cell Biol*, 126(2), pp. 457-464.
- [110] Gillery, P., Bellon, G., Coustry, F., and Borel, J. P., 1989, "Cultures of fibroblasts in fibrin lattices: models for the study of metabolic activities of the cells in physiological conditions," *J Cell Physiol*, 140(3), pp. 483-490.
- [111] Grassl, E. D., Oegema, T. R., and Tranquillo, R. T., 2003, "A fibrin-based arterial media equivalent," *J Biomed Mater Res A*, 66(3), pp. 550-561.
- [112] Long, J. L., and Tranquillo, R. T., 2003, "Elastic fiber production in cardiovascular tissue-equivalents," *Matrix Biol*, 22(4), pp. 339-350.
- [113] Robinson, P. S., and Tranquillo, R. T., 2005, "Effect of fibrin concentration on cell-induced remodeling and resulting mechanical properties of fibrin gel," *ASME Summer Bioengineering Conference*, ASME, Vail, Colorado.
- [114] Swartz, D. D., Russell, J. A., and Andreadis, S. T., 2005, "Engineering of fibrin-based functional and implantable small-diameter blood vessels," *Am J Physiol Heart Circ Physiol*, 288(3), pp. H1451-1460.
- [115] Ye, Q., Zund, G., Benedikt, P., Jockenhoevel, S., Hoerstrup, S. P., Sakyama, S., Hubbell, J. A., and Turina, M., 2000, "Fibrin gel as a three dimensional matrix in cardiovascular tissue engineering," *Eur J Cardiothorac Surg*, 17(5), pp. 587-591.
- [116] Yao, L., Swartz, D. D., Gugino, S. F., Russell, J. A., and Andreadis, S. T., 2005, "Fibrin-based tissue-engineered blood vessels: differential effects of biomaterial and culture parameters on mechanical strength and vascular reactivity," *Tissue Eng*, 11(7-8), pp. 991-1003.
- [117] Grassl, E. D., Oegema, T. R., and Tranquillo, R. T., 2002, "Fibrin as an alternative biopolymer to type-I collagen for the fabrication of a media equivalent," *J Biomed Mater Res*, 60(4), pp. 607-612.
- [118] Neidert, M. R., Lee, E. S., Oegema, T. R., and Tranquillo, R. T., 2002, "Enhanced fibrin remodeling in vitro with TGF-beta1, insulin and plasmin for improved tissue-equivalents," *Biomaterials*, 23(17), pp. 3717-3731.
- [119] Boublik, J., Park, H., Radisic, M., Tognana, E., Chen, F., Pei, M., Vunjak-Novakovic, G., and Freed, L. E., 2005, "Mechanical properties and remodeling of hybrid cardiac constructs made from heart cells, fibrin, and biodegradable, elastomeric knitted fabric," *Tissue Eng*, 11(7-8), pp. 1122-1132.
- [120] Arkudas, A., Tjiawi, J., Bleiziffer, O., Grabinger, L., Polykandriotis, E., Beier, J. P., Sturzl, M., Horch, R. E., and Kneser, U., 2007, "Fibrin gel-immobilized VEGF and bFGF efficiently stimulate angiogenesis in the AV loop model," *Mol Med*, 13(9-10), pp. 480-487.
- [121] Polykandriotis, E., Tjiawi, J., Euler, S., Arkudas, A., Hess, A., Brune, K., Greil, P., Lametschwandtner, A., Horch, R. E., and Kneser, U., 2008, "The venous graft as an effector of early angiogenesis in a fibrin matrix," *Microvasc Res*, 75(1), pp. 25-33.
- [122] Prajapati, R. T., Chavally-Mis, B., Herbage, D., Eastwood, M., and Brown, R. A., 2000, "Mechanical loading regulates protease production by fibroblasts in three-

- dimensional collagen substrates," *Wound Repair and Regeneration*, 8(3), pp. 226-237.
- [123] O'Callaghan, C. J., and Williams, B., 2000, "Mechanical strain-induced extracellular matrix production by human vascular smooth muscle cells: role of TGF-beta(1)," *Hypertension*, 36(3), pp. 319-324.
- [124] Seliktar, D., Black, R. A., Vito, R. P., and Nerem, R. M., 2000, "Dynamic mechanical conditioning of collagen-gel blood vessel constructs induces remodeling in vitro," *Annals of Biomedical Engineering*, 28(4), pp. 351-362.
- [125] Kanda, K., and Matsuda, T., 1994, "Mechanical stress-induced orientation and ultrastructural change of smooth muscle cells cultured in three-dimensional collagen lattices," *Cell Transplant*, 3(6), pp. 481-492.
- [126] Isenberg, B. C., and Tranquillo, R. T., 2003, "Long-term cyclic distention enhances the mechanical properties of collagen-based media-equivalents," *Annals of Biomedical Engineering*, 31(8), pp. 937-949.
- [127] Syedain, Z. H., Weinberg, J. S., and Tranquillo, R. T., 2008, "Cyclic distension of fibrin-based tissue constructs: evidence of adaptation during growth of engineered connective tissue," *Proc Natl Acad Sci U S A*, 105(18), pp. 6537-6542. Epub 2008 Apr 6524.
- [128] Altman, G. H., Horan, R. L., Martin, I., Farhadi, J., Stark, P. R., Volloch, V., Richmond, J. C., Vunjak-Novakovic, G., and Kaplan, D. L., 2002, "Cell differentiation by mechanical stress," *FASEB J*, 16(2).
- [129] Grenier, G., Remy-Zolghadri, M., Larouche, D., Gauvin, R., Baker, K., Bergeron, F., Dupuis, D., Langelier, E., Rancourt, D., Auger, F. A., and Germain, L., 2005, "Tissue reorganization in response to mechanical load increases functionality," *Tissue Engineering*, 11(1-2), pp. 90-100.
- [130] Yang, G., Crawford, R. C., and Wang, J. H., 2004, "Proliferation and collagen production of human patellar tendon fibroblasts in response to cyclic uniaxial stretching in serum-free conditions," *Journal of Biomechanics*, 37(10), pp. 1543-1550.
- [131] Isenberg, B. C., and Tranquillo, R. T., 2003, "Long-term cyclic distention enhances the mechanical properties of collagen-based media-equivalents," *Ann Biomed Eng*, 31(8), pp. 937-949.
- [132] Kulik, T. J., and Alvarado, S. P., 1993, "Effect of stretch on growth and collagen synthesis in cultured rat and lamb pulmonary arterial smooth muscle cells," *J Cell Physiol*, 157(3), pp. 615-624.
- [133] Shelton, J. C., Bader, D. L., and Lee, D. A., 2003, "Mechanical conditioning influences the metabolic response of cell-seeded constructs," *Cells Tissues Organs*, 175(3), pp. 140-150.
- [134] Balestrini, J. L., and Billiar, K. L., 2009, "Magnitude and duration of stretch modulate fibroblast remodeling," *J Biomech Eng*, 131(5), p. 051005.

CHAPTER 3

Equibiaxial cyclic stretch stimulates fibroblasts to rapidly remodel fibrin

(Balestrini, J. L., and Billiar, K. L., 2006, J Biomech, 39(16), pp. 2983-2990, reprinted with permission)

3.1. Introduction

During adult dermal healing, fibroblasts remodel the fibrin-rich provisional matrix by synthesizing, organizing, and crosslinking collagen and other matrix components to form a scar. In response to mechanical and biochemical cues, the collagen fibers increase in size and number, align in the direction of tension, and are arranged into bundles [1]. The remodeling process results in a dramatic compaction of the matrix and an increase in the tensile strength and stiffness of the scar [2, 3], yet the scar remains weaker than the native dermis that it replaces [1]. Heightened tissue stiffness combined with contracture often leads to reduced range of motion, undesirable aesthetics, patient discomfort, and in some cases severe deformity [4].

Clinicians have long recognized that the mechanical state of a wound during healing dramatically alters the structure and properties of the resulting scar. Dynamic splints, serial casting, z-plasty, massage, ambulation, range of motion exercises, and stretching techniques are commonly utilized to alter the appearance and properties of scars[4]. Furthermore, numerous animal studies have shown that stretching healing wounds results in a reduction in contracture and thickness and an increase in compliance and tensile strength of the scar [5-8]. Conversely, clinically undesirable results have also been attributed to the application of stretch including hypertrophic scarring, edema, and scar lengthening and widening [9, 10]. The observation that both positive and negative outcomes can result from altering the mechanical environment during healing is a troubling clinical dilemma [9]. Designing a treatment regimen that would result in superior mechanical properties without detrimental side effects requires a more thorough understanding of mechanobiology and the mechanisms underlying wound remodeling.

To investigate cell-mediated remodeling and wound contraction in a controlled mechano-chemical environment, *in vitro* three-dimensional wound healing models such as cell-populated collagen and fibrin gels have been utilized extensively [11, 12]. In these systems, uniaxial cyclic stretch stimulates the synthesis and crosslinking of collagen while increasing the matrix density, fiber alignment, stiffness, and tensile strength in the direction of stretch [13-18]. Whereas linear or circumferential alignment may be beneficial in tissue substitutes for such applications as tendons and blood vessels, uniaxial alignment does not accurately model the fiber architecture of planar tissues such as skin, pericardium, and heart valves. Furthermore, this alignment confounds the study of more subtle but important remodeling mechanisms such as compaction, crosslinking, and compositional changes of tissue.

Therefore, the aim of the present study is to determine the effects of cyclic stretch on the mechanical, morphological, and biochemical properties of fibroblast-populated fibrin gels. This investigation represents a first step in the investigation of mechanically induced remodeling processes that occur in planar tissues subjected to complex biaxial loading during healing. We hypothesize that cyclic stretch stimulates dermal fibroblasts to increase their synthesis and crosslinking of collagen and to rapidly condense the surrounding matrix. To minimize the confounding effects of in-plane fibril alignment on the mechanics of the matrix, our initial approach utilizes equibiaxial stretch, a technique that has been shown previously to result in a relatively uniform angular distribution of collagen fibers *in vivo* [6]. Cyclic stretch is therefore expected to result in a more compact and stronger tissue, even without the contribution of fiber alignment.

Fibrin gels populated with human dermal fibroblasts were produced based on the methods of Tuan *et al.* [12]. Into each 35 mm diameter flexible-bottom culture well (Flexcell Intl., Hillsborough, NC), 3 mL of solution with a final concentration of 0.2 U/mL thrombin, 3.8 mg/mL fibrinogen and 500,000 cells/mL was added. To resist gel detachment during stretch, the gels were polymerized for 24 hours into fibrous foam anchors (Flexcell) that were affixed to the outer 5 mm of the silicone membrane around the circumference of each well (Fig. 3.1).

3.2. Materials and methods

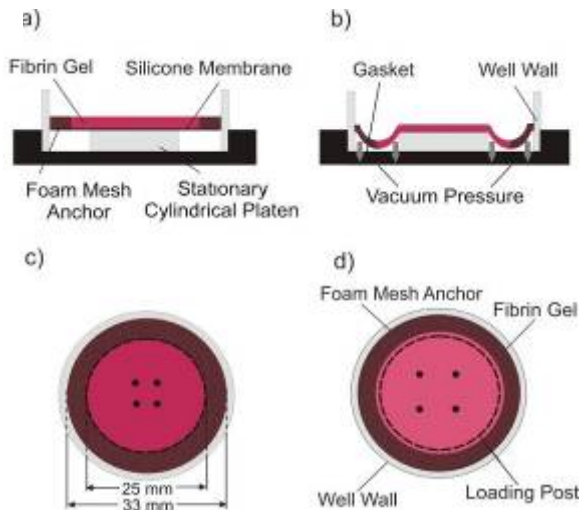


Fig. 3.1. Schematic of the method of stretching the fibroblast-populated fibrin gels (FGs): (a) Unloaded state. (b) Vacuum pressure is applied to the edges of the membrane, resulting in controlled equibiaxial stretch in the center of the rigid loading post. (c) Top view of the circular well showing dimensions of the well and loading post. (d) Top view showing equibiaxial stretch of the FG.

3.2.1. Fabrication of fibrin gels

The gels were cultured at 37° C with humidified 10% CO₂, and the culture medium (DMEM supplemented with 10% fetal bovine serum, 25 g/L L-ascorbate, 0.5 mL/L insulin, 100 units/mL penicillin G sodium, 100 µg/mL streptomycin sulfate, and 250 ng/mL amphotericin B) was changed every other day.

3.2.2. Application of stretch

To apply uniform equibiaxial cyclic stretch to the fibrin gels, a vacuum-driven loading device was utilized (FX-4000T, Flexcell Intl.). The device deformed the central region of the flexible bottom membrane to which the gels were attached by applying vacuum pressure to the membrane edges not supported by the 25 mm diameter cylindrical loading post (Fig. 3.1). The gels were cultured statically (control) or subjected to a sinusoidal waveform from 0% to 16% equibiaxial stretch at a frequency of 0.2 Hz for eight days.

3.2.3. Validation of strain field

The two-dimensional distribution of strain in the center of stretched samples was validated by image analysis (for more detailed information, please see Appendix). Specifically, the surface was texturized by dispersing black sand onto the fibrin gels and sequentially stretching the flexible bottom membranes with vacuum pressure levels that corresponded to 0, 5, 10, 15, and 20% equibiaxial (engineering) strain according to the manufacturer's instructions. At each pressure level, digital images were acquired using a machine vision system (DVT-600, DVT Corporation, Atlanta, GA) with a resolution of 0.067 mm/pixel at the chosen field of view. The components of the two-dimensional deformation field (u_1 and u_2 along the x_1 and x_2 camera axes, respectively) were determined from sequential speckle patterns using a custom phase correlation method (High Density Mapping software). The components of the Green's strains (E_{ij}) at each point on the gel were calculated using the equation:

$$E_{ij} = \frac{1}{2} \left(\frac{du_i}{dx_j} + \frac{du_j}{dx_i} + \sum_{\alpha=1}^2 \frac{du_\alpha}{dx_i} \frac{du_\alpha}{dx_j} \right), \quad (3.1)$$

where i and $j = 1..2$.

In the central 12 mm diameter region used for mechanical analysis, shear strain was negligible, the principal strains were equal ($E_P = E_1 = E_2$), and the strain field was uniform (COV \sim 6%). For consistency with previous studies, the principal stretch ratio, $\lambda = (1 + 2E_P)^{1/2}$ was calculated relative to the zero vacuum pressure reference state, and the equibiaxial engineering strain, $\varepsilon = (\lambda - 1) * 100\%$, was used to describe the strain level imposed on the tissues (e.g., $\varepsilon_{\max} = 16\%$).

3.2.4. Mechanical characterization

The strength of the samples was determined using a custom equibiaxial tissue inflation system described in detail in Billiar *et al.* [19] and in the Appendix. To minimize active cellular retraction prior to testing, the actin-rich cytoskeleton of the fibroblasts was disrupted with 6 μ M cytochalasin D (Sigma, St. Louis, MO) for 4 hours. Following treatment, the central 25 mm

Chapter 3: Equibiaxial cyclic stretch stimulates fibroblasts to rapidly remodel fibrin

section of each fibrin gel was removed from the silicon substrates; samples damaged during this removal process were not characterized mechanically. The thickness of each fibrin gel (n=11 static, n=13 stretched) was measured by placing a small reflective disk onto the sample, allowing the system to reach equilibrium, and recording the height using a laser displacement system (LDS) with $\pm 10 \mu\text{m}$ accuracy. The tension at failure, T (n=8 static, 11 stretched), was determined by the Law of Laplace for a spherical cap:

$$T = \frac{1}{2}PR, \quad (3.2)$$

where P is the burst pressure and R is the radius of curvature. The ultimate tensile strength (UTS) was defined as the tension at failure divided by the undeformed thickness of the fibrin gels. The extensibility, E, was defined as the (equibiaxial) Green's strain at the center of the sample at the failure pressure:

$$E = \frac{1}{2}[(\pi R * \arcsin(a/R))^2 - 1], \quad (3.3)$$

where the radius of the circular clamp, a, was 5 mm.

3.2.5. *Histological analysis*

Tissue samples (n= 2) used for histological evaluation were fixed in buffered formalin for 18-20 hours at 4° C and stored in 70% ethanol. They were then embedded in paraffin, cut into 4 μm sections, stained with hematoxylin and eosin, and examined with a Nikon Eclipse E600 microscope at a magnification of 200X.

3.2.6. *Transmission electron microscopy*

The organization and ultrastructural features of the matrix and cells were observed using transmission electron microscopy (TEM). Samples were fixed in 4% gluteraldehyde in 0.1 M Na cacodylate-HCl buffer (pH 7.2) for 2 hours at 4° C. The fixed samples were washed three times and left overnight in 0.5 M Na cacodylate-HCl buffer (pH 7.2), post-fixed for 1 hr in 1% OsO₄

(w/v), and stained en block for 20 minutes with 1% aqueous uranyl-acetate (w/v). After dehydration, the samples were transferred through two changes of propylene oxide, embedded in a mixture of SPON 812/Araldite 502 epoxy resin, and polymerized overnight at 70° C. The blocks were cut into ultra thin sections and examined on a Philips CM 10 transmission electron microscope (Philips; Eindhoven, Netherlands) at 80 Kv accelerating voltage.

3.2.7. Matrix alignment analysis

The in-plane alignment of the matrix was determined for a subset of samples (n=2) from each group by analyzing the birefringence of the matrix. Samples were placed between perpendicular linear polarization plates and rotated 180° in 15° increments, and the overall intensity and pattern of birefringence were measured.

3.2.8. Density, cell number and viability, and collagen content determination

The density of each sample was calculated by dividing its dry weight by its wet volume. Wet volume was determined by multiplying the thickness (measured using the LDS) by the area of each sample. The collagen content of a subset of samples (n = 6 from each group) was determined using the hydroxyproline assay first described by Woessner [20] assuming a conversion factor of 0.13 grams of hydroxyproline per gram of collagen [21]. The total amount of collagen was divided by the wet volume of each sample to obtain the collagen density. Cell number and viability were determined by enzymatic digestion of the fibrin gels with 0.05% trypsin and 2 mg/mL type 1 collagenase for 30 minutes. Samples were then mixed with trypan blue and the numbers of live and dead cells were quantified using a hemocytometer.

3.2.9. Inhibition of crosslinking

To determine the contribution of collagen crosslinking to the strength of the fibrin gels, beta-aminopropionitrile (BAPN, MP Biomedicals, Aurora, Ohio), a known inhibitor of lysyl oxidase-mediated collagen crosslinking, was added to the tissue-culture media at a concentration 1.0 mM every other day in selected groups of static and dynamically cultured samples.

3.2.10. Statistical analysis

Data are presented as mean \pm standard deviation in the tables. Control and treatment groups were compared using Student's *t*-tests with a level of $p < 0.05$ considered statistically significant. han stretched fibrin gels with cell-mediated compaction).

3.3. Results

3.3.1. Cyclic stretch increases tissue compaction and matrix density

From gross observation and qualitative handling, the stretched fibrin gels appeared thinner, less transparent, stronger, and stiffer than the static controls. Histological analysis revealed corresponding changes in the organization of the tissues at the microscopic level including a pronounced decrease in thickness and an increase in cell and matrix density in the stretched samples (Fig. 3.2). The stretched fibrin gels compacted to 3.4% of the original cast volume, approximately 14% of the thickness of the static controls, and were approximately ten times denser than the controls (Table 3.1). Cyclic stretch also passively compacted acellular fibrin gels cycled to 16% stretch resulting in an 86.8% reduction in thickness to $410 \pm 63 \mu\text{m}$ (approximately three times thicker than controls).

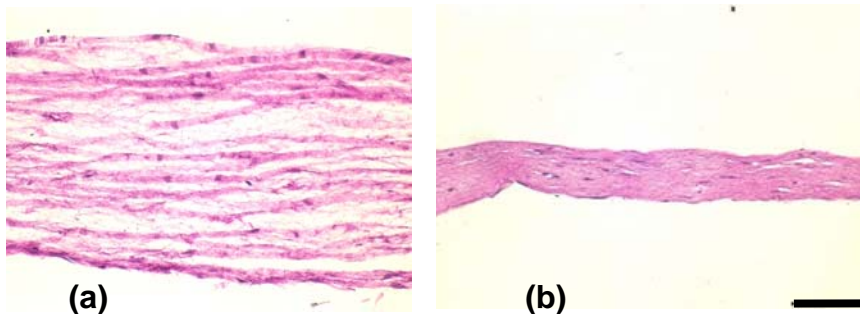


Fig. 3.2. Brightfield images of hematoxylin and eosin (H&E) stained sections of FGs after eight days of a) static culture and b) 16% cyclic stretch (original magnification 200X, scale bar = 100 μm). Stretch induced the fibroblasts to further compact the gels, resulting in a substantially denser matrix.

3.3.2. *Cyclic stretch increases tissue strength relative to static controls*

The UTS was ten times greater for stretched samples relative to controls due to a 30% increase in tension at failure combined with the aforementioned decrease in thickness. Extensibility was slightly lower in stretched fibrin gels than static controls but not statistically different.

Paralleling the strength data, the total collagen content was 15% greater in the stretched samples, resulting in a seven-fold increase in collagen density with stretch. No significant differences in cell number or viability were observed between the stretched fibrin gels and their respective static controls.

Table 3.1. Physical and biochemical properties of fibroblast-populated fibrin gels statically cultured or cyclically stretched (16% stretch, 0.2 Hz) for 8 days of culture. Triplicate samples were tested in each of the two experiments.

Group	Thickness (μm)	Density (g/cm ³)	Compaction (%)	UTS (kPa)	Failure Tension (N/m)	Extensibility	Collagen (μg)	Collagen Density (μg/cm ³)	Cell Number
Static	764 ± 129	0.03 ± 0.01	96.6 ± 0.31	12.9 ± 4	9.8 ± 2.69	2.02 ± 0.85	44.36 ± 5.59	132.9 ± 29	4.3*10 ⁶ ± 2.6*10 ⁵
Stretched	106 ± 25*	0.29 ± 0.11*	77.0 ± 1.37	119.2 ± 23*	13.1 ± 1.11*	1.56 ± 0.33	50.29 ± 6.16*	1047.3 ± 295*	4.5*10 ⁶ ± 2.2*10 ⁵

* Statistical difference between static and stretched groups ($p < 0.05$)

3.3.3. *Cyclic stretch changes cell morphology*

Transmission electron micrographs reveal a much denser, more organized arrangement of matrix fibrils in stretched samples than in controls (Fig. 3.3). Aggregates of fibrin bundles appear to be forming in the stretched fibrin gels, yet there was no significant difference between the fibril diameters in the stretched and static groups ($0.11 \pm 0.02 \mu\text{m}$ vs. $0.12 \pm 0.03 \mu\text{m}$). Compared to cells in static gels, fibroblasts in stretched fibrin gels appear to have a greater number of ribosomes, larger nuclei, and a greater amount of highly branched rough endoplasmic reticulum (arrows in Fig. 3.3). In the electron micrographs, neither collagen nor fibrin fibrils appear to be oriented in a predominant direction within the fibrin gels. En face examination under polarized

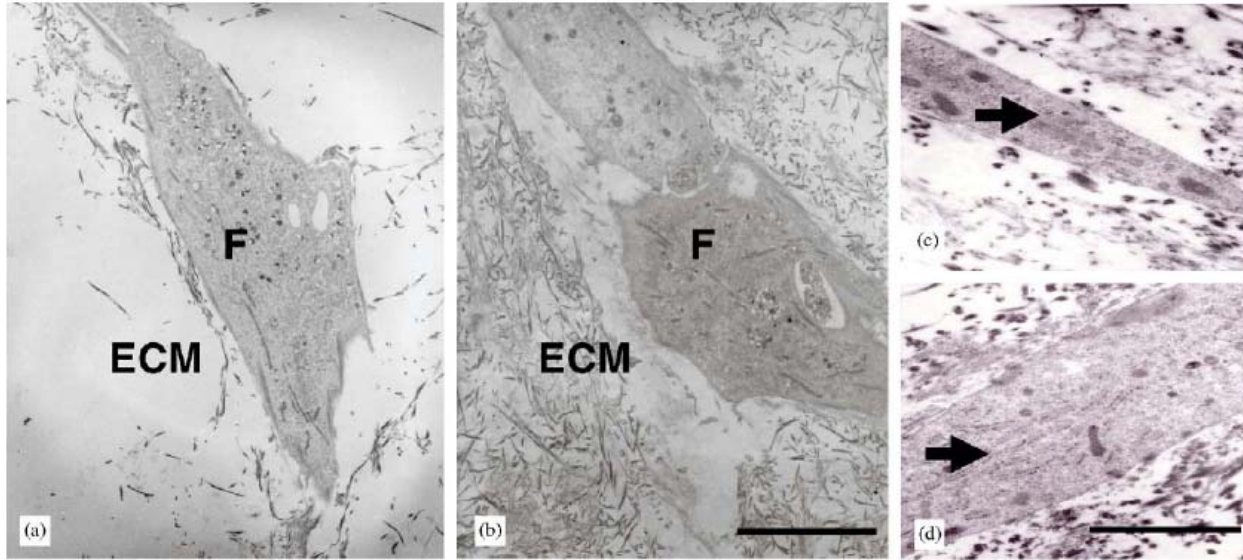


Fig. 3.3. TEM images of fibroblasts (F) and extracellular matrix (ECM) in static (a & c) and stretched FGs (b & d). Low magnification en face images show the increase in matrix density with stretch and collagen fibrils forming at the cell surface (a & b, original magnification 6,100X, scale bar = 10 μm). Extensive rough endoplasmic reticulum (ER) visible in high magnification transsection images (arrowheads) indicates a highly synthetic cell phenotype in both static and stretched gels, although widespread branching of the ER was only observed in the stretched gels (c & d, original magnification 43,400X, scale bar = 2 μm).

light further confirms the lack of in-plane alignment of the fibrils in the gels as the intensity and pattern of birefringence did not change with rotation of the sample between crossed-polarizers.

3.3.4. Collagen crosslinking impacts tissue compaction, UTS, and extensibility

Blocking of collagen crosslinking by BAPN reduced the compaction of stretched gels two-fold but produced no significant changes to the static gels (Table 3.2). The UTS of stretched samples decreased two-fold corresponding to their two-fold larger thickness relative to the non BAPN-treated samples; however, the tension at failure of the BAPN-treated and untreated groups was not significantly different. BAPN treatment significantly increased the extension at failure of the stretched gels.

Table 3.2. Effect of BAPN on the mechanical and biochemical properties of statically-cultured and cyclically-stretched (16% stretch, 0.2 Hz) fibroblast-populated fibrin gels after 8 days of culture.

Group	Thickness	UTS	Failure Tension	Extensibility
Static + BAPN/Static	0.96 ± 0.09	1.09 ± 0.16	0.99 ± 0.09	0.99 ± 0.23
Stretched + BAPN/Stretched	2.02 ± 0.49*	0.49 ± 0.11*	1.03 ± 0.01	1.44 ± 0.24

In order to highlight the effects of crosslinking, the BAPN-treated data were normalized to untreated data; all statistical analyses were performed on non-normalized raw data. Triplicate samples were tested in each of the two experiments.

* *Statistical difference between BAPN -treated and untreated groups ($p < 0.05$)*

3.4. Discussion

In this study, the influence of cyclic stretch on early-stage dermal wound remodeling was investigated by applying equibiaxial stretch to a model tissue *in vitro*. This novel methodology eliminates the overwhelming mechanical alterations that accompany fiber alignment in uniaxial systems and allows the study of more subtle strengthening mechanisms. Using this system, we were able to demonstrate that cyclic stretch stimulates fibroblasts to produce a stronger matrix by dramatically increasing compaction, matrix fiber reorganization, and collagen content without inducing in-plane fiber alignment.

3.4.1. Cyclic stretch increases cell-mediated and passive compaction

The most profound change we observed was the increase in compaction of the matrix with stretch. After only eight days in culture, stretched fibrin gels compacted nearly one hundred-fold to approximately one quarter of the density of native dermis (1.2 g/cm^3) [22]. Mechanically induced compaction has also been observed in uniaxially stretched fibrin and collagen gels, but it was far less pronounced than reported herein [14, 23]. Although the mechanism of stretch-induced compaction has not been elucidated, compaction may be enhanced by an increase in fibrin degradation as a result of increased matrix metalloprotease production [24]. Interestingly, the acellular gels also compacted substantially, indicating that much of the enhanced compaction upon stretch may be passive. Fibrin is an adhesive molecule and when condensed could form intermolecular bonds and stretch-induced entanglements. These data clearly demonstrate that the application of cyclic equibiaxial stretch alone is a powerful stimulus of matrix compaction.

3.4.2. Stretch does not modify cell number or viability

No significant differences in cell number or viability were observed between the stretched and static groups indicating that stretch increases the remodeling activity of the cells rather than their mitogenic activity. However, we cannot say with certitude that stretch did not alter cell proliferation in our study, as a change in cell proliferation in our system may have been balanced with a concomitant change in apoptosis.

3.4.3. Cyclic stretch induces cell-mediated strengthening of fibrin gels

Investigators that have applied uniaxial stretch to collagen and fibrin gels have observed substantial increases in tensile strength similar to those observed in our study [14, 23, 25]. Increased compaction (and thus decreased thickness), fibril alignment, enhanced entanglement of the fibrils, intermolecular cell-fibril and fibril-fibril bonding, and bundling of the fibrils are all hypothesized to contribute substantially to the increase in tensile strength of the model tissues exposed to mechanical stimulation [1, 14, 17, 23].

To account for the apparent increase in strength simply due to dividing by the smaller thickness of highly compacted samples, we also calculated failure tension (force/width). Our analysis indicates that while the majority of the ten-fold increase in UTS is due to a decrease in thickness, the stretched samples are still able to withstand significantly higher tension than statically cultured samples. As verified by histological and polarized light examination as well as TEM, there is no measurable in-plane alignment in the equibiaxially stretched fibrin gels, thus alignment does not appear to be the mechanism of strengthening. Furthermore, the average fibrin fibril diameter was similar to values found previously in polymerized gels [26] and was not altered by stretch. Thus, more subtle strengthening mechanisms such as collagen synthesis and crosslinking appear to contribute significantly to the increased strength of the mechanically stretched gels.

Chapter 3: Equibiaxial cyclic stretch stimulates fibroblasts to rapidly remodel fibrin

The total amount of collagen in the gels was low (<1% of the dry weight of the matrix) as expected for the short experimental duration in our study. The small level of collagen accumulation may also be due to attenuation of fibroblast collagen production by fibrin [27] and increased levels of collagenase production induced by stretch [13, 24, 28]. Nevertheless, the increase in collagen with stretch was statistically significant, highly correlated with matrix strength, and inversely correlated to matrix extensibility, indicating that collagen plays a role in the matrix mechanics. This finding is predicted by a simple composite model of a stiff network of collagen within a compliant fibrin matrix, and confirms that even a very small volume fraction of collagen has the potential to impact tissue stiffness profoundly. For example, a volume fraction of only 1% collagen (stiffness~25 kPa based on acellular collagen gels [29]) would increase the stiffness of a 3.4 mg/mL fibrin-only matrix from 750 Pa [30] to almost 1000 Pa.

Collagen crosslinking may also increase with stretch due to direct cellular stimulation or indirectly due to increased proximity of the cells and fibrils to each other with stretch-induced compaction [23]. Indeed, when lysyl oxidase-mediated collagen crosslinking was blocked with BAPN, the UTS of the stretched gels decreased two-fold. However, this drop in strength appears to be due to less pronounced compaction rather than a decrease in failure tension. The extensibility was also significantly increased with BAPN treatment in stretched groups. Interestingly, these crosslink-dependent changes did not occur in statically cultured fibrin gels.

3.4.4. Conclusions

The application of cyclic biaxial stretch is a promising approach for improving the quality of wound healing as well as for engineering functional tissue equivalents for the repair or replacement of diseased tissues. The goal now is to determine the optimal percentage, rate, duration, and/or direction of stretch that would produce superior mechanical and biochemical properties for each particular application.

3.4.5. Acknowledgements

The authors would like to thank Dr. Glenn Gaudette at the University of Massachusetts Medical School for the generous use of his extended phase image correlation software and Greg Hendricks for his electron microscopy expertise. We would also like to Danielle Dufour, Vanessa Lopez, Maria Mavromatis, and Jacquelyn Youssef for their technical assistance. This work was supported by Whitaker Research Grant 02-073 to KLB.

3.5. References

- [1] Clark, R. A. F., 1996, *The molecular and cellular biology of wound repair*, Plenum Press, New York.
- [2] Linares, H. A., 1996, "From wound to scar," *Burns*, 22(5), pp. 339-352.
- [3] Tomasek, J. J., Haaksma, C. J., Eddy, R. J., and Vaughan, M. B., 1992, "Fibroblast contraction occurs on release of tension in attached collagen lattices: dependency on an organized actin cytoskeleton and serum," *Anatomical Record*, 232(3), pp. 359-368.
- [4] Hardy, M. A., 1989, "The biology of scar formation," *Physical Therapy*, 69(12), pp. 1014-1024.
- [5] Brunius, U., Zederfeldt, B., and Ahren, C., 1967, "Healing of skin incisions closed by non-suture technique. A tensiometric and histologic study in the rat," *Acta Chir Scand*, 133(7), pp. 509-516.
- [6] Langrana, N. A., Alexander, H., Strauchler, I., Mehta, A., and Ricci, J., 1983, "Effect of mechanical load in wound healing," *Annals of Plastic Surgery*, 10(3), pp. 200-208.
- [7] Sussman, M. D., 1966, "Effect of increased tissue traction upon tensile strength of cutaneous incisions in rats," *Proceedings of the Society for Experimental Biology and Medicine*, 123(1), pp. 38-41.
- [8] Thorngate, S., and Ferguson, D. J., 1958, "Effect of tension on healing of aponeurotic wounds," *Surgery*, 44(4), pp. 619-624.
- [9] Arem, A. J., and Madden, J. W., 1976, "Effects of stress on healing wounds: I. Intermittent noncyclical tension," *Journal of Surgical Research*, 20(2), pp. 93-102.
- [10] Sommerlad, B. C., and Creasey, J. M., 1978, "The stretched scar: a clinical and histological study," *British Journal of Plastic Surgery*, 31(1), pp. 34-45.
- [11] Grinnell, F., 2000, "Fibroblast-collagen-matrix contraction: growth-factor signalling and mechanical loading," *Trends in Cell Biology*, 10(9), pp. 362-365.
- [12] Tuan, T. L., Song, A., Chang, S., Younai, S., and Nimni, M. E., 1996, "In vitro fibroplasia: matrix contraction, cell growth, and collagen production of fibroblasts cultured in fibrin gels," *Experimental Cell Research*, 223(1), pp. 127-134.
- [13] Altman, G. H., Horan, R. L., Martin, I., Farhadi, J., Stark, P. R., Volloch, V., Richmond, J. C., Vunjak-Novakovic, G., and Kaplan, D. L., 2002, "Cell differentiation by mechanical stress," *FASEB J*, 16(2).
- [14] Cummings, C. L., Gawlitta, D., Nerem, R. M., and Stegeman, J. P., 2004, "Properties of engineered vascular constructs made from collagen, fibrin, and collagen-fibrin mixtures," *Biomaterials*, 25(17), pp. 3699-3706.

- [15] Grenier, G., Remy-Zolghadri, M., Larouche, D., Gauvin, R., Baker, K., Bergeron, F., Dupuis, D., Langelier, E., Rancourt, D., Auger, F. A., and Germain, L., 2005, "Tissue reorganization in response to mechanical load increases functionality," *Tissue Engineering*, 11(1-2), pp. 90-100.
- [16] Isenberg, B. C., and Tranquillo, R. T., 2003, "Long-term cyclic distention enhances the mechanical properties of collagen-based media-equivalents," *Annals of Biomedical Engineering*, 31(8), pp. 937-949.
- [17] Seliktar, D., Black, R. A., Vito, R. P., and Nerem, R. M., 2000, "Dynamic mechanical conditioning of collagen-gel blood vessel constructs induces remodeling in vitro," *Annals of Biomedical Engineering*, 28(4), pp. 351-362.
- [18] Yang, G., Crawford, R. C., and Wang, J. H., 2004, "Proliferation and collagen production of human patellar tendon fibroblasts in response to cyclic uniaxial stretching in serum-free conditions," *Journal of Biomechanics*, 37(10), pp. 1543-1550.
- [19] Billiar, K. L., Throm, A. M., and Frey, M. T., 2005, "Biaxial failure properties of planar living tissue equivalents," *Journal of Biomedical Materials Research A*, 73A(2), pp. 182-191.
- [20] Woessner, J. F., Jr., 1961, "The determination of hydroxyproline in tissue and protein samples containing small proportions of this imino acid," *Archives of Biochemistry and Biophysics*, 93, pp. 440-447.
- [21] Eastoe, J. E., 1955, "The amino acid composition of mammalian collagen and gelatin," *Biochemical Journal*, 61(4), pp. 589-600.
- [22] Torvi, D. A., and Dale, J. D., 1994, "A finite element model of skin subjected to a flash fire," *Journal of Biomechanical Engineering*, 116(3), pp. 250-255.
- [23] Seliktar, D., Nerem, R. M., and Galis, Z. S., 2001, "The role of matrix metalloproteinase-2 in the remodeling of cell-seeded vascular constructs subjected to cyclic strain," *Annals of Biomedical Engineering*, 29(11), pp. 923-934.
- [24] Seliktar, D., Nerem, R. M., and Galis, Z. S., 2003, "Mechanical strain-stimulated remodeling of tissue-engineered blood vessel constructs," *Tissue Engineering*, 9(4), pp. 657-666.
- [25] Neidert, M. R., Wille, J. J., and Tranquillo, R. T., 2002, "Development and characterization of improved tissue engineered valve-equivalents using chemical and mechanical signaling," *Proceedings of the Second Joint EMBS/BMES Conference, IEEE, Houston, TX*, pp. 858-859.
- [26] Ferri, F., Greco, M., Giuseppe, A., Spirito, M., and Rocco, M., 2002, "Structure of fibrin gels studied by elastic light scattering techniques: Dependence of fractal dimension, gel crossover length, fiber diameter, and fiber density on monomer concentration," *Physica Review E*, 66, pp. 011913-011911,-011913-011913.
- [27] Clark, R. A., Nielsen, L. D., Welch, M. P., and McPherson, J. M., 1995, "Collagen matrices attenuate the collagen-synthetic response of cultured fibroblasts to TGF-beta," *Journal of Cell Science*, 108(Pt 3), pp. 1251-1261.
- [28] Prajapati, R. T., Chavally-Mis, B., Herbage, D., Eastwood, M., and Brown, R. A., 2000, "Mechanical loading regulates protease production by fibroblasts in three-dimensional collagen substrates," *Wound Repair Regen*, 8(3), pp. 226-237.
- [29] Roeder, B., Kokini, K., Sturgis, J., Robinson, P. J., and Voytik-Harbin, S., 2002, "Tensile mechanical properties of three-dimensional type 1 collagen extracellular matrices with varied microstructure," *Journal of Biomechanical Engineering*, 124.

Chapter 3: Equibiaxial cyclic stretch stimulates fibroblasts to rapidly remodel fibrin

- [30] Carr, M. E., and Carr, S. L., 1995, "Fibrin structure and concentration alter clot elastic modulus but do not alter platelet mediated force development," *Blood coagulation and fibrinolysis*, 6, pp. 79-86.

CHAPTER 4

Magnitude and duration of stretch modulate fibroblast remodeling of fibrin gels

(Balestrini, J. L. and Billiar, K. L. 2009.. J Biomech Eng 131, 051005, reprinted with permission)

4.1. Introduction

Cells within skin and other connective tissues are continuously subjected to a range of mechanical forces from external loading and cell-generated tension. These mechanical cues guide fibroblast-mediated tissue remodeling and ultimately regulate the structure of a stable and well-structured extracellular matrix (ECM) optimized to resist these loads [1]. When the ECM is disrupted due to injury, the loads applied to the cells are substantially altered which, in turn, leads to an increase in cell-generated forces and remodeling of the tissue architecture. The increase in cell-generated tension results in alignment of the collagen-rich ECM along these lines of tension, creating scar tissue with lower strength, compliance, and capacity to withstand multiaxial loads as compared to normal tissue. In addition, this increase in cell-generated force creates the potential for contracture and deformity [2].

Stretching wounds during healing (e.g., range of motion exercises, splinting, vacuum pressure) is used routinely by clinicians to attain improved tissue properties and manipulate healing rates and may aid in obtaining a stable bond between the skin and percutaneous devices [2-4]. In experimental models, the use of mechanical stimulation during wound healing has been shown to increase collagen production and decrease contracture of granulation tissue [5]. Alternatively, increased loading of the dermis is also associated with negative effects such as excessive collagen production and contracture, common processes found in many fibrocontractive diseases [6-8]. Clearly, determining loading regimens that promote the desired aspects of healing without stimulating detrimental side effects would be of obvious benefit.

Similar to observations *in vivo*, researchers have demonstrated that mechanical conditioning tissue models *in vitro* results in stronger, stiffer tissue as compared to statically cultured controls [8-15]. The most common three-dimensional (3D) tissue models utilized for mechanobiological studies are cell-populated collagen and fibrin gels [16]. Collagen gels have been extensively utilized as tissue models to investigate the interplay between tissue mechanics, cell-matrix interactions, and mechanobiology in a controlled *in vitro* manner as they allow for precise control over culture conditions, specimen composition, and boundary conditions [14, 17-19]. These connective tissue analogs form the dermal component of clinically-available tissue engineered skin replacements, yet they lack sufficient mechanical integrity and durability for clinical usage in load-bearing applications [20]. Fibrin gels were initially developed to model the early stages of connective tissue healing (fibroplasia) for mechanobiological studies, recently these constructs have emerged for use as tissue engineering scaffolds. Fibrin gels are initially very weak but, unlike collagen gels, do not inhibit ECM production and achieve tissue-like strength following sufficient synthesis and assembly of collagen [9, 20-25]. These systems therefore have a strong potential for use as tissue replacements in wound healing therapy and regenerative medicine and for restoring functionality to damaged or diseased tissue [21, 24, 26]. Although much has been learned about the mechanisms of strain-dependent remodeling by utilizing collagen and fibrin gels [10, 25, 27], the combinations of strain levels, ranges, and durations utilized thus far are not sufficient to characterize the complex relationships between mechanical loading parameters (magnitude, duration, etc.) and remodeling parameters (strength, stiffness, alignment, etc.). Quantitative dose-response curves would aid in the rational design of therapies and would assist in the understanding and prevention of scarring.

The goal of this investigation is to quantitatively study the relationship between stretch magnitude and duration on the changes in matrix mechanics and composition in a 3D planar model of wound healing. The present work follows a previous study where we observed that cyclic equibiaxial stretch at 16% for 24 hours per day dramatically increases the collagen content and tissue strength of fibroblast-populated fibrin gels [13]. In this study, these tissue models are cycled as little as 2% and as much as 16% equibiaxially for 6 or 24 hours per day. We hypothesize that the extent of matrix remodeling increases proportionally with the magnitude of stretch and the number of hours of stretch per day. This work will extend our knowledge of how

mechanical cues can be used to manipulate key properties of healing wounds and also contribute valuable information for the creation of custom tailored tissue equivalents based on cell-populated fibrin gels.

4.2. Materials and Methods

4.2.1. *Fabrication of fibrin gels*

Fibroblast-populated fibrin gels were produced as previously described [13]. Briefly, bovine fibrinogen and thrombin (Sigma, St. Louis, MO) were combined with passage 7-9 human foreskin fibroblasts (American Type Culture Collection, Manassas, VA) in Dulbecco's Modified Eagle Medium (DMEM, Mediatech, Herndon, VA) supplemented with 10% bovine calf serum, (BCS, HyClone, Logan, UT), 100 units/mL penicillin G sodium, 100 µg/mL streptomycin sulfate, and 250 ng/mL amphotericin B (Gibco, Grand Island, NY). The final concentrations of the constituents were 0.2 U/mL thrombin, 3.8 mg/mL fibrinogen (Sigma, St. Louis, MO), and 500,000 cells/mL. The fibrin and cell solution (3 mL) was poured into six 35 mm diameter untreated flexible-bottom culture wells with circular fibrous foam anchors (Flexcell Intl., Hillsborough, NC) and allowed to polymerize for 24 hours prior to mechanical stimulation. The gels were cultured at 37° C with humidified 10% CO₂. DMEM supplemented with 10% fetal bovine serum (FBS, Hyclone), 25 g/L L-ascorbate (Wako, Richmond, VA), 0.5 mL/L insulin (Sigma), 100 units/mL penicillin G sodium, 100 µg/mL streptomycin sulfate, and 250 ng/mL amphotericin B (Gibco) was changed every other day.

4.2.2. *Application of stretch*

A vacuum-driven loading device (FX-4000T, Flexcell Intl.) was utilized to apply uniform equibiaxial cyclic stretch to the fibrin gels as previously described [13]. The gels were cultured statically (control), or subjected to either continuous stretch (24 hr/day) or intermittent stretch (6 hr/day) with a sinusoidal waveform at 2, 4, 8 or 16% equibiaxial stretch at a frequency of 0.2 Hz for eight days. One limitation of the standard Flexcell system is that only one magnitude of stretch can be attained at any given time. Therefore, in the continuously stretched group there is

an individual set of parallel controls for each treatment group (i.e., each stretch magnitude); data from samples in the continuously stretched groups were normalized with respect to the parallel statically-cultured controls. At the conclusion of each experiment, samples were processed for biochemical, histological, or mechanical testing as described below.

To apply intermittent stretch, gels were cyclically stretched for 6 hours per day. The 6-well plates were then removed from the stretch device and cultured statically for the remaining 18 hours of each day for eight days. The same stretch magnitudes and frequency were used for the intermittently stretched fibrin gels as the continuously stretched gels. At the conclusion of each experiment, the gels were characterized identically to the continuously stretched gels (see below). In addition, sub-failure biaxial testing was performed on a subset of the samples from this group as described in the “Low force biaxial mechanical characterization” section. Since each of the four groups is cultured only six hours each day, all four magnitudes were performed in parallel with one statically-cultured control group.

4.2.3. Determination of cell number and total collagen content

Cell number was determined by liberating the cells from the inner 25 mm diameter area of the fibrin gels by treating the gels with 0.05% trypsin (Gibco) and 2 mg/mL type 1 collagenase (Sigma) for 30 min at 37°C. Samples (refer to Tables 2 and 3 for sample sizes) were stained with trypan blue and the cell number was quantified using a hemocytometer. Collagen content was quantified by the hydroxyproline assay [28]. The amount of collagen was estimated using a conversion of 0.13 grams of hydroxyproline per gram of collagen [29], and the accuracy of each assay was verified with a 1 mg/mL collagen standard (Sircol, Biocolor, Westbury, NY). Collagen density was quantified as the dry weight of collagen per volume of each gel, as determined by multiplying measured thickness (described below) by the area of inner 25 mm diameter section removed from the anchors for analysis.

4.2.4. *Determination of physical properties*

The thickness, ultimate tensile strength (UTS), failure tension, and extensibility of the samples were calculated as described in detail previously [13] and outlined briefly below. To eliminate active tissue retraction prior to testing, the actin-rich cytoskeletons of the fibroblasts were depolymerized by treating the all of the samples with 6 μ M cytochalasin D (Sigma) for four hours. Following cytochalasin D treatment, the central 25 mm section of each fibrin gel was cut from the anchors and carefully lifted from the flexible bottom membranes.

To perform a compaction assay, a standard method to measure the capacity of fibroblasts to remodel ECM components [30], sample thickness was quantified by placing a small reflective disk (1.3g, 13 mm diameter) onto the centermost region of the sample and allowing the tissue to reach equilibrium. The height was recorded using a laser displacement system, or LDS ($\pm 10 \mu$ m, LK-081, Keyence, Woodcliff Lake, NJ). Using a custom equibiaxial tissue inflation system [31], the tissue sample was circularly clamped and the centermost 5 mm section was inflated with isotonic room temperature saline until burst. The displacement was measured in the center of the sample by the LDS, and pressure during inflation was measured by a pressure transducer (± 0.13 kPa). The radius of curvature at failure, R , was determined from the sample height assuming a spherical cap geometry (validated in Billiar *et al.* [31]). The tension at failure, T , was then determined using the Law of Laplace, $T = \frac{1}{2}PR$, where P is the burst pressure. The UTS was defined as the tension at failure divided by the undeformed thickness of the fibrin gel (as measured by the LDS). The extensibility was defined as the (equibiaxial) Green's strain at the center of the sample at the failure pressure as defined in [32]. The sample numbers for each treatment group are given in Tables 2 and 3.

4.2.5. *Low-force biaxial mechanical characterization*

To investigate the effects of stretch magnitude on matrix stiffness, the Young's modulus of a subset of the intermittently stretched fibrin gels was determined using planar biaxial testing. Samples were removed from their silicone substrates and the thickness was measured with the LDS (as described above). To ensure the stiffness measurements would not be affected by the foam anchor, the anchor was cut radially into 20 equal sections from the fibrin-foam anchor

interface to the outer edge of the anchor. To attach the sample to the device, sixteen stainless steel hooks (four on each “side” of the sample) were attached to the fibrous foam anchor sections surrounding each sample; the four “corner” segments were not utilized as indicated by blank spaces around the edge of the sample in Figure 1. The sample was placed in a temperature-controlled, isotonic saline-filled bath (maintained at 37° C), and the hooks were attached with nylon suture to a dual pulley system which distributes equal force to each of the four hooks on each side of the sample. Each pulley system was attached to an actuator by a 7.6 cm plexiglass arm extending out of the bath either directly or via a torque transducer (0.15 N-m, Futek) which was used to measure force with ± 4 mN accuracy. Small styrofoam floats were placed at the base of each hook to maintain buoyancy of the sample.

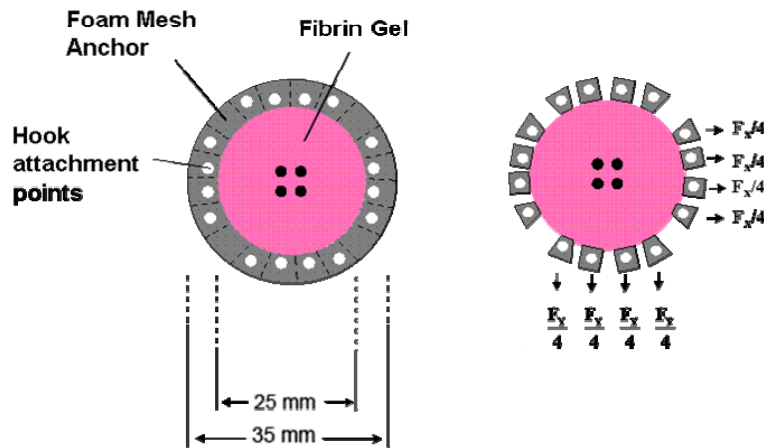


Fig 4.1. Schematics representing A) fibrin gel with foam anchor attached prior to and B) after loading onto the biaxial device. The dotted lines represent areas to be sectioned, and the holes represent areas the hooks will be placed. The four arrows in the x and y axis represent force at each of the tethering points. Note that the force is distributed equally at each loading point.

The actuators were drawn apart until the sample was restored to the original outer dimensions, and four small marker chips were affixed on the central region of the sample to form a 7 mm square region. Digital images were acquired using an analog video camera (XC-ST50, Sony) and an image acquisition board (PCI-1405, National Instruments, Austin, TX), and a custom video marker-tracking algorithm was used to track the markers. A sub-region was automatically positioned on each marker, and displacements were calculated using Labview (National Instruments). Each specimen was preconditioned with ten cycles to 10% equibiaxial engineering strain quasistatically at a strain rate of 0.01 s^{-1} . Engineering stress was calculated by dividing the force by the cross-sectional area of the tissue. The cross-sectional area of the tissue was measured by multiplying the sample width (the distance between the hooks, or 25 mm) by the tissue thickness. The Young’s modulus for each sample was determined by fitting data from the final equibiaxial protocol to the equation for a homogeneous linear elastic solid using MATLAB

(Mathworks, Inc., Natick, MA) software. The structural stiffness was calculated by multiplying the Young's modulus by the thickness of the sample.

4.2.6. Retraction assay

After the total culture period of 9 days, a subset of fibrin gels from each group was gently released from their wells and placed in a 35 mm Petri dish filled with warm culture media. The tissues are permitted to freely and rapidly retract within the petri dish, allowing for measurement of both the passive prestrain of the matrix (due to fibroblast pretension), and the active recontractile capacity of the cells (Figure 4). Digital images were acquired at 0, 1, 2, 3, 4, 5, 10, 15, 20, 25, and 30 minutes following release using a Flour-S MultiImager system (Biorad, Hercules, CA) and analyzed for gel area, A , as a function of time post-release. Total percent retraction ($R_T = (1-A/A_0) * 100\%$) was calculated at each time point. In order to determine the active retraction, R_A , passive retraction, R_o , and time constant of retraction, τ , the total retraction as a function of time, t , was fit to the equation:

$$R_T = R_A(1 - e^{-\frac{t}{\tau}}) + R_o. \quad (4.1)$$

The optimal parameter values (R_A , R_o , τ) were determined using MATLAB (Mathworks, INC.) by minimization of least squares error.

To ensure that our calculated value of the intercept, R_o , represents an accurate measurement of the passive component of the total retraction, a separate subset of samples was treated with 6 μ M cytochalasin D (for four hours), allowed to retract, and the resulting percent retraction compared to the calculated value of R_o (data not shown). As passive retraction is not a common engineering metric for remodeling, we also calculate the residual strain, or effective prestrain, in the matrix using the following equation:

$$\epsilon_{pre} = \frac{(d_f - d_i)}{d_i} \quad (4.2)$$

where the initial diameter (d_i) is defined as the dimension following release of prestress (calculated from the fit parameter R_0 above), and the final diameter ($d_f = 25$ mm) is defined as the diameter of the sample when attached to the anchor (with residual stress).

4.2.7. *Histological analysis*

Representative samples from each group were fixed in buffered formalin while still attached to the anchors for 18-20 hours at 4° C and stored in 70% ethanol for histological evaluation. The samples were then removed from their anchors and silicone membranes, embedded in paraffin, cut into 4 μ m sections, and then stained with hematoxylin and eosin (H&E). Micrographs were taken with a Nikon Eclipse E600 camera at a magnification of 200X.

4.2.8. *Statistical and regression analysis*

Data are presented as mean \pm standard deviation. For each treatment group, all remodeling metrics were normalized to the respective statically cultured control groups. To determine trends in remodeling metrics, the normalized data were first analyzed using a two-way ANOVA (SigmaStat, Systat Inc., San Jose, CA) to isolate factors with statistically significant effects and power. The factors analyzed in the ANOVA were stretch magnitude (M), duration of stretch per day (set to 0 for 24 hr/day and 1 for 6 hr/day), and the interaction term (I) between these factors (defined as the magnitude factor times the duration factor). If factors were found to have sufficient statistical significance ($p < 0.05$) and power (≥ 0.8) in the ANOVA, they were further analyzed for trends using regression analysis (SAS Institute Inc., Cary, NC). The coefficient of determination (R^2) and the root mean squared error (RMS) were used to assess the goodness of fit to the models.

4.3. Results

4.3.1. Effect of stretch on compaction

After nine days in culture, the fibroblasts rapidly condensed and reorganized the fibrin matrix in all groups as seen in the histomicrographs (Figure 2). By gross observation all gels appeared relatively uniform in thickness across the membrane (including the fibrin-anchor interface), and all cycled gels appeared less transparent and less hydrated than their statically cultured controls. Based on thickness measurements, both continuously stretched and intermittently stretched gels compacted in a dose-dependent manner with increasing stretch magnitude; although, the trends of compaction did differ slightly between these groups. In combination, compaction was linearly correlated to stretch magnitude with no significant correlation to the rest period or interactive term. Table 4.1 provides the regression models for compaction and other remodeling parameters as a function of all stretch factors, and Tables 4.2 and 4.3 list the raw data for each treatment group. Figure 3 represents these data graphically along with biochemical and mechanical data described in subsequent sections.

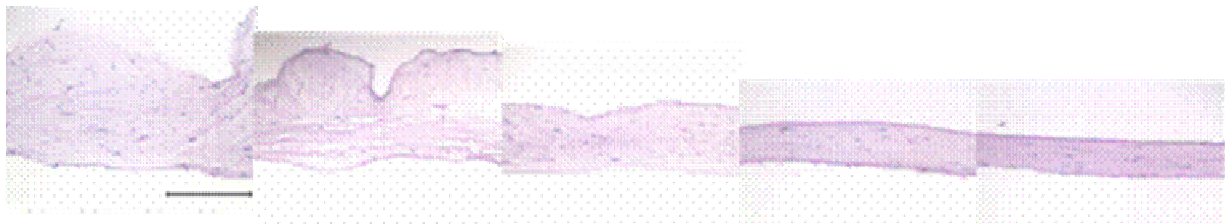


Fig. 4.2. Representative brightfield images of hematoxylin and eosin stained sections of fibrin gels stretched intermittently for eight days at 0, 2, 4, 8, and 16% stretch. These images demonstrate the dose-dependent decrease in thickness with stretch magnitude and the corresponding increase in protein and cell density as seen in both continuous and intermittently stretched groups. The indentations in the 0 and 2% stretch group are artifact of histological sectioning, and not present during culture. Original magnification 200x; scale bar = 100 μ m.

4.3.2. Effect of stretch on mechanical properties

All cycled gels were stronger than their respective controls in terms of both UTS and failure tension. There was an exponential increase in UTS with increasing stretch magnitude. Intermittently stretched gels in general had a larger UTS than continuously stretched gels (e.g., 35% stronger at 8% stretch and 26% at 16% stretch), but the impact of a rest period was not statistically significant (Figure 4.3, Table 4.1). In contrast, for failure tension there was a linear

dependence on both stretch magnitude the interaction between stretch magnitude and the rest period (Table 4.1). Specifically, the failure tension increased with increasing stretch magnitude in the intermittently stretched gels (Figure 4.1, Table 4.3) whereas the failure tension increased uniformly at all stretch magnitudes in gels cycled continuously (13-17% greater tension at failure relative to respective controls; Table 4.2). The extensibility increased with increasing stretch magnitude in the intermittent stretch group; no trend in extensibility with magnitude was observed in the continuously stretched group.

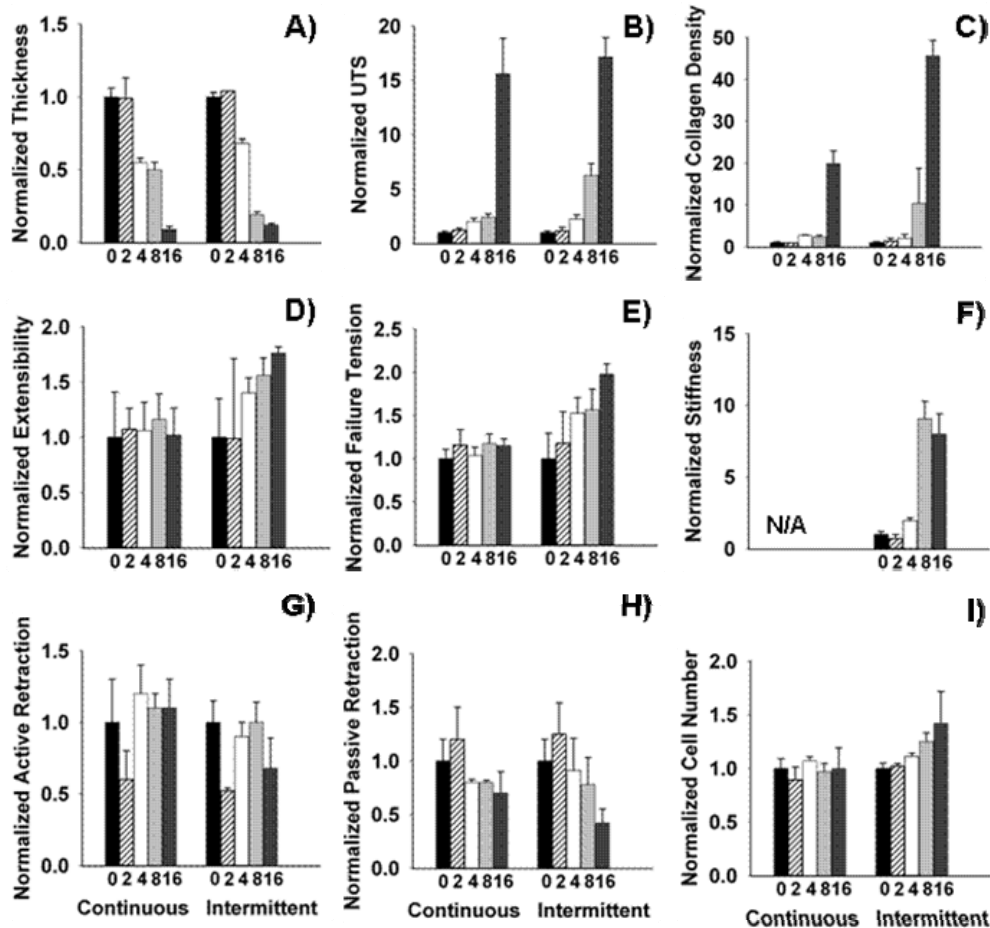


Fig. 4.3. A) Tissue thickness, B) UTS, C) collagen density, D) extensibility, E) failure tension, F) stiffness, G) active retraction, H) passive retraction and I) cell number of CS (24 hr/day), and IS (6 hr/day) fibrin gels cycled at 2, 4, 8, and 16% stretch for 8 days at 0.2 Hz, and normalized to statically cultured controls from each experiment. Note that UTS, stiffness, and collagen density are, by definition, directly dependent upon the thickness, whereas the other parameters are independent of the degree of compaction. For clarity, statistical models are provided

Table 4.1. Regression analysis for normalized remodeling metrics as a function of stretch magnitude (M), the length per day of stretch (CS vs. IS), and an interaction term (I, see statistical analysis methods). The fibroblast-populated fibrin gels were stretched continuously or intermittently at 0, 2, 4, 8 or 16% stretch for 8 days at 0.2 Hz. Note: although the passive retraction was determined to be significantly impacted by magnitude, and cell number was determined to be significantly impacted by both magnitude and the interaction term, they did not follow simple linear, exponential, or logarithmic regression models and are therefore not listed in the table.

Remodeling Metric	Regression Model	R ²	Root MSE
Thickness	= 0.99 - 0.06(M)	0.91	0.12
UTS	= 1.77 + (1.60 *10⁻⁶)exp^M	0.91	1.88
Failure Tension	= 1.05 + 0.06(M) - 0.05(I)	0.78	0.15
Collagen Density	= 2.23 + (4.90*10⁻⁶)exp^M - (2.81 *10⁻⁶)exp^I	0.93	3.41

4.3.3. Effect of stretch on cell number and collagen density

There was no change in cell number for gels stretched continuously in at any stretch level (Figure 4.3). When gels were stretched intermittently however, cell number increased with increasing stretch, peaking at 16% stretch (P< 0.001). Collagen density increased exponentially as a function of stretch magnitude, and there was significant interaction between magnitude and the rest period (Table 4.1).

Table 4.2. Raw mechanical, biochemical, and physiological data for continuously stretched gels cycled at 0, 2, 4, 8, and 16% stretch magnitudes for 8 days at 0.2 Hz. Each continuously stretched group was run with a separate statically cultured control group, thus the number of samples in the ‘0’ (static) group is very large.

% Stretch (Continuous)	Thickness (mm)	[n]	UTS (kPa)	Failure Tension (N/m)	Extensibility	[n]	Collagen Density (g/cm ³)	[n]	Cell Number (* 10 ⁶ cells)	[n]
0	1.29 ± 0.30	28	9.6 ± 3.0	11.3 ± 1.9	2.3 ± 0.4	20	0.13 ± 0.05	12	0.80 ± 0.18	12
2	1.15 ± 0.16	6	11.7 ± 1.8	13.3 ± 2.1	2.7 ± 0.5	6	0.09 ± 0.01	3	0.48 ± 0.07	3
4	0.76 ± 0.04	4	16.3 ± 2.2	12.5 ± 1.3	2.2 ± 0.5	3	0.20 ± 0.01	3	0.97 ± 0.04	3
8	0.42 ± 0.08	5	32.2 ± 4.6	15.5 ± 2.3	2.6 ± 0.6	5	0.49 ± 0.08	3	0.85 ± 0.07	3
16	0.13 ± 0.02	9	101.2 ± 21.2	13.2 ± 1.1	1.9 ± 0.4	9	2.91 ± 0.44	3	0.89 ± 0.17	3

Table 4.3. Raw mechanical, biochemical, and physiological data for intermittently stretched gels cycled at 0, 2, 4, 8, and 16% stretch magnitudes for 8 days at 0.2 Hz. All intermittently stretched treatment groups were tested simultaneously utilizing a single control group.

% Stretch (Intermittent)	Thickness (mm)	[n]	UTS (kPa)	Failure Tension (N/m)	Extensibility	[n]	Collagen Density (g/cm ³)	[n]	Cell Number (* 10 ⁶ cells)	[n]	Young’s Modulus (kPa)	Structural Stiffness (N/m)	[n]
0	1.53 ± 0.04	5	8.0 ± 2.3	12.2 ± 3.6	1.4 ± 0.5	4	0.16 ± 0.03	3	0.41 ± 0.21	2	7.2 ± 1.4	350 ± 72	3
2	1.60 ± 0.16	2	9.0 ± 2.8	14.3 ± 4.5	1.4 ± 1.0	2	0.22 ± 0.11	3	0.42 ± 0.91	2	5.1 ± 2.0	304 ± 140	2
4	1.05 ± 0.05	4	17.9 ± 3.0	18.6 ± 2.2	2.0 ± 0.2	4	0.32 ± 0.15	3	0.45 ± 0.13	2	14.2 ± 1.3	462 ± 103	2
8	0.39 ± 0.03	5	49.9 ± 8.7	19.1 ± 2.9	2.3 ± 0.2	5	1.67 ± 1.35	3	0.51 ± 0.33	2	65.5 ± 8.7	687 ± 149	2
16	0.18 ± 0.02	5	136.8 ± 14.2	24.1 ± 1.4	2.5 ± 0.1	5	7.36 ± 0.59	3	0.58 ± 0.16	2	57.3 ± 10.0	353 ± 58	3

4.3.4. *Effect of stretch on matrix retraction*

After release, all fibrin gels rapidly retracted due to a combination of prestress in the matrix and active cellular contraction, decreasing in projected area by approximately 60% or more within 10 minutes (e.g., see Figure 4.4). Overall trends in retraction for gels cycled at 0, 2, 4, 8, and 16% strain were very similar between gels cycled continuously (n =16, 2, 3, 3, and 7, respectively) and intermittently (n =3, 3, 3, 3, and 2, respectively). Although stretch magnitude was determined to be a statistically significant parameter governing passive retraction (R_o) per the ANOVA, the data does not follow a simple trend (linear, exponential, or logarithmic). Further, despite a consistent decrease in active cell-mediated matrix retraction (R_A) in the 2% stretched gels for both groups, there was no statistical dependence of this remodeling metric on the stretch magnitude or duration. The effective prestrain (ϵ_r) values for the groups cycled continuously to 0, 2, 4, 8, and 16% were 42 ± 17 , 17 ± 5 , 29 ± 1 , 30 ± 1 , and 25 ± 11 %, respectively, and the intermittently cycled groups were, 10 ± 2 , 13 ± 4 , 9 ± 3 , 8 ± 3 , and 4 ± 1 %, respectively.

The time constants of retraction for the groups cycled continuously to 0, 2, 4, 8, and 16% were 8 ± 3 , 5 ± 3 , 8 ± 1 , 7 ± 2 , and 7 ± 4 minutes, respectively. The time constants of retraction for the intermittently cycled groups to 0, 2, 4, 8, and 16% were 10 ± 2 , 13 ± 4 , 9 ± 3 , 8 ± 3 , and 4 ± 2 minutes, respectively. There was no correlation between stretch magnitude and the rate at which the matrices retracted, and there was no significant effect of the duration (6 vs. 24 hrs/day) on the rate of retraction.

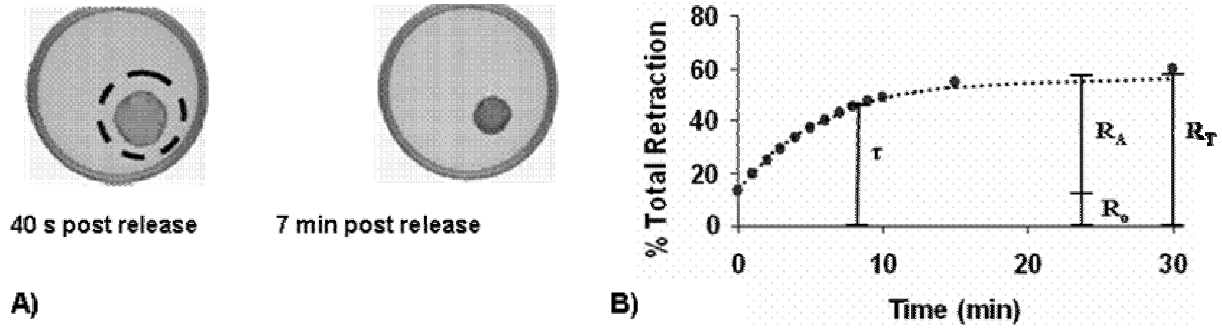


Fig. 4.4. A) Representative fibroblast-populated fibrin gel at 40 seconds and 7 minutes post release from its substrate. The dashed line represents the initial area of the fibrin gel that was dynamically cultured for 8 days then cut away from its circumferential anchors. Note the rapid decrease in projected-sectional area. B) Representative data of total matrix retraction as a function of time. The data are fit to an exponential increase equation as represented by the dotted line with three parameters; R_T (total retraction), R_A (active retraction), R_o (passive retraction), and τ (time constant), shown schematically in the figure. The bulk of the retraction occurs in less than 10 minutes ($\tau \sim 9$ min), and tensional homeostasis is reached by approximately 30 minutes.

4.3.5. Effect of intermittent stretch on the matrix stiffness

The elastic modulus increased slightly from control to 2% and 4%, increased to a maximum at 8%, and then dipped slightly down at 16% with intermittent stretch (Figure 5, Table 1). As biaxial tests were not performed on continuously stretched samples, the interaction between stretch magnitude and the rest period could not be determined.

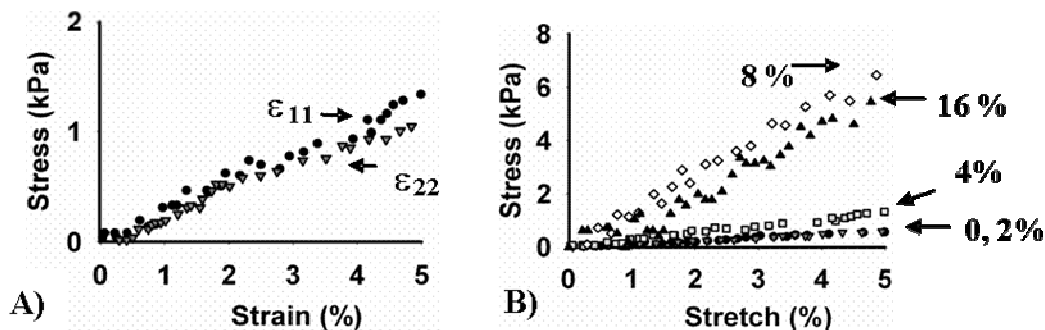


Fig. 4.5. A) Representative engineering stress-strain plot of equibiaxial loading along orthogonal '1' and '2' directions demonstrating isotropy of the matrix in a gel cycled intermittently at 4% strain for 8 days. Note that the '1' and '2' directions result in identical stress-strain profiles; this similarity is a result of the in-plane isotropy of the material. B) Representative stress-strain data from gels stretched at 0, 2, 4, 8, and 16% stretch for 6 hours a day at 0.2 Hz. Stiffness generally increases with increasing culture stretch magnitude, with a large increase between the 4% and 8% strain-conditioned groups, but no significant change between the 8% and 16% strain-conditioned groups.

4.4. Discussion

Establishing quantitative relationships between mechanical simulation and extracellular matrix remodeling is an important step towards rational design of manual therapies for wound healing and harnessing stretch as a means to custom tailor tissue analogs with specific requirements (e.g., strength, stiffness, contractility). In this study, using multiple levels of equibiaxial stretch, we determined that tissue strength, stiffness, and the accumulation of collagen increased with increasing stretch magnitude. Further, we discovered that while compaction and compaction-related remodeling (e.g., UTS) were highly dependent on stretch magnitude, stretch-induced increases in structural properties (e.g., failure tension) were contingent upon a rest period. These results demonstrate that the magnitude and the duration per day of stretch are both critical parameters in matrix remodeling and suggest that these two factors can be used independently or in concert to manipulate different aspects of remodeling.

4.4.1. *Cyclic stretch increases tissue strength in fibrin gels*

The data from this study confirm our previous results and the findings of others that cyclically stretching cell-populated biopolymer gels results in significant increases in mechanical properties [1, 8, 10-13, 19, 21, 23, 25, 27, 33-35]. We found that fibrin gels cycled continuously at 8% strain show comparable increases in UTS as collagen gels (~ 3 fold increase in gels stretched uniaxially at 10% strain for 8 days) [12] and even greater increases than reported in collagen-fibrin gels (~ 1.3 fold in gels stretched uniaxially at 10% strain for 8 days) [9]. Despite these large increases in tissue strength, the UTS of the fibrin gels (~ 30 kPa) is still substantially lower than those reported for collagen or collagen-fibrin gels (~ 60 kPa). As these gels are predominately composed of fibrin after only nine days in culture [13], and fibrin is generally weaker than collagen [9], this outcome is to be expected. Alternatively, the gels in this study may have lower UTS values than previously reported due to minimal in-plane alignment compared to gels cultured while being uniaxially stretched and tested uniaxially [13].

4.4.2. UTS increases exponentially as a function of stretch magnitude

In the present study, the UTS increased exponentially with increasing stretch, and this enhancement of tissue strength did not require continuous stimulation, exogenous growth factors, or extended culture duration – parameters previously thought to be required for a substantial increase in tissue strength [27, 35, 36]. It is unclear why notable increases in UTS require up to five weeks in other fibrin gel systems, although it may be due to passive decreases in thickness that may occur in the planar format relative to cylindrical geometries [35]. The substantial increase in UTS (relative to statically cultured gels) after only eight days of mechanical conditioning observed in this study was consistent with our previous data [13]. The similarity in trends in UTS between the intermittent and continuous groups was however unexpected. The intermittently stretched gels had higher collagen density, and increased collagen density typically results in increased tissue strength [11, 27].

4.4.3. Tissue compaction is both a passive and an active response to stretch

Compaction results in very large decreases in matrix volume (~ 80-95%), creates large changes in all intrinsic parameters, and can potentially obscure more meaningful changes resulting from cell-mediated remodeling. For example, stretch induced trends in thickness and UTS are inverse of one another (cf. Figures 2a and 2b), indicating that compaction, rather than true changes in fiber network strength, may dominate the observed increases in UTS. Further, if one were to only examine the UTS of our gels as the only metric of tissue strength, it would appear that the introduction of a rest period does not impact stretch-induced matrix strengthening. The effect of introducing the rest period is only made apparent when investigating changes in failure tension, a remodeling metric independent of tissue compaction, as described in the following section. In addition, we and others have shown that stretch-induced matrix compaction is not an entirely cell-mediated event. Acellular gels compact when stretched cyclically [9, 13], albeit significantly less than cell-populated gels (~ 3 fold less). These findings highlight the importance of measuring both intrinsic (compaction-dependent) and structural remodeling parameters to fully characterize changes in tissue properties due to mechanical conditioning.

4.4.4. Stretch-induced increases in failure tension are contingent on a rest period

To investigate cell-mediated changes in tissue strength without the confounding effects of changes in tissue thickness due to compaction, researchers have attempted to minimize or eliminate matrix compaction during cyclic loading by allowing cells to fully compact gels prior to mechanical conditioning [8, 10, 11, 35]. In this study, we elected not to precompact the matrix prior to experimentation; rather, we investigated the changes in failure tension (the ability of tissue to withstand tensile forces per unit length) in addition to measuring intrinsic matrix strength (UTS).

Trends in failure tension provided evidence that was not apparent in the trends of UTS: the introduction of a rest period during mechanical conditioning results in a stronger tissue construct. While intermittently stretched gels increased their tension prior to failure with increasing stretch in a dose-dependent manner, continuously stretched gels had only a slight increase in tissue strength. In fact, stretching gels continuously resulted in little enhancement in strength at higher stretch magnitudes despite increases in collagen density.

It is unclear why stretching gels intermittently rather than continuously results in an increase in failure tension. Although it would appear that the increase in cell number in the intermittently stretched gels could be the primary contributor to this increase in failure tension, the increase in cell number is slight. Further, there is evidence from previous studies that indicate that increases in cell number do not significantly improve tissue compaction, strength, or stiffness in fibrin gels cultured for a similar duration [24, 37]. It does appear that intermittently stretching gels results in an increase in the total amount of collagen produced per cell, not just an increase in the number of cells; a dramatic increase in collagen density could give rise to superior mechanical properties. It is also possible that by introducing a “rest period” during stimulation, one could alter the capacity of the cells to reorganize and remodel the surrounding collagen (e.g., enhanced crosslinking of the tissue). Although we previously reported that collagen crosslinking does not contribute significantly to the failure tension of continuously cycled fibrin gels [13], it is possible that allotting an 18 hour rest period each day may allow time for enhanced crosslinking of collagen in these systems.

Prior studies suggest that incorporating a rest period during mechanical loading regulates cells to utilize completely separate cell signaling pathways than when loaded continuously [38]. In addition, it is possible that intermittent stretch may simply be a method to disrupt the adaptation response of cells to a continuous stimulus, thus increasing the effectiveness of the stretch stimulus. This phenomenon has been shown to occur with incrementally increasing stretch magnitude on fibrin gels and results in higher UTS than continuous cycling at a given magnitude of stretch [35]. Although the mechanism remains unclear, these studies indicate that cells reorganize their matrix differently when the level of mechanical stimulation is varied.

4.4.5. *Matrix stiffness increases with intermittent stretch magnitude*

In addition to matrix strength, matrix stiffness is also an important measure of remodeling, and sufficient stiffness is an important parameter in determining the feasibility of using connective tissue equivalents *in vivo*. In the present study, the Young's modulus increased non-monotonically with increasing intermittent stretch with a peak at 8% strain. This non-monotonic increase in stiffness with stretch magnitude is consistent with a recent study utilizing continuous uniaxial stretch of valvular interstitial cell-populated fibrin gels [35], where it was determined that the Young's modulus was slightly less at the higher levels (15%) of strain than seen in intermediate levels of strain (10%).

To the best of our knowledge, these are the first measurements of stiffness of a fibrin gel via biaxial characterization. For comparison, collagen gels with similar cell and protein concentrations cycled at uniaxial 10% strain for 8 days and tested utilizing uniaxial pull to failure were approximately the same stiffness as the fibrin gels cycled at 8% in this study (58 vs 66 kPa) [12]. The fibrin gels tested in this study were slightly less stiff than previously reported for uniaxially cycled collagen/fibrin composite gels (10% strain) cultured under similar conditions (191-242 kPa) [9].

There are several limitations to the biaxial characterization measurements. During the biaxial testing, the fibrin gels ripped at the anchors at large bulk strains (above 10%) due to the low shear strength of the gels. Additionally, the 'effective' elastic modulus was estimated from a

single equibiaxial protocol following preconditioning assuming a Poisson's ratio of 0.25. This value was determined in preliminary experiments that utilized four different non-equibiaxial stretch protocols ($\varepsilon_{11}:\varepsilon_{22}=2:1, 1:2, \text{ and } 1:1$; data not shown). These protocols were run to allow for more complete constitutive modeling which we have left for future studies. Finally, because the biaxial characterization device was developed after the continuous stretch experiments, only measurements of the intermittently stretched gels could be made.

4.4.6. Tissue retraction is dependent on stretch magnitude

To quantify both the ability of the cells to impart residual strains in the matrix through remodeling activities and the cells' ability to actively contract the surrounding matrix, we utilized a retraction assay described previously [17]. Retraction, confusingly termed 'stress-relaxation' or 'release of tension' in previous studies utilizing collagen gels [30-32], occurs upon release of a compacted gel from the anchor and substrate. Whereas compaction occurs over hours to days and reflects cell traction-mediated remodeling of the gel [33, 34], passive retraction occurs immediately upon the release of prestress generated within the matrix by cells during compaction [35]. Active retraction occurs on the order of minutes following release and is due to cells actively contracting within the matrix; this active phase is indicative of the phenotype of the cells e.g., myofibroblasts contract the matrix to a greater extent than fibroblasts [18].

The passive retraction in both continuous and intermittently stretched gels was strikingly similar, demonstrating that the development of prestress across the matrix was dependent on the magnitude and not the duration of stretch. In addition, it appears that there is a decrease relative to controls in passive retraction at 2% strain in both groups. This decrease in passive prestress is not accompanied by any change in tissue compaction or cell number relative to controls, and is clearly correlated to the level of stretch applied. In contrast to previous reports, no significant increase in active retraction with dynamic culture was observed at any stretch magnitude [8, 39]. It has also been suggested that stretch-induced increases in cell contractility are due to alignment of cells and collagen fibrils in the direction of tension, thus creating a summation of contraction. In our system this alignment has been minimized by using equibiaxial strain, indicating that tissue alignment is not required for cells to impart forces across the matrix but may augment the

active contractility of the cells [13].

4.4.7. *Conclusions and summary*

In summary, in this study we systematically investigated how mechanical conditioning modifies cell-mediated remodeling of fibrin gels by measuring structural and intrinsic parameters and active and passive metrics, each of which gives different but valuable insight. For example, cyclically loading a sample at low strain (~5%) for a few hours each day appears to be more beneficial in terms of increases in resistance to tensile stretch, collagen content, and cell number than continuous stimulation at higher magnitudes of strain. In addition, the methods employed in this work provide valuable tools for investigating tissue remodeling in planar tissues and also for the determination of key parameters in the culture of functional tissue substitutes. The findings from this study provide a step towards characterizing culture conditions for tissue equivalents, developing improved wound healing treatments, and understanding tissue responses to changes in mechanical environments during growth, repair, and disease states.

4.4.8. *Acknowledgements*

The authors would like to thank Dr. Gaudette of Worcester Polytechnic Institute for the generous use of his extended phase image correlation software. We would also like to thank Dr. Jayson Wilbur for his assistance with statistical analysis, Dr. Marsha Rolle for her insightful commentary regarding the construction of the manuscript, and Angela Throm, Jeffery John, Christian Grove, Justine Roberts, Vanessa Lopez, Adriana Hera, Timothy Ebner, and Jacquelyn Youssef for their technical assistance. This work was supported in part by the U.S. Army Medical Research and Materiel Command (USAMRC); grant BFR08-1011-N00.

4.5. References

- [1] Bishop, J. E., Mitchell, J. J., Absher, P. M., Baldor, L., Geller, H. A., Woodcock-Mitchell, J., Hamblin, M. J., Vacek, P., and Low, R. B., 1993, "Cyclic mechanical deformation stimulates human lung fibroblast proliferation and autocrine growth factor activity," *Am J Respir Cell Mol Biol*, **9**(2), pp. 126-133.
- [2] Rudolph, R., Berg, J. V., and Ehrlick, H. P., 1992, *Wound Healing: Biochemical and Clinical Aspects*, W.B. Saunders Co., Philadelphia, PA.
- [3] Deva, A. K., Buckland, G. H., Fisher, E., Liew, S. C., Merten, S., McGlynn, M., Gianoutsos, M. P., Baldwin, M. A., and Lendvay, P. G., 2000, "Topical negative pressure in wound management," *Med J Aust*, **173**(3), pp. 128-131.
- [4] Siegel, H. J., Long, J. L., Watson, K. M., and Fiveash, J. B., 2007, "Vacuum-assisted closure for radiation-associated wound complications," *J Surg Oncol*, **96**(7), pp. 575-582.
- [5] Clark, R. A. F., 1996, *The Molecular and Cellular Biology of Wound Repair*, Plenum Press, New York.
- [6] Aarabi, S., Bhatt, K. A., Shi, Y., Paterno, J., Chang, E. I., Loh, S. A., Holmes, J. W., Longaker, M. T., Yee, H., and Gurtner, G. C., 2007, "Mechanical load initiates hypertrophic scar formation through decreased cellular apoptosis," *FASEB J*, **21**(12), pp. 3250-3261.
- [7] Arem, A. J., and Madden, J. W., 1976, "Effects of stress on healing wounds: I. Intermittent noncyclical tension," *J Surg Res*, **20**(2), pp. 93-102.
- [8] Seliktar, D., Black, R. A., Vito, R. P., and Nerem, R. M., 2000, "Dynamic mechanical conditioning of collagen-gel blood vessel constructs induces remodeling in vitro," *Ann Biomed Eng*, **28**(4), pp. 351-362.
- [9] Cummings, C. L., Gawlitta, D., Nerem, R. M., and Stegemann, J. P., 2004, "Properties of engineered vascular constructs made from collagen, fibrin, and collagen-fibrin mixtures," *Biomaterials*, **25**(17), pp. 3699-3706.
- [10] Isenberg, B. C., and Tranquillo, R. T., 2003, "Long-term cyclic distention enhances the mechanical properties of collagen-based media-equivalents," *Ann Biomed Eng*, **31**(8), pp. 937-949.
- [11] Kim, B. S., Nikolovski, J., Bonadio, J., and Mooney, D. J., 1999, "Cyclic mechanical strain regulates the development of engineered smooth muscle tissue," *Nat Biotechnol*, **17**(10), pp. 979-983.
- [12] Seliktar, D., Nerem, R. M., and Galis, Z. S., 2003, "Mechanical strain-stimulated remodeling of tissue-engineered blood vessel constructs," *Tissue Eng*, **9**(4), pp. 657-666.
- [13] Balestrini, J. L., and Billiar, K. L., 2006, "Equibiaxial cyclic stretch stimulates fibroblasts to rapidly remodel fibrin," *J Biomech*, **39**(16), pp. 2983-2990.
- [14] Kessler, D., Dethlefsen, S., Haase, I., Plomann, M., Hirche, F., Krieg, T., and Eckes, B., 2001, "Fibroblasts in mechanically stressed collagen lattices assume a "synthetic" phenotype," *J Biol Chem*, **276**(39), pp. 36575-36585.
- [15] Grenier, G., Remy-Zolghadri, M., Larouche, D., Gauvin, R., Baker, K., Bergeron, F., Dupuis, D., Langelier, E., Rancourt, D., Auger, F. A., and Germain, L., 2005, "Tissue reorganization in response to mechanical load increases functionality," *Tissue Eng*, **11**(1-2), pp. 90-100.
- [16] Pedersen, J. A., and Swartz, M. A., 2005, "Mechanobiology in the third dimension," *Ann Biomed Eng*, **33**(11), pp. 1469-1490.

- [17] Hinz, B., and Gabbiani, G., 2003, "Cell-matrix and cell-cell contacts of myofibroblasts: role in connective tissue remodeling," *Thromb Haemost*, **90**(6), pp. 993-1002.
- [18] Tomasek, J. J., Haaksma, C. J., Eddy, R. J., and Vaughan, M. B., 1992, "Fibroblast contraction occurs on release of tension in attached collagen lattices: dependency on an organized actin cytoskeleton and serum," *Anat Rec*, **232**(3), pp. 359-368.
- [19] Wille, J. J., Elson, E. L., and Okamoto, R. J., 2006, "Cellular and matrix mechanics of bioartificial tissues during continuous cyclic stretch," *Ann Biomed Eng*, **34**(11), pp. 1678-1690.
- [20] Grassl, E. D., Oegema, T. R., and Tranquillo, R. T., 2002, "Fibrin as an alternative biopolymer to type-I collagen for the fabrication of a media equivalent," *J Biomed Mater Res*, **60**(4), pp. 607-612.
- [21] Swartz, D. D., Russell, J. A., and Andreadis, S. T., 2005, "Engineering of fibrin-based functional and implantable small-diameter blood vessels," *Am J Physiol Heart Circ Physiol*, **288**(3), pp. H1451-1460.
- [22] Neidert, M. R., Lee, E. S., Oegema, T. R., and Tranquillo, R. T., 2002, "Enhanced fibrin remodeling in vitro with TGF-beta1, insulin and plasmin for improved tissue-equivalents," *Biomaterials*, **23**(17), pp. 3717-3731.
- [23] Ye, Q., Zund, G., Benedikt, P., Jockenhoevel, S., Hoerstrup, S. P., Sakyama, S., Hubbell, J. A., and Turina, M., 2000, "Fibrin gel as a three dimensional matrix in cardiovascular tissue engineering," *Eur J Cardiothorac Surg*, **17**(5), pp. 587-591.
- [24] Yao, L., Swartz, D. D., Gugino, S. F., Russell, J. A., and Andreadis, S. T., 2005, "Fibrin-based tissue-engineered blood vessels: differential effects of biomaterial and culture parameters on mechanical strength and vascular reactivity," *Tissue Eng*, **11**(7-8), pp. 991-1003.
- [25] Boublik, J., Park, H., Radisic, M., Tognana, E., Chen, F., Pei, M., Vunjak-Novakovic, G., and Freed, L. E., 2005, "Mechanical properties and remodeling of hybrid cardiac constructs made from heart cells, fibrin, and biodegradable, elastomeric knitted fabric," *Tissue Eng*, **11**(7-8), pp. 1122-1132.
- [26] Nerem, R. M., 2007, "Cell-based therapies: From basic biology to replacement, repair, and regeneration," *Biomaterials*, epub, ahead of print.
- [27] Boerboom, R. A., Rubbens, M. P., Driessen, N. J., Bouten, C. V., and Baaijens, F. P., 2008, "Effect of strain magnitude on the tissue properties of engineered cardiovascular constructs," *Ann Biomed Eng*, **36**(2), pp. 244-253.
- [28] Woessner, J. F., Jr., 1961, "The determination of hydroxyproline in tissue and protein samples containing small proportions of this imino acid," *Arch Biochem Biophys*, **93**, pp. 440-447.
- [29] Eastoe, J. E., 1955, "The amino acid composition of mammalian collagen and gelatin," *Biochem J*, **61**(4), pp. 589-600.
- [30] Bell, E., Ivarsson, B., and Merrill, C., 1979, "Production of a tissue-like structure by contraction of collagen lattices by human fibroblasts of different proliferative potential in vitro," *Proc Natl Acad Sci U S A*, **76**(3), pp. 1274-1278.
- [31] Billiar, K. L., Throm, A. M., and Frey, M. T., 2005, "Biaxial failure properties of planar living tissue equivalents," *J Biomed Mater Res A*, **73**(2), pp. 182-191.
- [32] Ahlfors, J. E., and Billiar, K. L., 2007, "Biomechanical and biochemical characteristics of a human fibroblast-produced and remodeled matrix," *Biomaterials*, **28**(13), pp. 2183-2191.

- [33] Altman, G. H., Horan, R. L., Martin, I., Farhadi, J., Stark, P. R., Volloch, V., Richmond, J. C., Vunjak-Novakovic, G., and Kaplan, D. L., 2002, "Cell differentiation by mechanical stress," *FASEB J*, **16**(2), pp. 270-272.
- [34] Chun, J., Tuan, T. L., Han, B., Vangsness, C. T., and Nimni, M. E., 2003, "Cultures of ligament fibroblasts in fibrin matrix gel," *Connect Tissue Res*, **44**(2), pp. 81-87.
- [35] Syedain, Z. H., Weinberg, J. S., and Tranquillo, R. T., 2008, "Cyclic distension of fibrin-based tissue constructs: evidence of adaptation during growth of engineered connective tissue," *Proc Natl Acad Sci U S A*, **105**(18), pp. 6537-6542. Epub 2008 Apr 6524.
- [36] Clark, R. A., Nielsen, L. D., Welch, M. P., and McPherson, J. M., 1995, "Collagen matrices attenuate the collagen-synthetic response of cultured fibroblasts to TGF-beta," *J Cell Sci*, **108**(Pt 3), pp. 1251-1261.
- [37] Grassl, E. D., Oegema, T. R., and Tranquillo, R. T., 2003, "A fibrin-based arterial media equivalent," *J Biomed Mater Res A*, **66**(3), pp. 550-561.
- [38] Nishimura, K., Blume, P., Ohgi, S., and Sumpio, B. E., 2007, "Effect of different frequencies of tensile strain on human dermal fibroblast proliferation and survival," *Wound Repair Regen*, **15**(5), pp. 646-656.
- [39] Wakatsuki, T., Kolodney, M. S., Zahalak, G. I., and Elson, E. L., 2000, "Cell mechanics studied by a reconstituted model tissue," *Biophys J*, **79**(5), pp. 2353-2368.

CHAPTER 5

Applying controlled non-uniform deformation for *in vitro* studies of cell mechanobiology

(Jenna L Balestrini, Jeremy K Skorinko, Adriana Hera, Glenn R Gaudette, Kristen L Billiar submitted in part to *Biomechanics and modeling in mechanobiology*, 2009)

5.1. Introduction

Connective tissues routinely have a wide range of mechanical loads imparted on them that are vital for the normal health and homeostasis of cells within these tissues [1-3]; these loads have also been demonstrated to regulate the growth, maintenance, and pathogenesis of many of these tissues [4, 5]. To investigate how these mechanical signals regulate cell behavior in a controlled environment, cells are often plated on an elastic membrane that is deformed equibiaxially or uniaxially as uniformly as possible [6-8]. These classical studies have demonstrated the profound effect of stretch on the biological responses of cells including changes in the shape of epithelial cells [9], reorientation of fibroblasts and smooth muscle cells [10], increases in proliferation rates [11], alteration of migratory behavior [12], and changes in the expression and synthesis of a variety of contractile and regulatory proteins [11, 13, 14].

Although past investigations have provided a wealth of information regarding the response of cells to homogeneous mechanical stimulation, there is very little known about how cells respond to the complex strain fields found *in vivo*. Strain patterns *in vivo* are often anisotropic (different magnitudes along different directions) and inhomogeneous with local gradients of strain magnitude [15, 16]. These non-uniformities in strain direction and magnitude are especially pronounced near local areas of increased stiffness e.g., in tissues undergoing clinical intervention with the addition of stents, prosthetics, etc., or during disease onset such as the formation of stiff fibrotic foci [2, 3]. Strain anisotropy has also been shown to be an important regulator in cell activity. For example, fibroblasts and smooth muscle cells will elongate and align perpendicular

to the direction of principal strain under uniaxial and strip biaxial stretch (i.e., pure uniaxial strain without transverse strain) [6, 17, 18]. Further, there is significant difference in cell proliferation, shape, orientation, and synthetic activity [19-21] between fibroblasts stretched biaxially and uniaxially. However, these studies typically consist of extremely anisotropic strain that is simply compared to equibiaxial strain; therefore, the more subtle but potentially important responses to intermediate biaxial states of strain found *in vivo* have been ignored.

In addition to strain direction, there is overwhelming evidence demonstrating that cell synthetic and proliferative activities are regulated by the magnitude of the strain stimulus [14, 17, 22, 23]. Despite this knowledge, there is very little information regarding how cells will respond to gradients of strain magnitude as seen *in vivo*. Cells have been shown to alter migration and proliferation in response to gradients of stiffness ('durotaxis' or 'durokinesis')[24], yet the effects of gradients of strain on cell migration ('tendotaxis') have only recently begun to be considered [25]. Early cell stretching systems involved inflation of circularly clamped membranes, and inadvertently created radially symmetric strain gradients [25-28]. These systems are however no longer utilized extensively due to complex fluid stresses and difficulty in evaluating the strain field (caused by the out of plane motion of the membrane). Given the similarities between stiffness-dependent and strain-dependent cell behavior in terms of increases in synthetic and contractile activity, strain gradients and gradients of strain anisotropy are likely to have profound effects on cell biology.

The goal of this study is to develop a culture system that produces non-uniform strain patterns for studying the effects of strain magnitude, anisotropy, and gradients on cells in culture. We describe herein a simple method in which a circular rigid inclusion is affixed to the center of a radially stretched membrane (in a commercially available vacuum driven device) to create strain gradients based upon a numerical analysis performed by Moore and colleagues [29]. In addition, using ring inserts that limit the deformation capacity of the stretch device, we are also able to run multiple strain magnitudes simultaneously and decouple both strain magnitude and strain gradient effects. Custom high resolution deformation mapping software is utilized to verify the distribution of radial and circumferential stretch ratios across the membrane. As a demonstration of the utility of the method, we measure fibroblast orientation within a single culture well along lines of minimum principal strain.

5.2. Materials and Methods

5.2.1. Experimental Approach

Rigid circular inclusions were affixed to the center of radially stretched homogenous circular membranes to create an *in vitro* system capable of simultaneously producing multiple strain magnitudes and differential ratios of axial stretch within the same culture well. The approach was based on numerical simulations by Moore and colleagues [29], which demonstrate that symmetric but highly non-uniform strain fields can theoretically be produced by a stretching the edge of a membrane with a small circular rigid inclusion in the center.

The rigid inclusion alters both the strain magnitude and anisotropy co-localizing the highest radial strains with the greatest strain anisotropy at the edge of the inclusion. To separate these effects, it is advantageous to run parallel experiments at different strain magnitudes, both with rigid inclusions and without (i.e., homogeneous equibiaxial strain). To alter the magnitude of strain without the use of additional pressure control units, we adapted a system developed by Boerboom et al. [30] to limit the distension of the compliant culture membrane. A series of annular rings (see Fig. 5.1a-c) of different heights placed around the cylindrical “loading platens” allow the user to achieve different strain levels in each well of the 6-well culture plate. These rings enable both the decoupling of magnitude and gradient effects, and they also allow for the use of a single control (as opposed to a control for each level of strain magnitude) in mechanobiological studies.

5.2.2. Fabrication of the rigid inclusion model system

To create a non-uniform strain field as simulated in Mori et al. [29], 5mm, 10mm, and 15mm diameter glass coverslips (Deckgläser, Germany) were adhered to the center of 35mm diameter collagen coated flexible bottom Bioflex culture wells (Flexcell International, NC) using Silastic Medical Adhesive (Dow Corning, Midland, MI). The glue was allowed to cure for 48 hours, and

the 6 well plates were rinsed and sterilized by washing with ethanol and subsequently rinsing with deionized water, and then UV sterilized for 10 minutes. To apply cyclic stretch the Flexcell FX-4000T (Flexcell International) was cycled up to 35kPa vacuum pressure (corresponding to ‘6%’ equibiaxial strain in unmodified well) using a square waveform at 0.2Hz and a 25mm diameter platen.

5.2.3. *Ring inserts to limit strain*

Delrin rings with thicknesses ranging from 6-10mm, an outer diameter of 35mm, and an inner diameter of 25mm were fabricated. The ring inserts were placed on the perimeter of the loading posts and silicone lubrication was placed on the loading post and ring (Fig. 5.1a-c). Unaltered 6-well Bioflex plates were placed onto the baseplate and markers composed of 4 ink dots placed across the membrane. Vacuum pressure was then applied at approximately 52 and 89kPa (corresponding to ‘10%’ and ‘20%’ applied strain in an unmodified system), and images were taken using a digital SLR camera (6 megapixel, Cannon EOS). Displacement of the markers was measured using Image J (version 1.38, NIH). To ensure that the strain across the membrane remained homogeneous across the membrane with the addition of inserts, the strain distribution across the membrane was assessed with inserts that restricted global strain to 10% strain using an image correlation method (as described in section 2.4). All measurements were repeated on an additional set of wells.

5.2.4. *Strain field verification*

For the strain field verification, a mixture of silicon carbide particles (40 μ m diameter) and retro-reflective beads (60 μ m diameter) was applied to create a random light intensity distribution in the region of interest (ROI) on plates with 5, 10 and 15mm diameter cover slips affixed. Digital images were acquired at 50 frames per second using a 1280 x 1024 pixel resolution CMOS camera (Photron; San Diego CA; Model # Fastcam-X 1280 PCI) with 8 bit pixel depth while the flexible-bottom plates were cycled at 0.2Hz with vacuum pressures ranging from 0-35kPa (corresponding to 0-6% equibiaxial strain in the unmodified state, i.e., the ‘applied strain’). To

verify the pressures corresponding to each level of applied strain used for strain field mapping ('2%', '4%', and '6%'), a pressure transducer (Millar instruments; Houston, TX; Model # SPR-524) was inserted into the vacuum tubing between the Flexlink pressure controller and the baseplate. The pressure was simultaneously obtained with the images using an analog-digital converter (National Instruments; Austin, TX; Model # PCI-6023E) and the camera connected to a one-gigabyte frame grabber board (Photron; San Diego, CA).

The two-dimensional distribution of strain in the center of stretched samples was determined using digital image analysis. Specifically, the components of the two-dimensional deformation field (u_1 and u_2 along the X_1 and X_2 camera axes, respectively) were determined from the images by measuring light distribution patterns using High Density Mapper (HDM) software [5]. In brief, HDM converts the light distribution to the spectral domain using a fast Fourier transform (FFT) and through the use of an interference function the displacement and rotation are found. The displacements are then converted back from the spectral domain to cartesian coordinates using an inverse FFT. The chosen field of view (FOV) resulted in a camera resolution of 0.018mm/pixel. Displacements were measured using a 0.58mm (32 pixel) sub-image size with a corresponding step size of 0.29mm (16 pixel shift) yielding a 17 x 41 matrix of u_1 and u_2 values for a 5mm x 12mm ROI. To remove spurious data points (e.g., due to reflection) deformation components (u_i) were filtered in MATLAB (Mathworks, Natick, MA) using a Gaussian filter with a 3x3 window size, a standard deviation of 0.25. To determine the total deformation in the loading cycle, the displacement components were summed for the loading phase. The local displacement gradients (du_i/dX_j) were obtained from regressions over five points to minimize noise inherent in differentiating measured signals. The deformation gradient tensor, F , was calculated at each location using the following equations:

$$F_{ij} = \frac{\partial x_i}{\partial X_j} = \frac{\partial (X_i + u_i)}{\partial X_j} = \begin{bmatrix} \lambda_1 & \kappa_1 \\ \kappa_2 & \lambda_2 \end{bmatrix}; \quad (5.1)$$

where λ_i and κ_i are the stretch ratio and shear components, respectively. As the chosen geometry and loading utilized in this system are radially symmetric, the deformation in Cartesian coordinates, $F(X_1, X_2)$ was then transformed to polar coordinates, $F'(r, \theta)$ by the relationship:

$$F' = \beta F \beta^T ; \quad (5.2)$$

$$\text{where } \beta = \begin{bmatrix} \cos \theta & \sin \theta \\ -\sin \theta & \cos \theta \end{bmatrix}, \theta = \tan^{-1} \left(\frac{y - y_{center}}{x - x_{center}} \right), r = \sqrt{(y - y_0)^2 + (x - x_0)^2},$$

θ is the angle of rotation counter-clockwise from the horizontal, and r is the radius from the center. In long hand, Eqn. 5.2 can be written:

$$\begin{aligned} F'_{11} &= F_{11} \cos^2 \theta + F_{22} \sin^2 \theta + (F_{12} + F_{21}) \sin \theta \cos \theta = \lambda_r \\ F'_{22} &= F_{11} \sin^2 \theta + F_{22} \cos^2 \theta - (F_{12} + F_{21}) \sin \theta \cos \theta = \lambda_\theta \\ F'_{12} &= (F_{22} - F_{11}) \cos \theta \sin \theta + F_{12} \cos^2 \theta - F_{21} \sin^2 \theta = \kappa'_1 \\ F'_{21} &= (F_{22} - F_{11}) \cos \theta \sin \theta + F_{21} \cos^2 \theta - F_{12} \sin^2 \theta = \kappa'_2 \end{aligned} \quad (5.3)$$

Unlike the values of F which were evenly spaced in Cartesian space by the step size, $dX=0.29\text{mm}$, and could simply be averaged by taking the mean of a column of data, the mean values of F' at particular radial increments, dr , required binning of the data. Thus, to obtain the mean values for each well as a function of radius, the λ_r , λ_θ , κ_1 , and κ_2 matrices were vectorized and ordered by radius then binned and averaged with a binsize of 0.29mm (same value as the step size for HDM analysis). Average data for four wells in each treatment group are presented as mean \pm standard error of the mean (SEM).

5.2.5. Strain field verification for 3D model systems

To determine if the strain distribution in the 3D rigid inclusion systems were comparable to strain distributions in the 2D rigid inclusion systems and to verify that the fibrin gels would remain adhered to the rigid inclusions for the entire experimental duration, strain fields were assessed as was described in section 5.2.4. Briefly, fibrin gels were cast into wells with a 5 mm glass coverslip (described in section 5.2.7), allowed to polymerize overnight, and cycled for 8 days at '6%' applied strain (32 kPa vacuum pressure) at 0.2 Hz. Media was removed from the fibrin gels, the gels were covered in silicone carbide particles, cycled to '6%' applied strain and imaged for image analysis.

5.2.6. Statistical analysis and modeling

To facilitate calculation of radial and circumferential stretch ratios at a given radius, the mean stretch ratio versus radius data were modeled using regression analysis (Sigmastat, Systat Software, Inc., Richmond, California) for each inclusion size and applied strain level. The stretch ratio data were fit to the following equations:

$$\begin{aligned} \lambda_r &= \lambda_0 + a \exp(-br^*) \\ \lambda_\theta &= \lambda_0 + a[1 - \exp(-br^*)] \end{aligned} \quad (5.5)$$

$$r^* = \frac{(r - r_{inclusion})}{r_{outer}}; \quad (5.6)$$

where λ_θ and λ_r are the circumferential and radial stretch ratios, respectively, λ_0 , a and b are model parameters, r^* is the normalized radius, r is distance from the center, $r_{inclusion}$ is the inclusion radius, and r_{outer} is the outer radius (12.5mm in our wells). To test the utility of the model to predict data not utilized for the parameter optimization (i.e., alternative pressures), the data for ‘2%’ and ‘4%’ applied strain were interpolated by scaling the output of the model generated with the ‘6%’ parameters by 1/3 and 2/3, respectively, with b held constant. For example, $\lambda_{0_2\%} = (\lambda_{0_6\%} - 1)/3 + 1$, $a_{2\%} = a_{6\%}/3$, and $b_{2\%} = b_{6\%}$ (note: 1 is subtracted from λ_0 to obtain engineering strain from stretch ratio for scaling).

For direct comparison with predictions from numerical analysis, the data from Mori *et al.* [29] were linearly scaled from 10% to 6% applied strain and then interpolated for our slightly smaller inclusion sizes. Specifically, digitized radial and circumferential stretch ratios for an isotropic membrane stretched 10% at the outer circumference (Fig. 3 in Mori *et al.*) were scaled to 6% strain by subtracting 1 (to obtain engineering strain), multiplied by 0.6, and adding 1 (to re-obtain stretch ratios). The validity of this method of scaling was confirmed with comparison to multiple strain level predictions by Mori *et al.* (5% to 25%, Fig. 2 in Mori *et al.*). To approximate the results for the normalized inclusion sizes ($r_{inclusion}/r_{outer}$) used in this study (0.2, 0.4, and 0.6) from those used by Mori *et al.* (0.25, 0.5, 0.75), the scaled stretch ratio vs. r^* curves

were fit to equations 2.6 above. In the case of radial stretch ratio, in order to avoid overparameterization, the variable b was held constant at $b=6$, and λ_0 and a were fit (resulting in $R^2 > 0.98$ for all curves). Curve fitting was utilized to obtain the following approximate relationships between these parameters and the normalized inclusion sizes:

$\lambda_0 = 1.05(r_{inclusion}/r_{outer})^2 - 0.536(r_{inclusion}/r_{outer}) + 1.18$ and $a = -0.047(r_{inclusion}/r_{outer}) + 0.096$, λ_0 and a were then interpolated for $r_{inclusion}/r_{outer} = 0.2, 0.4, \text{ and } 0.6$ using these relationships. The digitized curves for circumferential stretch ratio, could all be fit well with a single set of parameters ($\lambda_0=1$, $a=0.094$, and $b=6$) with $R^2 > 0.95$ thus, for simplicity, no further parameter optimization was done. The interpolated parameter values were used in Eqns. 5.6 to generate curves for comparison with our data.

5.2.7. Demonstration of cell orientation to non-homogeneous strain field created by rigid inclusion in two and three dimensional models

As a demonstration of the utility of this method for mechanobiological studies, a proof of concept study was performed wherein cell orientation with respect to changing anisotropy of stretch across the membrane created by the rigid inclusion was investigated. Therefore, 2D and 3D models were created to examine cellular response to these changes in strain distribution. To create the 2D system, human dermal foreskin fibroblasts (American Type Culture Collection, Manassas, VA) were cultured in Dulbecco's Modified Eagle Medium (DMEM, Mediatech, Herndon, VA) and supplemented with 10% bovine calf serum, (BCS, HyClone, Logan, UT), 100 units/mL penicillin G sodium, 100 $\mu\text{g}/\text{mL}$ streptomycin sulfate, and 250 ng/mL amphotericin B (Gibco, Grand Island, NY). Passage 7-9 human foreskin fibroblasts were seeded into six 35mm diameter collagen-coated Bioflex culture wells at a density of 6,000 cells/cm² and allowed to adhere to the substrate overnight prior to stretching. The fibroblasts were cultured at 37° C with humidified 10% CO₂, and fed DMEM supplemented with 10% fetal bovine serum (FBS, Hyclone), 25 g/L L-ascorbate (Wako, Richmond, VA), 0.5 mL/L insulin (Sigma, St. Louis, MO), 100 units/mL penicillin G sodium, 100 $\mu\text{g}/\text{mL}$ streptomycin sulfate, and 250 ng/mL amphotericin B (Gibco) was changed every other day.

After 2 days of continuous sinusoidal ‘2%’ applied strain (8kPa vacuum pressure) at 0.2Hz, the cells were fixed and permeabilized with 5.3% formaldehyde and 4 μ M Triton X-100 (Calbiochem, Gibbstown, NJ) for 30 minutes and blocked with 1% bovine serum albumin (BSA, Sigma) in PBS for 30 minutes. To visualize cells, F-actin was detected using Alexa Fluor 488 phalloidin stain (Molecular Probes, Eugene, Oregon) and DNA was detected using Hoechst 33342 stain (Molecular Probes) according to manufacturer’s instructions. All fluorescence images were acquired using a Nikon Eclipse microscope (magnification= 200x). Cell orientation was determined by fitting the perimeter of each cell (as made apparent by phalloidin staining) to an ellipse using Image J software (NIH) and measuring the orientation of the long axis. Due to symmetry, the cell orientations were converted from 360° measurements to 0-90° and binned every 15°. A minimum of 50 cells were counted for each image, two wells were examined per treatment group and three images were taken per well.

To investigate tissue architecture changes in response to non-uniform strain fields in 3D model systems, fibrin gels were cast onto 5 mm inclusion model systems that were prepared as described in the above section (5.2.6). To ensure that the fibroblast-populated fibrin gels were attached to the glass coverslips, the rigid inclusion system was plasma cleaned prior to casting the gels within these systems. Fibrin gels were produced and cultured as previously described [31]. Bovine fibrinogen and thrombin (Sigma, St. Louis, MO) were combined with passage 7-9 human foreskin fibroblasts (American Type Culture Collection, Manassas, VA) in Dulbecco’s Modified Eagle Medium (DMEM, Mediatech, Herndon, VA) and 10% bovine calf serum, (BCS, HyClone, Logan, UT), 100 units/mL penicillin G sodium, 100 μ g/mL streptomycin sulfate, and 250 ng/mL amphotericin B (Gibco, Grand Island, NY) were added to the media. The final concentrations of each component of the gels were 0.2 U/mL thrombin, 3.8 mg/mL fibrinogen (Sigma, St. Louis, MO), and 500,000 cells/mL.

After mixing, the fibrin and cell solution (3 mL) was poured into six 35 mm diameter flexible-bottom culture wells with circular fibrous foam anchors and a 5 mm glass coverslip. Gels were allowed to polymerize for 24 hours prior to mechanical stimulation and cultured at 37° C with humidified 10% CO₂. Gels were fed with DMEM supplemented with 10% fetal bovine serum (FBS, Hyclone), 25 g/L L-ascorbate (Wako, Richmond, VA), 0.5 mL/L insulin (Sigma), 100

units/mL penicillin G sodium, 100 µg/mL streptomycin sulfate, and 250 ng/mL amphotericin B (Gibco) every other day.

After 8 days of sinusoidal ‘6%’ applied strain at 0.2Hz for 6 hr/day, cells were fixed and stained for F-actin and nuclei using the same protocol as the 2D system. Cells were visualized and imaged across the matrix using confocal microscopy and qualitatively examined for orientation with respect to principal strain. All fluorescence images in 3D were acquired using a Leica SP5 confocal imaging system (magnification= 200x). In order to investigate matrix reorganization with respect to non-homogeneities produced in our system, a subset of samples were analyzed histologically. Representative samples from each group were fixed in buffered formalin while still attached to the anchors for 18-20 hours at 4° C and stored in 70% ethanol for histological evaluation. The samples were then removed from their anchors and silicone membranes, embedded in paraffin, cut into 5 µm sections, and then stained with hematoxylin and eosin (H&E). Micrographs were taken with a Nikon Eclipse E600 camera at a magnification of 200X, and thickness of each sample were measured using SPOT 4.0 imaging software (Diagnostic Instruments, MI).

5.3. Results

The radial and circumferential strain distributions were assessed in a 5 mm wide section of the image that spanned from the center of the inclusion to the edge of the platen (area of strain contour in Fig. 5.1d). Due to the combination of edge effects near the rounded edge of the loading post and out-of-plane displacement of the membrane (with respect to the camera) at the edge of the platen, our analysis was limited to the central 20mm region as opposed to the entirety of the 35mm membrane, i.e., $0 < r < 10\text{mm}$ or $0 < r^* < 0.8$.

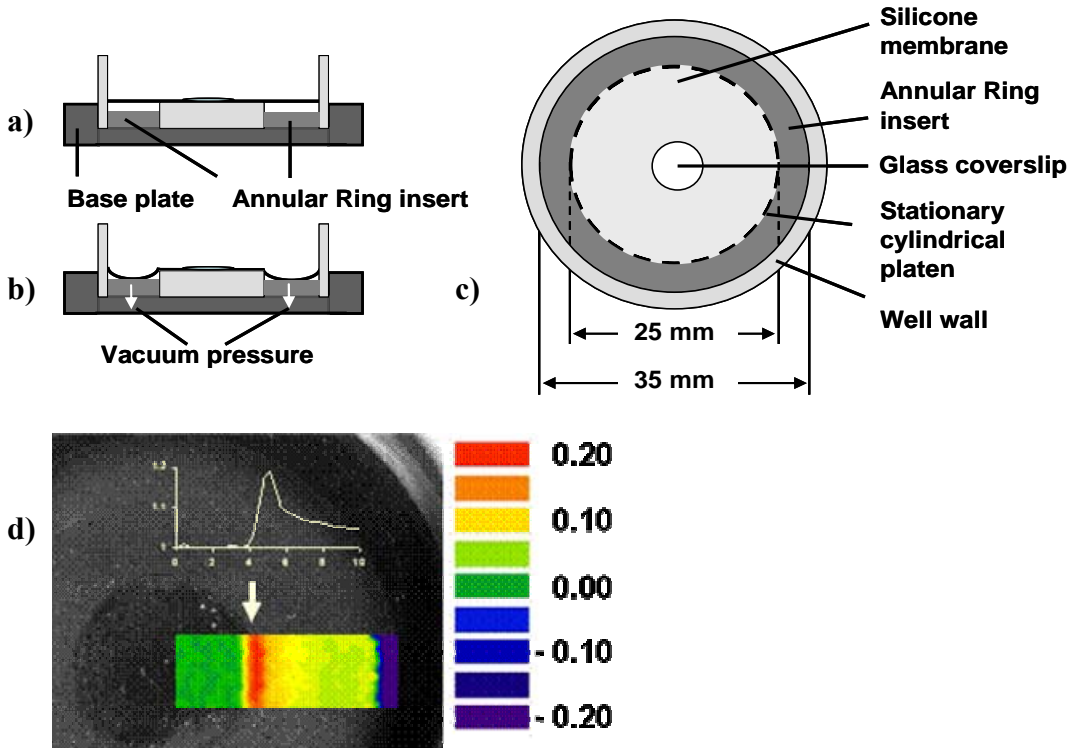


Fig. 5.1 Schematics of the of the rigid inclusion system with a ring insert shown: a) undeformed and b) deformed cross-sections and c) aerial view d) representative line and contour plots of radial strain (λ_r) across a 5mm section of the membrane that was modified using 10mm inclusion, covered in light reflective beads, and deformed using 35kPa of vacuum pressure ('6%' applied strain). The white arrow indicates the edge of the inclusion. Note: due to substantial edge effects ($r > 10\text{mm}$), the useful cell culture area is restricted to the central 20mm of the 35mm diameter membrane.

5.3.1. Effect of the subimage size on the resolution of strain distribution

A subimage size of 32 pixels with a step size of 16 (pixel shift) was determined to give the optimum balance between distance resolution and noise reduction (Fig. 5.2). Decreasing the subimage size to 16 pixels with a pixel shift of 8 (lowest level that led to correlation) resulted in the highest peak stretch ratio values ($\lambda_r = 1.22$), yet also yielded the highest noise levels. Due to this increase in noise, several data sets could not be analyzed using the lower subimage size. Using the mid-range subimage size (32 pixels with a pixel shift of 16) resulted in a slightly lower peak stretch ratio value ($\lambda_r = 1.19$), which we term 'blunting' of the peak, yet produced less noise than the smaller subimage size configurations. Applying a larger subimage size (64 pixels with a pixel shift of 16) yielded even lower peak stretch ratio values ($\lambda_r = 1.18$) and a lower noise level. This increase in subimage size also results in an increase in averaging of the data points and

decrease in gradients; the impact of this averaging is made evident by observing where the λ_r begins to rise from 1.0 with respect to the inclusion edge (e.g., in Fig. 5.2c the ‘ramp up’ of the gradient begins ~ 4 mm from the center, whereas the edge of the inclusion is actually at 5mm). Therefore, in order to maintain accurate phase correlation while minimizing noise, a subimage size of 32 with a pixel shift of 16 was utilized for the strain field data reported below.

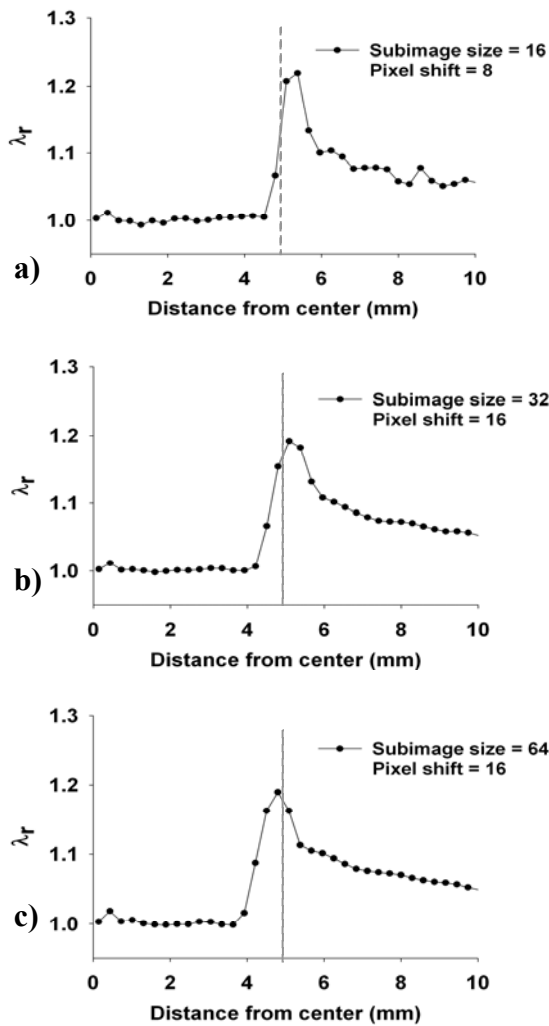


Fig. 5.2 Representative radial stretch ratio, λ_r versus radius for a 10mm inclusion system cycled to ‘6%’ applied strain (35kPa vacuum pressure). The grey line represents the edge of the inclusion. Two-dimensional displacements were analyzed with a subimage size:pixel shift ratio of a) 16:8, b) 32:16, and c) 64:16. The curves become smoother and less noisy with increasing subimage size but the peaks are also increasingly “blunted” as evidenced by the decreasing λ_{max} of 1.22, 1.19, and 1.18 for subimage sizes of 16, 32, and 64, respectively. In addition, the increase in averaging with increasing subimage size results in an offset of the λ_r gradient with respect to the inclusion edge.

5.3.2. *Effect of the rigid inclusion on strain distribution in 2D*

Adhering rigid inclusions to the center of radially stretched membranes produces gradients of radial and circumferential stretch that are a function of both the amount of vacuum pressure applied and the size of the inclusion. In all cases, the radial strain increases to a maximum at the edge of the inclusion and decreases exponentially with increasing radial distance towards the outer edge (Fig. 5.3a,c). This peak in radial strain yielded maximum radial stretch ratios of 1.15, 1.19, and 1.24 for 5, 10, and 15mm inclusions, respectively, for ‘6%’ applied strain (Fig. 5.3a). Conversely, the circumferential strain is lowest adjacent to the inclusion, and increases rapidly with increasing radial distance from the inclusion (Fig. 5.3b,d) producing maximal circumferential stretch ratios of 1.07, 1.05, and 1.03 for 5, 10, and 15mm inclusions, respectively, for ‘6%’ applied strain (Fig. 5.34b). The rate of change in strain along the radius is also highest in the radial direction at the edge of the inclusion, corresponding strain gradients of -15.1, -22.8, and -33.8%/mm for 5, 10, and 15mm inclusions, respectively, for ‘6%’ applied strain. The strain gradients across the membrane are presented for the three different inclusion sizes at ‘6%’ applied strain (Fig. 5.4a) and for the 10mm inclusion at ‘2%’, ‘4%’, and ‘6%’ applied strain (Fig. 5.4b).

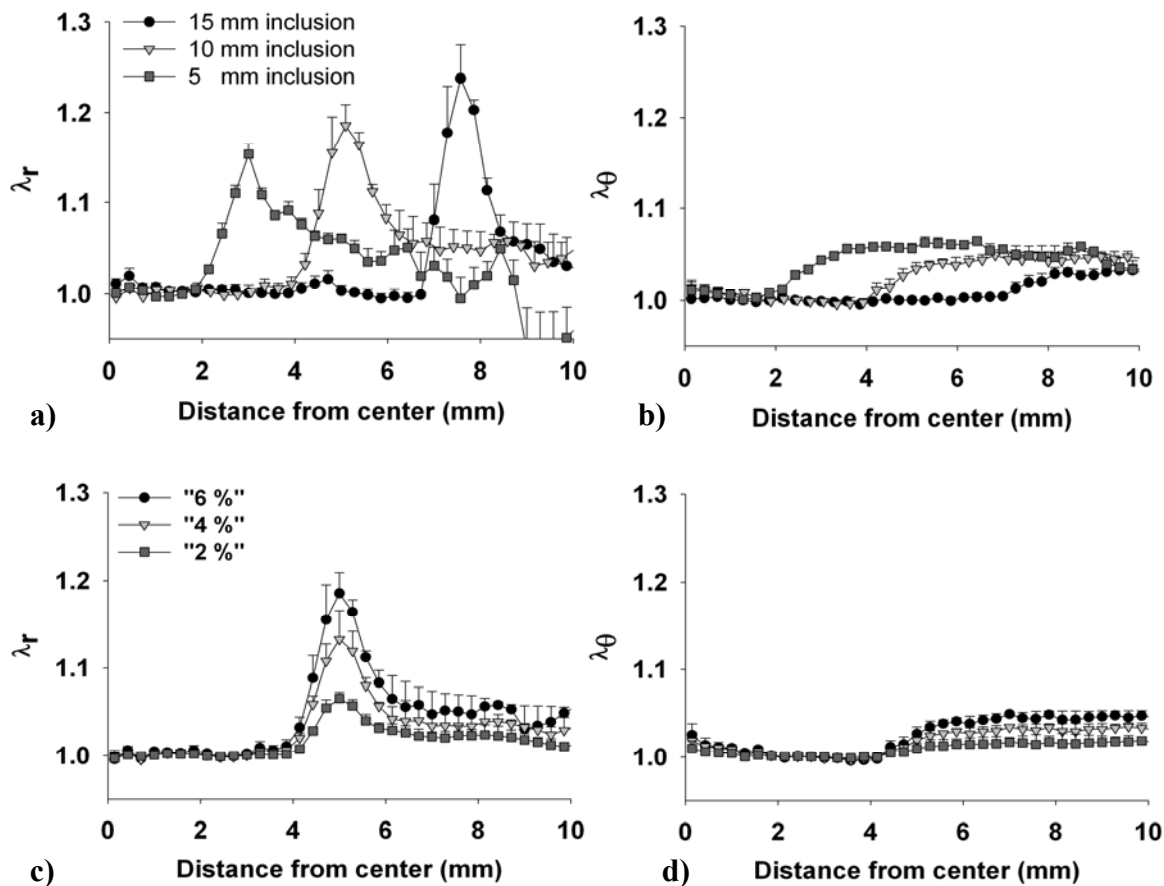


Fig. 5.3. Effect of increasing inclusion size and applied strain on the deformation of the membrane. a) Radial and b) circumferential stretch ratios across 35mm diameter silicone membranes cycled to ‘6%’ applied strain. c) Radial and d) circumferential stretch ratios across a membrane with a 10mm inclusion for ‘2%’, ‘4%’, and ‘6%’ applied strain. Note that the inclusion remains central above the 25mm diameter stationary cylindrical platen during cycling due to radial symmetry. Mean \pm SEM plotted; n=4 wells for each curve.

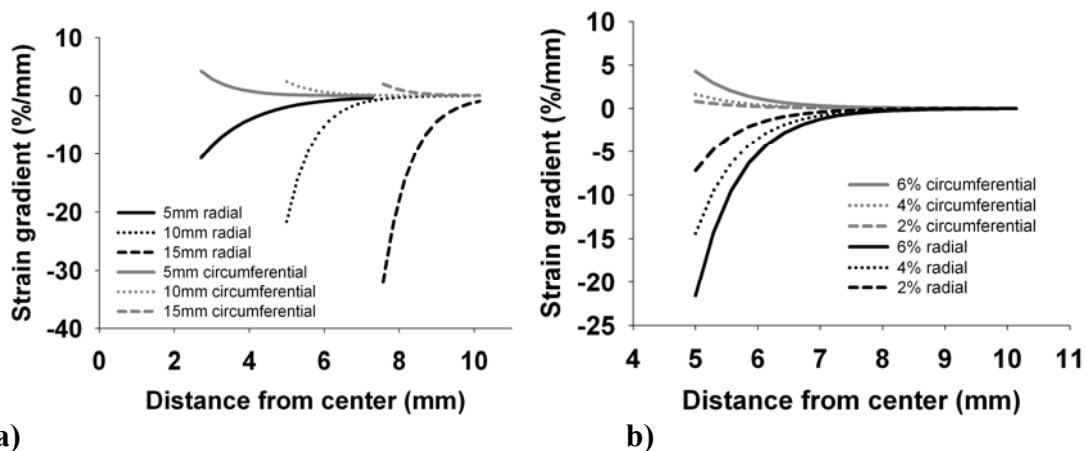


Fig. 5.4 Strain gradients for a) ‘6%’ applied strain for different inclusion sizes (5mm, 10mm, and 15mm) and for b) 10mm inclusion at ‘2%’, ‘4%’, and ‘6%’ applied strain. Note in (a) that -10%/mm (and lower) radial

gradient can be obtained with all three inclusion sizes, but the corresponding radial strains for these inclusions (Fig. 5.4) are very different (1.17, 1.11, 1.01); the anisotropy of stretch are also somewhat different at these radii. Also note in (b) that the strain gradients decrease with decreased applied strain, but the strain anisotropy is not a function of applied strain, thus different gradients can be tested while the anisotropy is constant at a given radius.

Table 5.1: Optimal parameter values for stretch ratio vs. radius curves and interpolated parameters for '2%' and '4%' curves based on optimal parameters for '6%' curves. These parameters can be used with Eqns. 2.6 to calculate the radial and circumferential stretch ratios and associated anisotropy and gradients at any radial location with applied strains up to '6%' for each inclusion size.

λ_r						λ_θ				
<u>5mm inclusion</u>	6% (fit)	4% (fit)	4% (predicted)	2% (fit)	2% (predicted)	6% (fit)	4% (fit)	4% (predicted)	2% (fit)	2% (predicted)
yo	1.026	0.980	1.017	1.011	1.009	1.016	1.016	1.010	1.005	1.005
a	0.168	0.129	0.112	0.065	0.056	0.043	0.016	0.029	0.020	0.014
b	9.38	4.38	9.35	8.38	9.35	16.3	15.2	16.3	13.2	16.3
R ²	0.926	0.934	0.904	0.848	0.848	0.824	0.806	0.840	0.892	0.883
<u>10mm inclusion</u>	6% (fit)	4% (fit)	4% (predicted)	2% (fit)	2% (predicted)	6% (fit)	4% (fit)	4% (predicted)	2% (fit)	2% (predicted)
yo	1.044	1.030	1.029	1.016	1.015	1.028	1.020	10.018	1.010	1.009
a	0.151	0.110	0.101	0.050	0.050	0.019	0.012	0.012	0.007	0.006
b	17.9	18.2	17.9	13.1	17.9	16.6	15.1	16.6	11.0	16.6
R ²	0.947	0.954	0.958	0.920	0.928	0.836	0.810	0.809	0.865	0.819
<u>15mm inclusion</u>	6% (fit)	4% (fit)	4% (predicted)	2% (fit)	2% (predicted)	6% (fit)	4% (fit)	4% (predicted)	2% (fit)	2% (predicted)
yo	1.016	1.012	1.011	1.000	1.005	1.017	1.005	1.011	1.000	1.006
a	0.256	0.185	0.171	0.122	0.085	0.014	0.017	0.010	0.012	0.005
b	17.2	17.6	17.2	16.7	17.2	19.8	41.1	19.8	56.5	19.8
R ²	0.967	0.968	0.968	0.965	0.969	0.801	0.939	0.855	0.865	0.682

5.3.3. Results of regression analysis and modeling

The radial and circumferential stretch ratio versus radius curves were fit well by three-parameter exponential models (Eqns. 5.6) with $R^2 > 0.8$ in all cases and generally $R^2 > 0.9$ in the radial direction with residuals evenly distributed about the mean (Table 5.1, Fig. 5.5). The data for the '2%' and '4%' applied strain cases are predicted well by scaling the curves for the '6%' applied strain by 1/3 and 2/3, respectively (keeping b constant) (e.g., Fig. 5.4 c,d). Only in the case of the 15mm inclusion in the circumferential direction were the R^2 values slightly lower for the predicted curves than the individually fit curves. Thus, the strain pattern appears to be

independent of applied strain and the strain magnitude proportional to applied strain. There is no clear relationship between the parameters values for the different inclusion sizes (data not shown).

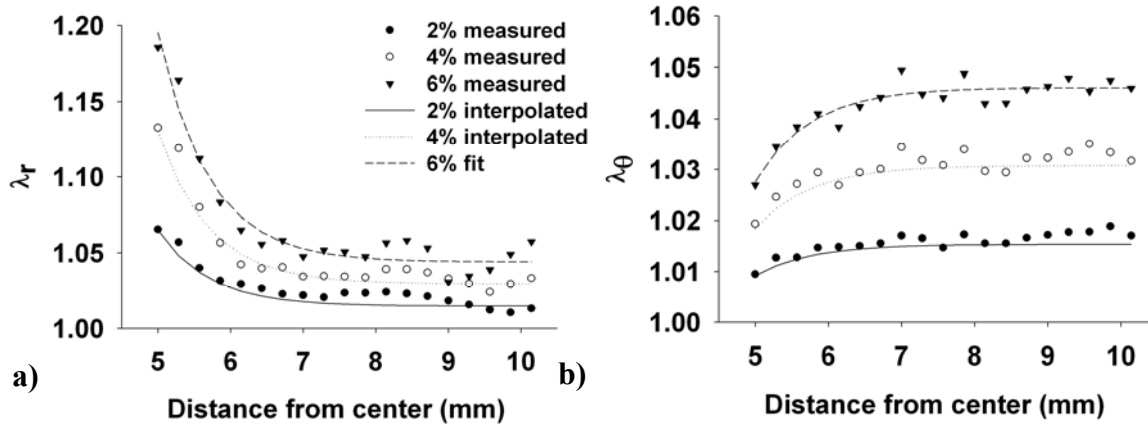


Fig. 5.5 a) Radial and b) circumferential stretch ratio data plotted from the edge of the 10mm diameter inclusion towards the stretched edge of the membrane (same mean data shown in Fig. 5.4 c&d plotted without SEM for clarity). The plots demonstrate the goodness of fit of the ‘6%’ applied strain (top curve) with the model (Eqns. 5.6, $R^2 = 0.95$ radial and $R^2 = 0.84$ circumferential) and the accuracy of the predicted curves for the ‘2%’ and ‘4%’ applied strain cases.

The resulting distribution of radial and circumferential strains across the membrane creates a continuous range of strain anisotropy from strip biaxial at the edge of the inclusion to equibiaxial strain near the edge of the membrane (Fig. 5.6). The strain anisotropy is highly dependent on inclusion size with maximum strain anisotropy ($\lambda_r - 1 / \lambda_\theta - 1$) of 3.9, 7.1, and for systems with inclusion sizes 5, 10, or 15mm in diameter, respectively. Since the strain field is proportional to the vacuum pressure, the anisotropy is not affected by the applied strain level.

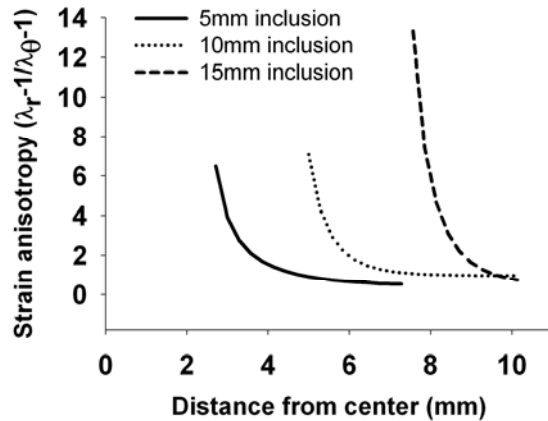


Fig. 5.6 Stretch anisotropy for ‘6%’ applied strain as a function of radial distance from center for each inclusion size. The plots demonstrate the continuous variation of anisotropy from strip biaxial (i.e., pure uniaxial with no transverse strain) at the edge of the inclusion, to equibiaxial near the outer edge.

Curves generated from fit parameters for our data (Table 5.1) are plotted with normalized radius ($r_{inclusion}/r_{outer}$) in Fig. 5.7. As mentioned previously, data are only plotted to 80% of the platen radius due to edge effects causing poor reproducibility beyond this region. Digitized data from Moore and colleagues [29] scaled to ‘6%’ applied strain and interpolated to the relative size of the inclusions utilized in this study are also plotted for comparison (Fig. 5.7). The general trends of measured strain distribution in the radial and circumferential direction were similar to those predicted, although our measured peak values of radial strain and steepness strain gradients were substantially higher. Theoretically, the circumferential stretch ratio is zero at the edge of the inclusion; however, due to measurement limitations this value is not observed (see Discussion). Further, unlike the predicted circumferential stretch ratios which approach 1.06 at the outer radius regardless of inclusion size due to the displacement boundary condition, the measured stretch ratios level off at progressively lower values as the size of the inclusion increases.

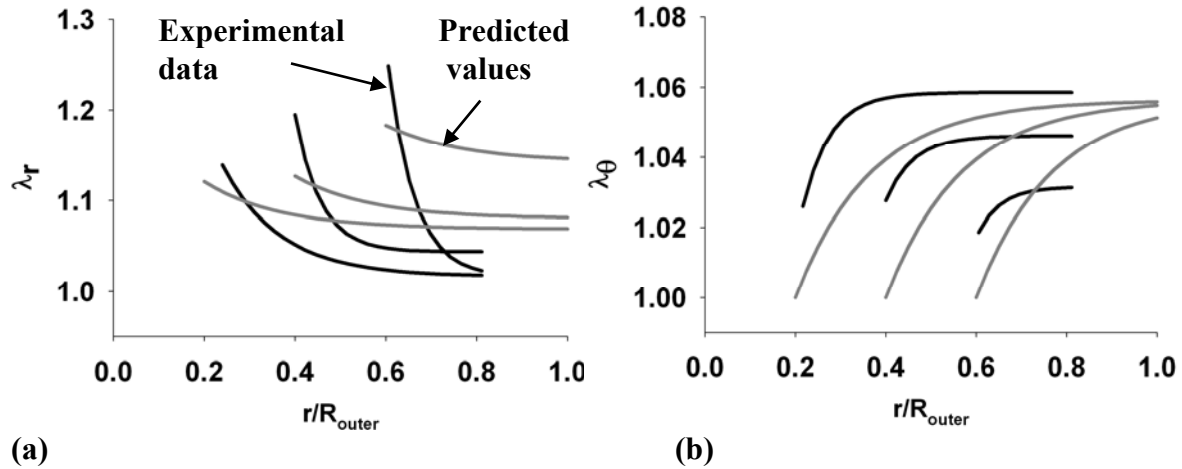


Fig. 5.7 Comparison of ‘6%’ applied strain data for a) radial and b) circumferential directions from this study (black lines) and scaled data from Mori et al., 2005 (grey lines). For direct comparison, curves are generated from fit parameters for our data and from digitized data from Mori et al. scaled to ‘6%’ applied strain and interpolated to the relative size of the inclusions utilized in this study (see Methods for details). Note that the radial stretch ratios at the edge of the inclusion underrepresent the true peak strain due to the subimage size (32 pixels, 0.58 mm) required for the displacement mapping, and that the circumferential stretch ratio at the edge of the inclusion is physically constrained at 1.0, yet could not be measured

5.3.4. Effect of ring inserts on global strain distribution

By placing Delrin rings around the platens to limit the travel of the membrane, the vacuum-driven stretching device was modified to simultaneously apply different levels of ‘applied strain’ at a single vacuum pressure (Fig. 5.8). With the inserts in place, there was no increase in average ‘applied strain’ across the membrane when pressures were increased from 52kPa (corresponding to 10% equibiaxial strain without inserts) to 89kPa (corresponding to 20% equibiaxial strain without inserts) (refer to Appendix). The addition of inserts with heights of 6.0, 6.5, 7.0, and 7.5mm resulted in average equibiaxial applied strains of 13.0%, 5.5%, 3.1%, and 0.1% respectively (all with 89kPa applied vacuum, Fig. 5.8). The height to strain data was fit logarithmically (ring height = $-0.685\text{LN}(\% \text{ strain}) + 4.58$, $R^2 = 0.99$). This relationship predicts that a 6.15mm ring height would yield ‘10%’ applied strain. The strain resulting from 6.15mm inserts with 89kPa vacuum was $e_r = 9.52\% \pm 1.5\%$ and $e_\theta = 9.75\% \pm 1.4\%$, as measured using HDM (n=2). Due to the lower resolution of images used for assessing homogeneity across the entirety of the membrane in response to the addition of inserts, for this analysis the standard deviation for the Gaussian filter was increased to 0.5.

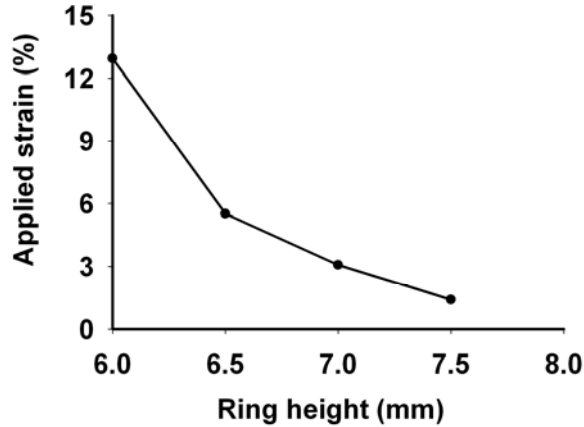


Fig. 5.8. A) Relationship between the height of the Delrin inserts and the resulting applied strain for a mechanically loaded silicone membrane. Inserts with a height less than 6mm did not result in a notable decrease in strain magnitude. A sample size of two was utilized for each measurement.

5.3.5. *Effect of an inhomogeneous strain field created by rigid inclusion in 3D*

After 8 days of cycling at ‘6%’ applied strain, strain distributions in the 3D inclusion systems (fibrin gel cast onto a 5mm coverslip) were similar to 2D systems in terms of radial and circumferential stretch ratios (Fig. 5.9), indicating that there does appear to be a strain gradient through the thickness of the fibrin gel. Despite these overall similarities in strain distribution, peak radial values were blunted $\lambda_{r_{\max}} = 1.14$ and there was apparent deformation on the surface of the inclusion that is not evident in the 2D systems.

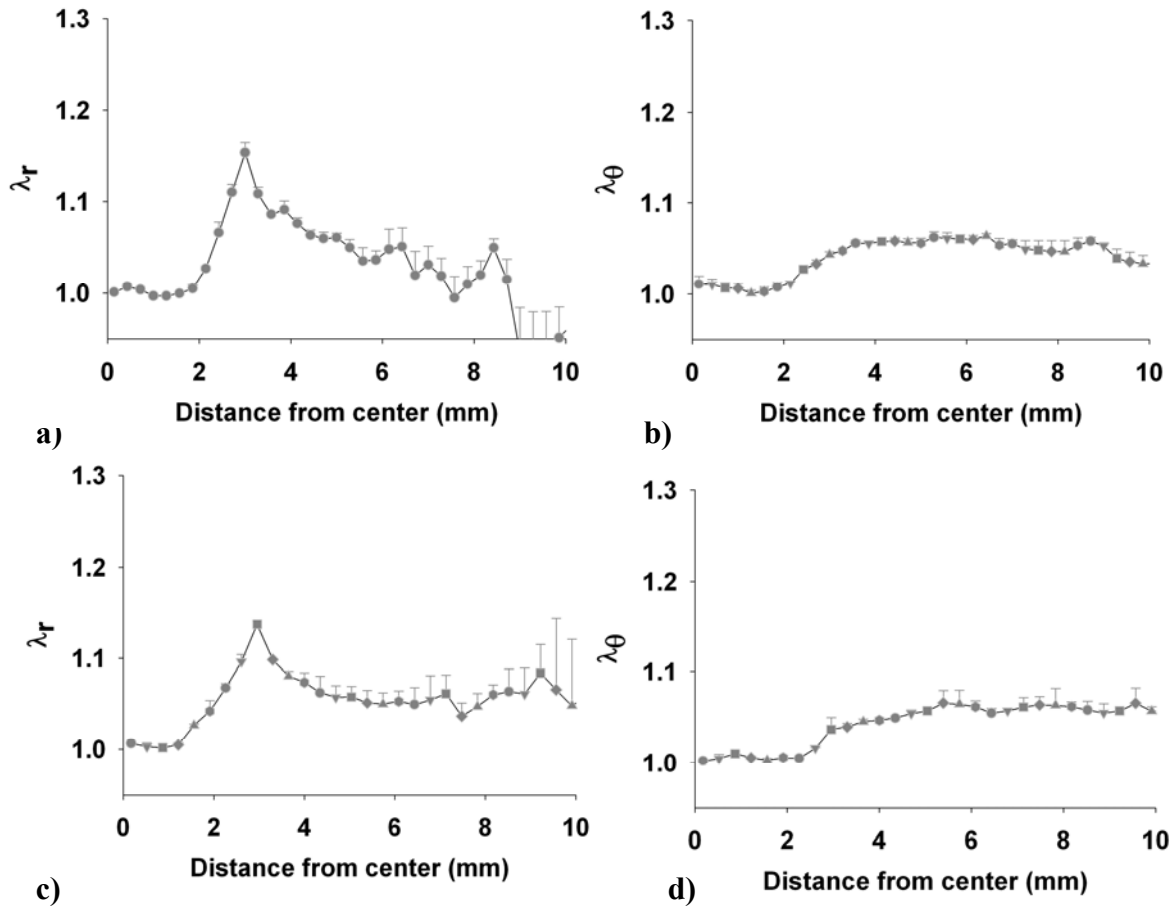


Fig. 5.9. Effect of deformation of the 5mm inclusion system with and without a fibroblast-populated fibrin gel. a) 2D radial and b) circumferential stretch ratios across silicone membranes cycled to ‘6%’ applied strain c) 3D radial and d) circumferential stretch ratios across a fibrin gel cycled to ‘6%’ applied strain. Note that although the strain distributions are similar between 2D and 3D systems, the peak radial values in the 3D system are blunted as compared to the 2D system. Mean \pm SEM plotted; n=2 and n=4 wells for 3D and 2D data, respectively.

5.3.6. *Effect of an inhomogeneous strain field created by rigid inclusion on cell orientation in 2D*

To demonstrate that cell orientation is impacted even under low strain conditions, fibroblasts were conditioned for 2 days using ‘2%’ applied strain (vacuum pressure of 13kPa) with 5mm diameter inclusions. Fibroblasts oriented themselves in the direction of principal strain, with preferred alignment most pronounced in the ‘strip biaxial’ zone. Representative images of cells and the cell orientation angle distributions are shown in Fig. 5.10. In the ‘strip biaxial zone’ (2.8mm from the center, $\lambda_r-1/\lambda_\theta-1 \sim 6.5$), 80% of cells oriented perpendicular to principal strain (between 0-15° with respect to Cartesian coordinates), which is parallel to the edge of the

inclusion. Cells in the ‘biaxial zone’ (3.3mm from the center, $\lambda_r-1/\lambda_\theta-1 \sim 2.8$) also oriented themselves to the direction of perpendicular to strain, although this response was less than seen in the ‘strip biaxial zone’ (58% oriented between 0-15°). Cells in the ‘equibiaxial zone’ (4.7mm from the center, $\lambda_r-1/\lambda_\theta-1 \sim 1.03$) and cultured on the control stretched sample showed no preferred alignment (23% orientated between 0-15°).

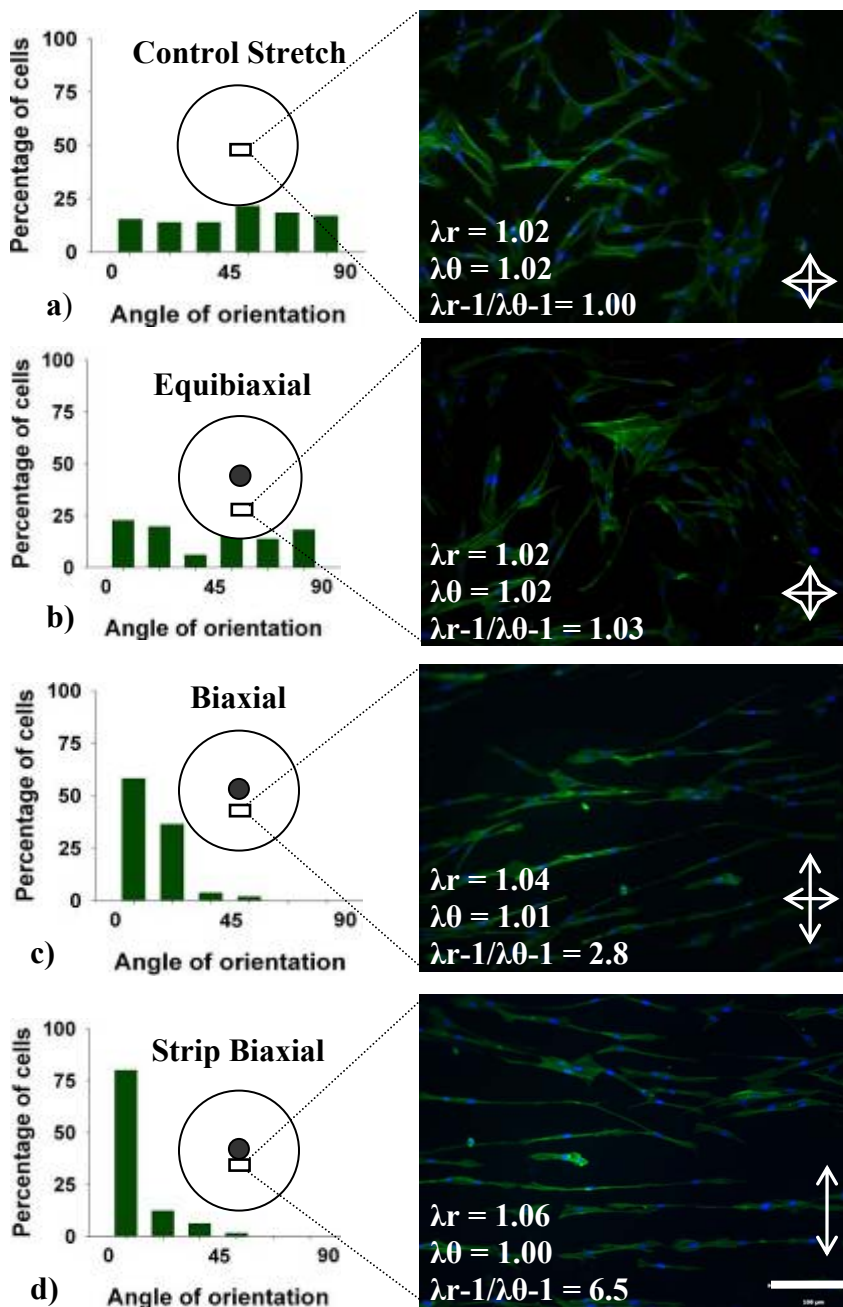


Fig. 5.10. Representative images of human dermal fibroblasts cultured on membranes with 5mm diameter inclusions for two days at 0.2Hz at ‘2%’ applied strain. Cells fluorescently stained with phallotoxin and Hoechst, and the corresponding cell orientation angle in response to a) equibiaxial stretch control (no inclusion), and for in the rigid inclusion model at b) equibiaxial strain (4.7mm from center), c) biaxial (3.3mm from center), and d) strip biaxial (2.7mm from center). The boxes in the schematics demonstrate the location in the wells that the images were acquired. Scale bar represents 100 μ m. Arrows in the bottom right corner indicate directions and relative magnitudes of stretch.

5.3.7. *Effect of an inhomogeneous strain field created by rigid inclusion on cell orientation in 3D*

To investigate cell orientation in response to non-homogeneous strain in 3D, fibroblast-populated fibrin gels were cast into wells with 5mm diameter inclusions, conditioned for 8 days at 6 hours per day using ‘6%’ applied strain (vacuum pressure of 35kPa). Representative confocal images of cells and histological micrographs are shown in Fig. 5.11. Gross observation indicated that gels stretched with a centrally adhered inclusion were substantially thinner and more transparent around the inclusion, and this transparency was not apparent in the stretched controls. Similar to fibroblasts in 2D, fibroblasts in 3D oriented themselves in the direction of principal strain, with preferred alignment most pronounced in the ‘strip biaxial’ zone near the inclusion and not preferred in the ‘equibiaxial zone’. Histological images reveal that fibroblasts compacted their surrounding matrix in response to increasing radial strain magnitude, i.e. the tissue in the ‘strip biaxial’ zone was substantially more compacted than in the biaxial or equibiaxial zone, and tissue appeared to increase in thickness with increasing distance from the inclusion. In addition, both the fiber density and cell number appear to be substantially lower in the inclusion samples (globally) than in stretched controls, resulting in areas that were 4 fold thinner than statically-cultured controls.

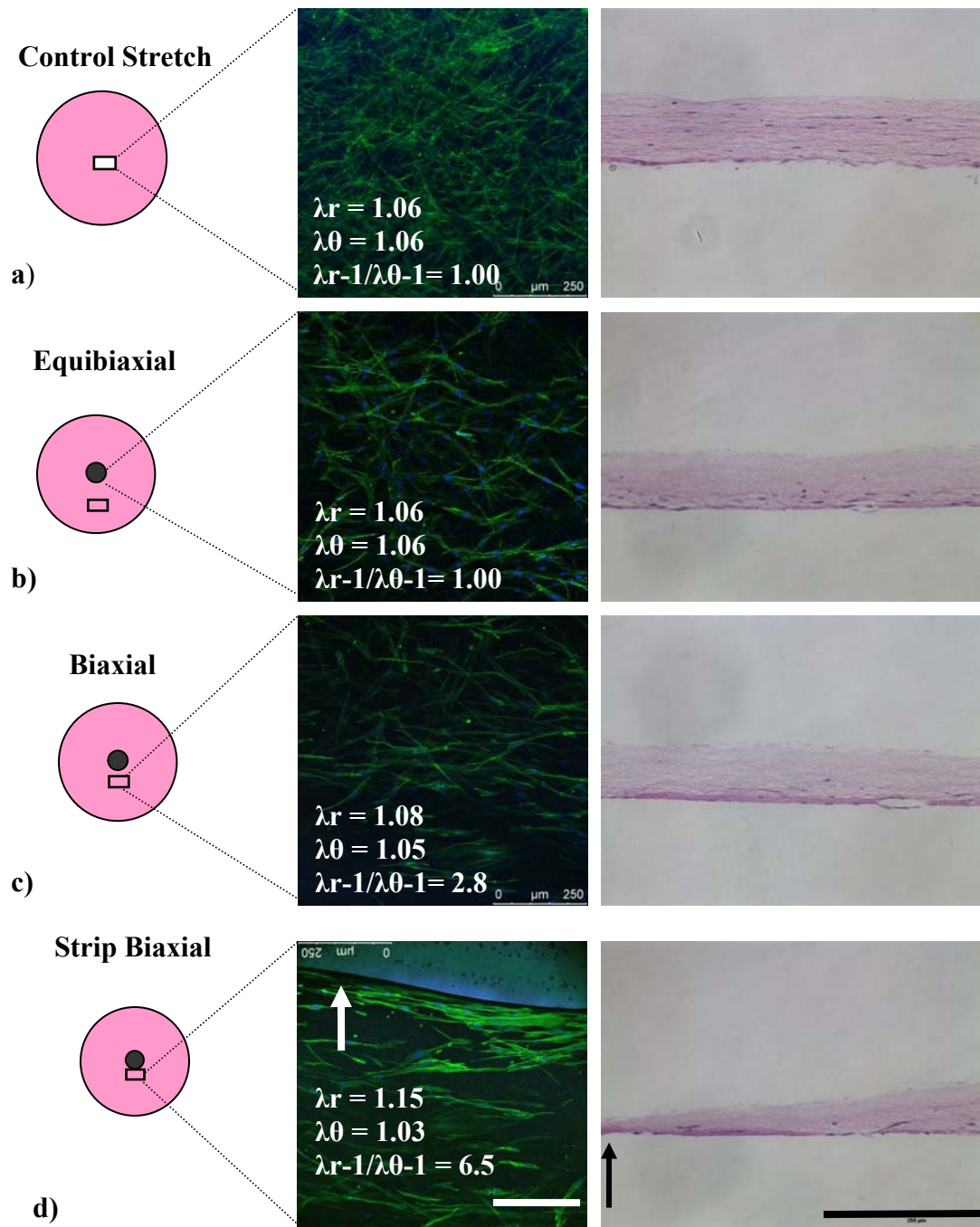


Fig. 5.11. Representative confocal and histological H&E images of human dermal fibroblasts cultured in fibrin gels with 5mm diameter inclusions for eight days at 0.2Hz at '6%' applied strain. Cells fluorescently stained with phallotoxin and Hoechst, and the corresponding cell orientation in response to a) equibiaxial stretch control, and for in the rigid inclusion model at b) equibiaxial strain (5 mm from center), c) biaxial (3 mm from center), and d) strip biaxial (2.5 mm from center). Histological images shown here are from radial cross sections from each sample. Arrows represent the edge of the inclusion. The boxes in the schematics demonstrate the location in the wells that the images were acquired. Scale bar represents 250 μm .

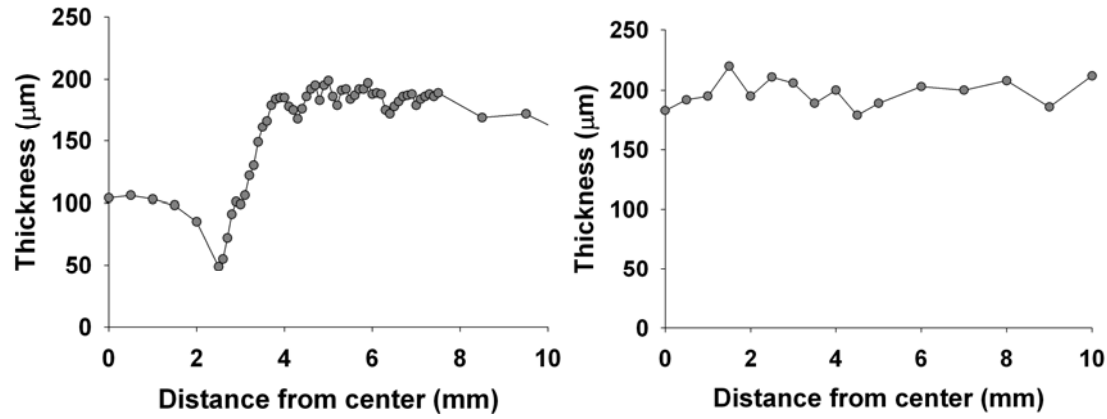


Fig. 5.12. Representative thickness of fibrin gels taken from histological H&E images of human dermal fibroblasts cultured in fibrin gels a) with and b) without (equibiaxial stretched control) 5mm diameter inclusions for eight days at 0.2Hz at ‘6%’ applied strain. Arrow represents the edge of the inclusion (corresponding to 45 µm)

5.4. Discussion

In this report, we describe the development and validation of an experimental system for the study of strain magnitude and anisotropy effects on cell behavior *in vitro*. By adding a rigid circular inclusion to the center of a radially stretched membrane we are able to create controlled gradients of strain in the radial and circumferential directions resulting in a continuous spectrum of stretch magnitudes and axial ratios of stretch, ranging from strip biaxial to equibiaxial stretch. At a given vacuum pressure, the inclusions create up to a 4-fold increase in maximum radial strain as compared to an unaltered membrane (23.7% peak strain versus 6% equibiaxial strain), a gradient of radial strain up to 33.8%/mm, and a maximal strain anisotropy ($\lambda_r-1/\lambda_\theta-1$) of 13.3. Regression models relating stretch to radial position, applied strain (vacuum pressure), and inclusion size facilitate calculation of strain gradients, stretch ratios, and amounts of anisotropy applied to cells under particular sets of experimental conditions. Additionally, we demonstrate that strain values can be independently altered on a per well basis with the addition of ring inserts. Finally, our pilot study demonstrates the utility of the device for use in 2D and 3D systems by determining the effect of graded levels of strain anisotropy on cell orientation and tissue reorganization.

5.4.1. Gradients of strain can be 'tuned' by altering applied strain or the inclusion size

To isolate the effects of gradients, specific regions of membranes with different sized inclusions can be examined at various levels of applied strain. By judiciously choosing combinations of these parameters, one may obtain regions with desired levels of stretch gradient, magnitude, and anisotropy. The gradients in a specific region may be calculated by taking the derivatives of Eqns. 5.6 with respect to radius and utilizing the appropriate coefficients for the regression models presented in Table 5.1 (note: the 'b' value must be divided by the outer radius to obtain gradient in physical units e.g., mm^{-1}). The corresponding stretch ratios are obtained directly from Eqns. 5.6 for the given radius, and the anisotropy is calculated by dividing the radial and circumferential strains. For example, the 10mm inclusion can be used to investigate the differential cell response for three different radial stretch gradients, -10, -5, and -2.5 %/mm, by applying 6% strain and examining the cells at $r = 5.54, 6.03, \text{ and } 6.51\text{mm}$, respectively. As a control for anisotropy, the same gradients can be obtained by applying '4%' strain and examining the cells at $r = 5.256, 5.741, \text{ and } 6.23\text{mm}$, respectively. Under these conditions both the radial gradients and radial stretch ratios are identical, but the circumferential stretch is lower resulting in slightly higher anisotropy. Alternately, the same gradients (-10, -5, and -2.5 %/mm) can be obtained with the 5 mm inclusion by applying '6%' strain and examining the cells at $r = 2.81, 3.73, \text{ and } 4.66\text{mm}$, respectively. For the smaller inclusion, the radial strains and anisotropy are generally higher. If subjecting cells to continuous gradients of strain and anisotropy is not desired in a particular study, cells could be constrained to specific stretch patterns by simply utilizing contact printing with surface proteins to create cell attachment in areas with very specific stretch regimes.

5.4.2. Benefit of a planar, radially symmetric system

Clearly, a purely one-dimensional gradient of strain magnitude would allow more straightforward analysis of the effects of strain gradients on cell behavior than coupled gradients of strain magnitude and anisotropy. In theory, a one-dimensional gradient could be

accomplished by uniaxially stretching a membrane produced with a gradient of stiffness or thickness; however, in practice, each of these scenarios would produce complex two-dimensional strain patterns due to the non-uniform stress patterns in the membrane and uneven lateral contraction (Poisson effect) along the length of the membrane. Recently, in an analogous method as used herein, Mooney and colleagues [25] affixed a rigid glass material to the bottom of a uniaxially stretched planar compliant culture substrate in an effort to produce a one-dimensional strain gradient. Unfortunately, the two-dimensional deformation field resulting from this modification was not fully analyzed, thus the effects of the inclusion and culture well boundaries on the strain field are not clear. In particular, because this system consists of a membrane that is roughly square, the shear and transverse strains may be substantial resulting in cells being subjected to complex local strain patterns. The radially symmetric nature of our design yields consistent two-dimensional strain gradients with low shear strain.

The orthogonal radial and circumferential strain gradients produce controlled anisotropy levels that span between uniaxial, strip biaxial and equibiaxial strain (Fig. 5.10). These differential strain patterns can be utilized to investigate cell behavior under a variety of mechanical conditions. One application for this system would be investigating cell reorientation to stretch. In 2D systems, fibroblasts and many other cell types have been shown to align to the direction of minimum principal strain which is perpendicular to the direction of pure uniaxial stretch i.e., strip biaxial with zero transverse strain [21] or slightly off axis in standard uniaxial stretch due to with negative transverse strain produced by the Poisson effect [6, 12]. However, to our knowledge, no studies exist which examine how cells respond to strain anisotropies that span in between these orientations of stretch or along a continuous gradient of strain. In our preliminary 2D study, substantial fibroblast reorientation is demonstrated with only slight stretch anisotropy ($\lambda_r-1/\lambda_\theta-1 = 2.8$ at $r = 3.3\text{mm}$, 1.04:1.01), and more pronounced orientation is observed at higher levels of anisotropy ($\lambda_r-1/\lambda_\theta-1 = 6.5$ at $r = 2.8$, 1.06:1.00). Studies utilizing our system could also be used to test the robustness of models of stretch-induced cytoskeletal reorganization and combined effects with small molecules which alter orientation [32].

Interestingly, our study differs with findings from previous studies where fibroblasts in a 3D matrix oriented themselves towards the direction of principal strain [1, 33]. It is possible that

the dramatic increase in strain magnitude (i.e., strain gradient) at the edge of the inclusion induced a heightened level of matrix remodeling, resulting in substantial degradation of the matrix and a lack of scaffolding. In a previous study by Seliktar and his colleagues, an increase in strain magnitude resulted in an increase in the production of MMP-2 and MMP-9, proteolytic enzymes involved in matrix degradation [34]. Both confocal and histological images near the edge of the inclusion (i.e., strip biaxial zone) indicate that this area of the tissue is substantially less cell-populated than any other area of the gel or in stretched controls. In addition, polarized light microscopy was attempted without success due to the insufficient amount of matrix fibers in the inclusion samples (see appendix).

5.4.3. Isolating anisotropy, gradient and magnitude effects

Although the observed cell orientation in response to the direction of stretch is consistent with previous studies [21], it is important to note that the magnitude of strain was different in the regions analyzed in this study (e.g., 6% radial strain in the strip biaxial region yet only 2% radial strain in the equibiaxial region). The non-uniformities produced by the inclusion simultaneously alter both the strain magnitude and anisotropy; therefore, isolating these two effects requires utilizing proper controls. As the pattern of anisotropy is independent of applied strain (both radial and circumferential strains are proportional to applied strain as shown in Fig. 5.6), cells exposed to the same anisotropy but different strain magnitudes can be studied by examining cells at the same radial position exposed to different levels of applied strain. The applied strain can be altered either globally (for all 24 wells) by changing the applied vacuum pressure or locally by applying a high level of vacuum to all wells and adding inserts to limit membrane deformation differently in each well. This modification, first proposed by Boerboom et al. [30], allows for multiple strain magnitudes (and thus controls) to be run in parallel on the Flexcell system without the use of multiple pressure control units. Interestingly, although the trends of restricted deformation as a function of insert size are similar to those previously reported [30], the relationship between applied strain and ring height differs. This discrepancy is likely due to physical alterations to the membrane in the previous study and differences in our platen design (e.g., equibiaxial as opposed to uniaxial design). To examine specific strain fields of interest,

one could utilize contact printing using surface proteins (e.g., collagen I) to culture cells in specific loading areas. This method would allow for the isolation of cellular response by minimizing cell-cell contact or paracrine soluble factors secreted by neighboring cells undergoing different strain patterns.

5.4.4. Optimization of effective resolution

As described in the methods, to acquire accurate measurements of strain while minimizing noise, we employed a high density displacement mapping technique (HDM) with subpixel resolution, utilized an optimal subimage size, and filtered the data to remove spurious points. HDM measures the displacement of random light intensity patterns created by surface markers using phase correlation rather than image cross-correlation, resulting in an accuracy of 0.09 pixels and a precision of 0.02 pixels [35]. Despite the high accuracy of this technique, as with all image analysis-based strain field measurement methods, the effective spatial resolution is limited by resolution of the camera, the need for finite sized sub-regions, filtering of spurious values (e.g., due to reflections), and averaging or smoothing necessary for taking derivatives (du/dx). Although a high resolution camera is used (1280 x 1024 pixels), small sub-regions of multiple pixels (e.g., 32x32) must be analyzed for accurate correlation of displacement and the reduction of noise. Measuring the relative displacement of sub-regions rather than individual pixels effectively ‘blunts’ the data and reduces the effective resolution (c.f., Fig. 5.3a, b, and c). For example, although the ‘absolute resolution’ of HDM is based on a subpixel displacement, the difference in strain between any two locations (i.e., ‘gradient resolution’) is limited by the pixel shift (16 pixels \sim 0.3mm). In addition, taking derivatives of displacement over five data points (16 pixels each) also contributes to the overall smoothing of data and lowering of the gradient resolution. The point-by-point removal of spurious data using the 2D Gaussian filter is accomplished by using a small window size (3x3) and low standard deviation, thus erroneous data points were removed with minimal filtering of surrounding data and a negligible decrease in the effective resolution.

5.4.5. Our findings of symmetric strain gradients support the predictions of Moore and colleagues

The general trends of strain distribution in our study were similar to those predicted by Moore and colleagues [29], although our measured peak values of radial strain and steepness strain gradients were much higher (Fig. 5.8). Variance from the predicted results can be attributed to both theoretical differences (e.g., different boundary conditions) and experimental limitations (e.g., averaging of sub-regions of the membrane necessary for accurate correlation). In terms of boundary conditions, the strain is applied differently in our system than in the numerical analysis. In the numerical analysis, a displacement is applied to the outer boundary of the membrane resulting in a defined circumferential strain at the outer radius and sequentially higher radial strains with increasing inclusion size due to the decreasing ‘gauge length’. In contrast, our method of loading involves a vacuum pressure being applied to the lower surface of the membrane between the edge of the platen and the fixed outer boundary (Fig. 5.2b). Because the inclusion restricts the free motion of the membrane, at a given pressure the displacement at the edge of the platen decreases with increasing inclusion size. This increase in effective global stiffness creates lower circumferential and radial strains at the boundary than would occur with a displacement boundary condition (e.g., circumferential strain near the edge of the platen with a 10mm inclusion is less than 5% when vacuum pressure corresponding to ‘6%’ strain is applied, see Fig. 5.4d). The second source of variance from the numerical analysis results from physical restrictions: the peak strains and strain gradients are effectively ‘blunted’ due to limitations in the ‘gradient resolution’ (discussed in the above section); and the rate of increase in radial strain at the edge of the platen is physically limited since a step increase to the peak value predicted at the edge of the inclusion in the numerical study is not physically possible. At present it is unclear why we observe higher radial strains and steeper gradients than predicted by Moore and colleagues, as the experimental limitations should result in lower peak strain values and less steep curves.

5.4.6. Restrictions to utilizing the proposed system

It should be noted that there are a few restrictions to using the proposed rigid inclusion system. In order to ensure radial symmetry of the strain distribution, it is essential that the glass coverslip be evenly attached (even distribution of silicone glue across the coverslip) and absolutely central to the membrane. Also, due to edge effects necessitating the restriction of cell attachment the central 20mm region of membrane, using larger diameter inclusions will result in a limited area for cell attachment. Specifically, using 5, 10, and 15mm inclusion result in a total usable surface areas of 295, 236, and 138mm² (94, 75, or 44% of the total surface area), respectively. Finally, utilizing the ring inserts to manipulate strain magnitude will effectively blunt the waveforms resulting in a ‘square’ waveform. This adjustment in waveform may not be appropriate for all studies (e.g., studies requiring a sinusoidal or other special waveform). To mitigate the effects of this alteration in the loading curve, validations in this study were performed using a square waveform.

5.4.7. Conclusions and summary

Our new model system allows for the simultaneous study of cells exposed to different stretch magnitudes and deformation patterns within a single well and provides a method for directly studying the effect of gradients of stretch and stretch anisotropy on cell biology. The commercial availability of the apparatus utilized in our system and the straightforward modifications to the wells allow for adoption in laboratories without access to complex equipment. Studies using this device and method could provide valuable information on cellular adaptation to complex or changing mechanical environments produced by clinical interventions (e.g., stents, prostheses, etc.), and possibly help understand mechanism underlying propagation of stiff fibrotic foci as observed in diseases such as idiopathic pulmonary fibrosis. In the future, we will examine the use of this system in three-dimensional studies in combination with cytokines such as TGF- β to assess gradient affects on cell-mediated remodeling as seen during wound healing and fibrocontractive diseases. In conclusion, this system represents a new tool which may assist in the understanding the relationship between the complex and dynamic mechanical extracellular environment and cell behavior.

5.4.8. Acknowledgements

The authors would like to thank Piyush Ramuka for his assistance with MATLAB, Neil Whitehouse for his assistance with machining, and Tim Ebner, Roxanne Skowran, Angela Throm, and Andrew Capulli for their technical assistance in the laboratory. In addition, the authors would like to thank Dr. Daniel Tschumperlin for his valuable discussions on the topic of strain inhomogeneity and cell behavior. This work was supported in part by the U.S. Army Medical Research and Materiel Command (USAMRC); grant BFR08-1011-N00 (KLB), and by the American Heart Association; Scientist Development Grant 0635013N (GRG).

5.5 References

- [1] Eastwood, M., McGrouther, D. A., and Brown, R. A., 1998, "Fibroblast responses to mechanical forces," *Proc Inst Mech Eng [H]*, 212(2), pp. 85-92.
- [2] Giannone, G., and Sheetz, M. P., 2006, "Substrate rigidity and force define form through tyrosine phosphatase and kinase pathways," *Trends Cell Biol*, 16(4).
- [3] Ingber, D. E., 1997, "Tensegrity: the architectural basis of cellular mechanotransduction," *Annu Rev Physiol*, 59, pp. 575-599.
- [4] Zhang, S., Garbutt, V., and McBride, J. T., 1996, "Strain-induced growth of the immature lung," *J Appl Physiol*, 81(4), pp. 1471-1476.
- [5] Aarabi, S., Bhatt, K. A., Shi, Y., Paterno, J., Chang, E. I., Loh, S. A., Holmes, J. W., Longaker, M. T., Yee, H., and Gurtner, G. C., 2007, "Mechanical load initiates hypertrophic scar formation through decreased cellular apoptosis," *FASEB J*, 21(12), pp. 3250-3261.
- [6] Mudera, V. C., Pleass, R., Eastwood, M., Tarnuzzer, R., Schultz, G., Khaw, P., McGrouther, D. A., and Brown, R. A., 2000, "Molecular responses of human dermal fibroblasts to dual cues: contact guidance and mechanical load," *Cell Motil Cytoskeleton*, 45(1), pp. 1-9.
- [7] Lee, A. A., Delhaas, T., McCulloch, A. D., and Villarreal, F. J., 1999, "Differential responses of adult cardiac fibroblasts to in vitro biaxial strain patterns," *J Mol Cell Cardiol*, 31(10), pp. 1833-1843.
- [8] Nishimura, K., Blume, P., Ohgi, S., and Sumpio, B. E., 2007, "Effect of different frequencies of tensile strain on human dermal fibroblast proliferation and survival," *Wound Repair Regen*, 15(5), pp. 646-656.
- [9] Arold, S. P., Wong, J. Y., and Suki, B., 2007, "Design of a new stretching apparatus and the effects of cyclic strain and substratum on mouse lung epithelial-12 cells," *Ann Biomed Eng*, 35(7), pp. 1156-1164. .
- [10] Loesberg, W. A., Walboomers, X. F., van Loon, J. J., and Jansen, J. A., 2005, "The effect of combined cyclic mechanical stretching and microgrooved surface topography on the behavior of fibroblasts," *J Biomed Mater Res A*, 75(3), pp. 723-732.

- [11] Breen, E. C., Fu, Z., and Normand, H., 1999, "Calcyclin gene expression is increased by mechanical strain in fibroblasts and lung," *Am J Respir Cell Mol Biol*, 21(6), pp. 746-752.
- [12] Raeber, G. P., Lutolf, M. P., and Hubbell, J. A., 2008, "Part II: Fibroblasts preferentially migrate in the direction of principal strain," *Biomech Model Mechanobiol*, 7(3), pp. 215-225. .
- [13] Katsumi, A., Naoe, T., Matsushita, T., Kaibuchi, K., and Schwartz, M. A., 2005, "Integrin activation and matrix binding mediate cellular responses to mechanical stretch," *J Biol Chem*, 280(17), pp. 16546-16549.
- [14] Wang, J. H., Yang, G., and Li, Z., 2005, "Controlling cell responses to cyclic mechanical stretching," *Ann Biomed Eng*, 33(3), pp. 337-342.
- [15] Hashima, A. R., Young, A. A., McCulloch, A. D., and Waldman, L. K., 1993, "Nonhomogeneous analysis of epicardial strain distributions during acute myocardial ischemia in the dog," *J Biomech*, 26(1), pp. 19-35.
- [16] Oomens, C. W., van Ratingen, M. R., Janssen, J. D., Kok, J. J., and Hendriks, M. A., 1993, "A numerical-experimental method for a mechanical characterization of biological materials," *J Biomech*, 26(4-5), pp. 617-621.
- [17] Dartsch, P. C., Hammerle, H., and Betz, E., 1986, "Orientation of cultured arterial smooth muscle cells growing on cyclically stretched substrates," *Acta Anat (Basel)*, 125(2), pp. 108-113.
- [18] Kulik, T. J., and Alvarado, S. P., 1993, "Effect of stretch on growth and collagen synthesis in cultured rat and lamb pulmonary arterial smooth muscle cells," *J Cell Physiol*, 157(3), pp. 615-624.
- [19] Berry, C. C., Cacou, C., Lee, D. A., Bader, D. L., and Shelton, J. C., 2003, "Dermal fibroblasts respond to mechanical conditioning in a strain profile dependent manner," *Biorheology*, 40(1-3), pp. 337-345.
- [20] Shelton, J. C., Bader, D. L., and Lee, D. A., 2003, "Mechanical conditioning influences the metabolic response of cell-seeded constructs," *Cells Tissues Organs*, 175(3), pp. 140-150.
- [21] Wang, J. H., Goldschmidt-Clermont, P., Moldovan, N., and Yin, F. C., 2000, "Leukotrienes and tyrosine phosphorylation mediate stretching-induced actin cytoskeletal remodeling in endothelial cells," *Cell Motil Cytoskeleton*, 46(2), pp. 137-145.
- [22] Balestrini, J. L., and Billiar, K. L., 2009, "Magnitude and duration of stretch modulate fibroblast remodeling," *J Biomech Eng*, 131(5), p. 051005.
- [23] Boccafoschi, F., Bosetti, M., Gatti, S., and Cannas, M., 2007, "Dynamic fibroblast cultures: response to mechanical stretching," *Cell Adh Migr*, 1(3), pp. 124-128. .
- [24] Lo, C. M., Wang, H. B., Dembo, M., and Wang, Y. L., 2000, "Cell movement is guided by the rigidity of the substrate," *Biophys J*, 79(1), pp. 144-152.
- [25] Yung, Y. C., Vandenburgh, H., and Mooney, D. J., 2009, "Cellular strain assessment tool (CSAT): precision-controlled cyclic uniaxial tensile loading," *J Biomech*, 42(2), pp. 178-182.
- [26] Gilbert, J. A., Weinhold, P. S., Banes, A. J., Link, G. W., and Jones, G. L., 1994, "Strain profiles for circular cell culture plates containing flexible surfaces employed to mechanically deform cells in vitro," *J Biomech*, 27(9), pp. 1169-1177.

- [27] Williams, J. L., Chen, J. H., and Belloli, D. M., 1992, "Strain fields on cell stressing devices employing clamped circular elastic diaphragms as substrates," *J Biomech Eng*, 114(3), pp. 377-384.
- [28] Winston, F. K., Macarak, E. J., Gorfien, S. F., and Thibault, L. E., 1989, "A system to reproduce and quantify the biomechanical environment of the cell," *J Appl Physiol*, 67(1), pp. 397-405.
- [29] Mori, D., David, G., Humphrey, J. D., and Moore, J. E., Jr., 2005, "Stress distribution in a circular membrane with a central fixation," *J Biomech Eng*, 127(3), pp. 549-553.
- [30] Boerboom, R. A., Rubbens, M. P., Driessen, N. J., Bouten, C. V., and Baaijens, F. P., 2008, "Effect of strain magnitude on the tissue properties of engineered cardiovascular constructs," *Ann Biomed Eng*, 36(2), pp. 244-253.
- [31] Balestrini, J. L., and Billiar, K. L., 2006, "Equibiaxial cyclic stretch stimulates fibroblasts to rapidly remodel fibrin," *J Biomech*, 39(16), pp. 2983-2990.
- [32] Kaunas, R., Nguyen, P., Usami, S., and Chien, S., 2005, "Cooperative effects of Rho and mechanical stretch on stress fiber organization," *Proc Natl Acad Sci U S A*, 102(44), pp. 15895-15900.
- [33] Hinz, B., and Gabbiani, G., 2003, "Mechanisms of force generation and transmission by myofibroblasts," *Curr Opin Biotechnol*, 14(5), pp. 538-546.
- [34] Seliktar, D., Nerem, R. M., and Galis, Z. S., 2001, "The role of matrix metalloproteinase-2 in the remodeling of cell-seeded vascular constructs subjected to cyclic strain," *Annals of Biomedical Engineering*, 29(11), pp. 923-934.
- [35] Kelly, D. J., Azeloglu, E. U., Kochupura, P. V., Sharma, G. S., and Gaudette, G. R., 2007, "Accuracy and reproducibility of a subpixel extended phase correlation method to determine micron level displacements in the heart," *Med Eng Phys*, 29(1), pp. 154-162.

CHAPTER 6

Conclusions and future work

6.1. Overview

This thesis describes an investigation of how mechanical factors present in connective tissue during wound healing regulate cell-mediated matrix remodeling and changes in tissue architecture. Harnessing the relationship between stretch and matrix remodeling will provide new insights into the fundamental processes of wound healing, hyperplasia, and fibrosis and assist in creating tissue-engineered constructs with custom-tailored properties. We specifically isolate stretch effects on cell function independent of passive matrix in-plane alignment, established functional dose-response curves to quantify the relationship between stretch and remodeling, and developed a novel system to study the complex non-uniform nature of strains observed in connective tissue.

6.2. Isolating the effects of mechanical loading on cell-mediated matrix remodeling during fibroplasia

6.2.1. Minimizing fiber alignment to isolate stretch effects

We began our investigation of how mechanical cues influence fibroblast behavior in the early stages of wound healing by isolating the effects of mechanical stimulation on 3D planar tissue models. Previous to our original study, researchers had demonstrated significant increases in mechanical properties of uniaxially stretched cell-populated biopolymer gels [1-14], although it was unclear if these increases were cell-mediated or simply a result of passive alignment of the tissue. By applying equibiaxial stretch to fibroblast-populated fibrin gels, we were successful in minimizing in-plane alignment

previously observed in these uniaxially stretched systems [1, 15] and demonstrated that cyclic stretch actively stimulates fibroblasts to produce a stronger matrix by profoundly increasing tissue compaction, matrix fiber reorganization and collagen content. In addition, collagen cross-linking was found to play a major role in stretch-induced tissue compaction and compaction derived matrix strength but not the structural strengthening during this early culture period.

Increases in tensile strength in mechanically conditioned tissue equivalents have been suggested to result from increases in tissue compaction (often due to a decreased tissue thickness) [16, 17], fibril alignment, enhanced entanglement of the fibrils due to the increase in matrix density [9], intermolecular cell-fibril and fibril-fibril bonding, bundling of the fibrils, and crosslinking [18]. Previous investigators that utilized uniaxial stretch to collagen gels [16], fibrin gels [19], and collagen/fibrin blends [17] also observed substantial increases in tensile strength. Although our study indicates that the majority of increases in stretch-induced mechanical properties are primarily due to a decrease in tissue thickness, we did observe the presence of more subtle cell-mediated strengthening mechanisms such as collagen synthesis and crosslinking that were increased and contributed to the increased strength of the mechanically stimulated gels.

6.2.2. Establishing the relationship between stretch magnitude, duration of stimulation per day, and matrix remodeling

After determining that mechanical conditioning actively stimulates fibroblast remodeling behavior in fibrin gels, we sought to investigate how cells responded to different levels and durations (length per day) of mechanical conditioning. Using methodology developed in the previous study, we cycled fibrin gels for 2, 4, 8 or 16 % strain for either 6 (intermittent) or 24 (continuous) hours per day. As a result, we determined that stretch-induced fibroblast remodeling behavior was profoundly impacted by both the magnitude and duration of strain per day, as evidenced by dose-dependent responses of several functional remodeling metrics. We determined that tissue strength, stiffness, and the

Chapter 6: Conclusions and future work

accumulation of collagen increased with increasing stretch magnitude in all samples, and that cycling intermittently rather than continuously did not reduce the level of tissue compaction, UTS, or tissue retraction between these groups. Interestingly, stretch magnitude-dependent increases in cell number, extensibility, failure tension, and net collagen accumulation were contingent upon the introduction of a rest period during stimulation. It appears that reducing the mechanical loading time increases cellular capacity to remodel their surrounding tissue into a more cell populated, collagen-dense and functionally stronger tissue.

Although it is well known that mechanical stretch regulates a variety of aspects of cell function through a variety of mechanisms (e.g., regulation of cell cycle, integrin production, integrin confirmation, cell signaling pathways), which of these underlying mechanisms are altered by increasing the magnitude or introducing a rest period during mechanical conditioning is not yet understood. It is however becoming clear that cells within mechanically loaded tissues undergo an “adaptation response” to continuous signaling (one magnitude, stretched continuously); cells exposed to a constant mechanical stimuli initially demonstrate heightened activity but return to baseline levels after sustained mechanical stimulation [20-22]. For example, smooth muscle cells that are stretched continuously have been shown to undergo cell cycle arrest or “growth arrest” via the prevention of phosphorylation of key regulatory proteins involved in the transition from the late G₁ phase to the S phase [23]. It is therefore possible that utilizing intermittent stretch may disrupt this adaptation response by allowing for the continuation of cell cycle events, thus increasing the effectiveness of the mechanical conditioning on cell proliferation and matrix synthesis. This premise is supported by recent work from Tranquillo and colleagues where incrementally increasing stretch magnitude in fibrin gels resulted in higher ECM production, UTS, and cell number than cycling continuously at a given magnitude of stretch [14].

In addition, the introduction of a rest period, or the increase in stretch magnitude could have profound effects on cell activity by through the release of mediators, such as MMPs and transforming growth factor- β , which can regulate matrix remodeling processes such

as proliferation and matrix deposition. Finally, it has been suggested that the effects of cyclic stretch on cell proliferation and ECM production is matrix dependent and mediated by integrin binding to specific matrix proteins [24]. In the event of an increase in collagen or other ECM proteins as seen in our intermittent stretched samples, it is likely that the cell-ECM couplings would also be affected. It has also been established that incorporating a rest period during mechanical loading regulates fibroblasts to utilize completely separate cell signaling pathways than when loaded continuously [25]. Hu et al. demonstrated that mechanical stresses may directly alter receptor conformation to initiate signaling pathways normally used by growth factors; therefore, it is possible that differential stretch regimes would induce alterations in integrin upregulation and conformation resulting in the usage of separate signaling pathways [26]. Although it remains unclear as to which of these underlying mechanisms enhances cellular response during intermittent cycling, it is clear that cells reorganize and remodel their matrix differently when the level of mechanical stimulation is varied, and that this phenomenon should be investigated in future studies.

6.2.3. Determining passive and active stretch effects

Although we have demonstrated that mechanically stimulated cells actively compact their matrix through remodeling mechanisms (e.g., collagen crosslinking), it is important to note that the compaction of fibrin gels is in part a passive event. In our first study, we observed that cyclically stretching acellular fibrin gels resulted in a significant decrease in thickness relative to statically-cultured acellular fibrin gels. The passive compaction of the fibrin could simply be due to the increased proximity of fibers when stretched; fibrin is an adhesive molecule and, when condensed, could form intermolecular bonds between fibrils and stretch-induced entanglements. This phenomenon of passive compaction has been previously noted; Cummings *et al.* [27] also observed compaction of acellular gels, although not as marked as found in our first study. Passive compaction, or compaction that is not cell-mediated, can be problematic when attempting to isolate active cellular remodeling mechanisms. In addition, increases in passive tissue

compaction could also be impacting cell behavior and therefore remodeling activity. The increase in matrix density would result in an increase in cell density, potentially increasing functional cell-cell and cell-matrix interactions [17] and therefore remodeling capacity of the resident cells. Therefore, it is important to investigate the overall impact of stretch on the active and passive contributions to regulating cell function.

Measurements that are typically utilized to quantify intrinsic material properties and thus matrix remodeling are generally dependent on thickness (e.g., matrix density, UTS, Young's modulus), and therefore it can be difficult to isolate the active cellular contribution to these metrics. As seen in our first two studies, compaction results in very large decreases in matrix volume creating large changes in all intrinsic parameters; stretch-induced compaction could therefore obscure active (or more subtle) forms of cell-mediated remodeling. This scenario is illustrated in our second study where we investigated strain-magnitude dependent increases in UTS in continuously and intermittently stretched gels resulted at increasing strain magnitudes resulted in similar amounts of UTS. When comparing the strength of these tissues using UTS as a metric, the mechanical properties of these tissues is quite similar and is not significantly impacted by the duration of the stretch stimulus. When we examined structural properties of these tissues (i.e., not normalized to thickness), cycling fibrin gels intermittently rather than continuously resulted in a stronger tissue construct in terms of failure tension. Only by examining both intrinsic and structural properties were we capable of fully characterizing changes in tissue properties due to the different regimens of mechanical conditioning. Based on our findings, other researchers have begun to investigate both structural and intrinsic measurements of matrix properties [28].

6.3. Developing relevant mechanobiological models of wound healing in planar connective tissues

6.3.1. Fibrin gels as models of early wound healing

Chapter 6: Conclusions and future work

Although the bulk of studies investigating mechanoregulation in three-dimensional wound healing systems utilize collagen gels, we elected to utilize fibrin gels for our studies. Collagen gels are an excellent model of end-stage wound healing (remodeling) or fibrosis. However as we seek to investigate mechanical regulation in the initial stages of wound healing (i.e., fibroplasia), fibrin gels are a more appropriate model system. Fibrin, in combination with other components of the extracellular matrix, plays a vital role in the fibroproliferative response in wound healing through multiple mechanisms including a direct stimulation of cytokine production, modification of cytokine and growth factor activity, and modulation of the expression of matrix protein degrading proteases and their inhibitors [29, 30]. In addition, it has recently been suggested that fibrin may play a larger role in the tensile strength and remodeling of the provisional matrix than previously thought [31, 32]. The tensile strength is significantly lower during early stages of wound healing in fibrinogen-deficient mice, despite finding higher collagen levels [31]. These findings are supported by a study where scorbutic (scurvy-induced) animals maintained a normal rate of wound size reduction despite the obvious lack of collagen production [33]. In Chapter 3, we showed that aggregates of fibrin were observed in TEM micrographs of cyclically stretched fibrin gels, but they were not apparent in the statically grown fibrin gels. These formations suggest that cells could potentially be reorganizing and bundling fibrin; these bundles could potentially provide an interim source of mechanical stability prior to sufficient collagen accumulation and maturation. These findings are however quite preliminary, and further morphological investigation is required.

In the studies presented in this thesis, we elected to utilize neonatal fibroblasts as opposed to adult dermal fibroblasts or fibroblasts from alternative connective tissue types (e.g., lung fibroblasts). Neonatal fibroblasts are utilized extensively as models of connective tissue [25, 32, 34-39]; these cells produce more extracellular matrix and have a faster proliferation rate in culture than adult dermal fibroblasts [34]. In addition, due to the large amount of literature available on neonatal fibroblast response to mechanical stimulation, comparisons of our findings to previous research were feasible. In addition, previous research not included in this thesis indicated that dermal fibroblasts are

Chapter 6: Conclusions and future work

substantially less proteolytic than alternative fibroblast cell types (e.g., lung fibroblasts, valvular interstitial cells), enabling the investigation of mechanical regulation of fibroblast behavior without the necessity of using proteolytic inhibitors. In these studies, we elected not to block proteolytic activity using inhibitors in order to better understand how mechanical loading impacts matrix remodeling; although we did not directly measure proteolytic activity, we wanted to more accurately represent the response of cells to stretch in terms of protein degradation and synthesis. In addition, we did not utilize exogenous TGF- β 1 (growth factor) as it is well known that cyclic stretch and TGF- β 1 have synergistic effects on cell function [40], and we sought to isolate the impact of mechanical stretch alone on cell activity.

It is important to note that although fibrin gels as *in vitro* models do allow for the investigation of mechanobiological response of cells to mechanical cues, there are several limitations to using these analogs. Because these are simplified models of connective tissue, they do not include other important constituents found *in vivo* including immune system components (e.g., macrophages), exogenous growth factors (e.g., EN-1, TGF- β , EGF, etc) and alternative cell types in addition to fibroblasts found in connective tissue (e.g., epithelial and endothelial cells). In addition, the systems utilized in these studies do not allow for the investigation of fibroblast infiltration into the matrix, nor do they model interactive effects of chemoattractants and cell function. Further, because fibroblasts readily degrade the surrounding fibrin at a rapid rate, experimental duration using these systems is somewhat limited. Therefore it is difficult to ascertain the effects of longer term stimulation on cell function and measure therefore the functional changes in the tissue that would require more substantial culture durations (e.g., markers seen during pathological onset, appreciable collagen production). In order to circumvent fibroblast-mediated fibrin degradation, one option would be to utilize protease inhibitors such as ϵ -ACA or Aprotinin as done previously, or adjust the balance of protein synthesis and degradation by adding soluble factors such as TGF- β 1 that promote matrix production by fibroblasts. Future studies utilizing these factors would allow for the investigation of long term tissue remodeling as a function of mechanical loading, and also allow for the

investigation of modifying fibrin gel composition for use as tissue equivalents in regenerative medicine.

6.3.2. *Modeling the complex mechanical environment of connective tissue*

Although past investigations have provided a wealth of information regarding the response of cells to homogeneous mechanical stimulation, there is very little known about how cells respond to the complex strain fields found *in vivo*. In most studies, cells are plated on substrata that are deformed equibiaxially or uniaxially as uniformly as possible [25, 41, 42]. Although uniaxially stretched systems produce complex strain distributions as a result of edge effects present at the grips of the device, researchers typically focus on the area that is most uniformly deformed [25, 41, 42]. Strain distributions *in vivo* are often non-uniform, anisotropic (i.e., deformed at different magnitudes at different directions) and produce local gradients of strain magnitude [43, 44].

We sought to develop an experimental system to produce complex but reproducible non-homogeneous strain patterns for the study of strain magnitude, anisotropy, and gradient effects on cells in culture. The commercially available system utilized in our first two studies (i.e., a Flexcell device) was modified by simply affixing glass coverslips (5, 10, or 15mm diameter) to the center of 35mm diameter flexible-bottomed culture wells. To isolate the effects of strain magnitude, we utilized ring inserts previously reported by Boerboom [4] that allowed for multiple strain magnitudes to be run in parallel. By rigorously validating 2D and 3D deformation fields using high density mapping, we determined that the addition of the rigid inclusion creates strong circumferential and radial strain gradients and produces a continuous range of stretch anisotropy ranging from strip biaxial to equibiaxial strain. Further, we also determined that even at low levels of applied strain, the addition of a rigid inclusion results in a substantial increase in strain magnitudes at the edge of the inclusion (e.g., a sample with a 5 mm inclusion cycled to “2%” applied strain will have a 3 fold increase in strain).

Chapter 6: Conclusions and future work

To investigate how this system impacts cellular behavior in 2D and 3D systems, either dermal fibroblasts were seeded (5mm inclusions and cycled to ‘2%’ applied strain for 2 days), or fibroblast-populated fibrin gels were cast directly into culture wells (5mm inclusions and cycled to ‘6%’ applied strain for 8 days at 6 hours per day) and mechanically conditioned. Cells in 2D and 3D systems oriented themselves to the direction of principal strain as seen previously [45], with the highest level of alignment at the edge of the inclusion. In the 3D inclusion system, fibroblasts compacted their matrix in a response to increasing strain magnitude as was observed in Chapter 4 in uniformly stretched samples. As a result there was substantial compaction at the edge of the inclusion and a subsequent gradient of tissue thickness across the tissue. Interestingly, the histological images of fibroblasts cycled within the inclusion system appear to be degraded more extensively, as evidenced by sparse fibrin arrangement and low cellularity compared with stretched controls. Although the strain magnitude at the edge of the inclusion is substantially higher than maximum strain levels in stretched control (15% versus 6% strain magnitude, respectively), there appears to be global degradation of the tissue, even in areas where strain magnitude is identical to control values (e.g., 6% strain at 5 mm from the center). In our previous study where gels were cycled intermittently at 16% strain, this level of degradation was not present (refer to Figure 4.2).

Although not investigated in this preliminary experiment, it appears that the inhomogeneities produced in our system could be increasing the proteolytic activity in cells. If true, this finding would suggest that even at low levels of applied stretch (e.g., due to normal breathing), the introduction of an inclusion (e.g., stiff fibrotic focus or a prosthetic) would profoundly impact global strain distributions and greatly enhancing matrix remodeling. This strain distribution-dependent enhancement of matrix remodeling could play a critical role in the persistence and propagation of disease, or be dictate the success or failure of device implantation. Further, with the addition of increased collagen and subsequent increase of peak radial strains (due to the increase in inclusion size), it is possible that the addition of a stiff fibrotic foci in a mechanically loaded tissue (e.g., the lungs) could be creating a self-propagating disease. Experiments investigating fibrotic disease onset or the remodeling following implantation of devices as a function strain

distributions would assist in the understanding of the role of mechanics during these states of repair and are discussed in the future studies section of this thesis (6.5).

6.4. Mechanical conditioning for use in regenerative medicine

Currently, most tissue equivalents lack sufficient mechanical integrity and durability for clinical usage in load-bearing applications [46]. Mechanical conditioning has become a primary strategy to address these limitations in tissue strength and has been met with some success [47]. In this thesis, we determined that the UTS of tissues increased exponentially with increasing stretch magnitude (over the range studied), and this enhancement of tissue strength did not require large strain levels, continuous stimulation, exogenous growth factors such as TGF- β , or extended culture duration – all parameters previously thought to be required for a substantial increase in tissue strength [4, 14, 36]. For example, we determined that after only eight days of mechanical conditioning with as little as 8% strain, stretched fibrin gels become approximately 6-fold stronger, 10-fold more collagen dense, 9-fold stiffer, and 20% more cell populated. In order to harness stretch as a means and to custom tailor tissue analogs with specific requirements (e.g., strength, stiffness, contractility), quantitative relationships between mechanical simulation and extracellular matrix remodeling are required. Our results demonstrate that the magnitude and the duration per day of stretch are both critical parameters in matrix remodeling and suggest that these two factors can be used independently or in concert to manipulate different aspects of remodeling. In addition, the use of non-uniform strain could be particularly useful for the creation of tissue analogs with girded matrix properties. These tissue equivalents could be beneficial at the interfaces between tissues with different material properties (and therefore different loading conditions, or at the interface of a prosthesis).

6.5. Future work

It remains unclear as to why introducing a rest period by using intermittent stretch increases fibroblast ability to produce more net collagen content, increase in number and strengthen their matrix as compared with continuously cycled fibroblasts. In order to

Chapter 6: Conclusions and future work

determine the effects on intermittent stretch on cell cycle events, proliferation could be measured by [³H]-thymidine incorporation [23], cell number counts over time (i.e., at specific time points), or by histological staining for proliferative markers (e.g., by staining for KI 67+ cells) [48]. The percentage of cells in the G₀/G₁, S and G₂/M phase of the cell cycle can be determined by cell cycle analysis using specific markers in conjunction with flow cytometry [23].

An alternative application of the 2D inclusion system developed in our final study could be the use of contact printing with surface functionalization proteins to create cell attachment in areas with very specific stretch regimes. Surface proteins such as collagen I could be placed within one specific area of known strain anisotropy per well, thus eliminating cell-cell communication and soluble factors between fibroblasts undergoing differential strain regimes. Alternative potential modifications of the system include the addition of PDMS micro grooves on the surface of the silicone membrane to study contact guidance and orientation dependence, investigating the impact of electrical signaling in conjunction with dynamic conditioning, or even altering the surface stiffness to investigate combined effects of durotaxis and tendotaxis.

Preliminary evidence from our 3D inclusion study suggests that introducing gradients of strain magnitude and anisotropy could profoundly stimulate cell remodeling activity. Alternative measures of tissue architecture and matrix remodeling should also be assayed. Although we attempted to analyze fiber orientation in our inclusion system with polarized light microscopy [49], there was not enough material remaining post conditioning to acquire accurate measures of fiber orientation. In future studies, an antifibrotic inhibitor (ϵ -ACA, 3 mg/ml) could be utilized to restrict fibrin degradation and investigate long-term effects of mechanical conditioning, or continuous strain could be utilized to attain a lesser level of matrix remodeling. In addition, functional measures of remodeling could be assayed for by measuring matrix stiffness (refer to Appendix for methods and preliminary data), collagen deposition, or cellularity.

Studies using the 3D rigid inclusion system could also provide valuable information on cellular adaptation to complex or changing mechanical environments produced by

Chapter 6: Conclusions and future work

clinical interventions (e.g., stents, prostheses, etc.), possibly helping to understand mechanisms underlying propagation of stiff fibrotic foci as observed in diseases such as idiopathic pulmonary fibrosis. Currently it is unclear if the stretch-induced remodeling responses seen in these studies are indicative of fibrotic disease progression, normal healing, or protection from a fibrotic response. In particular in our final study, it is unclear if the heightened level of matrix remodeling at the edge of the inclusion would be considered normal or fibrotic healing.

Fibrotic-like remodeling can be evaluated by examining the cell phenotypes within the tissue, the persistence of these cell types, the accumulation of net collagen over time, and the production of profibrotic and anti-fibrotic factors. For example, it is well accepted myofibroblast persistence plays a critical role in the onset of several fibrotic diseases. The location of myofibroblasts and the percentage of the total cell population in the fibrin gel (compared to fibroblasts) can be determined by measuring the amount of α -SMA relative to total cell number (e.g., staining histologically or removing the cells from their matrix and sorting with FACS), and the persistence could be determined with by performing a duration study where numbers of these cells in response to mechanical stimulation are tracked over time. Endogenous profibrotic factors such as TGF- β 1 [50], fibroblast growth factor (FGF-2) [51], interleukin-1 (IL-1) [51-53], and connective tissue growth factor (CTGF) [51] could also be measured and compared with anti-fibrotic factors such as tissue inhibitor of metalloproteinases (TIMPs) [41, 48, 54, 55] (e.g., TIMP 1,2,3, 4) and collagenases (e.g., collagenase-1 and collagenase-2) [48] to ascertain a profibrotic response of fibroblasts to differential strain regimes. Further, the inclusion of a proteolytic inhibitor would allow for the extended culture duration of these equivalents, and allow for the examination of changes in tissue architecture, composition, and material properties in response to the addition of an inclusion over time. If cell-mediated remodeling resulted in global changes in tissue properties including “pathological” levels of tissue stiffness or collagen accumulation and composition (i.e., levels and amounts that compare to that of scar tissue [56]), this result would indicate a fibrotic response.

Chapter 6: Conclusions and future work

Specific integrin expression could also be an indicator of fibrotic activity. Integrins link the cell cytoskeleton to the extracellular matrix and have been found to regulate cell adhesion and migration, modulate growth factor sensitivity, transduce external forces into intracellular signals, and transmit cell-generated tension [57]. Specific integrins have been shown to mediate myofibroblast differentiation and function, particularly those specific for collagen ($\alpha_1\beta_1$, $\alpha_2\beta_1$) and fibronectin ($\alpha_5\beta_1$) [58, 59]. For example, Swartz and colleagues demonstrated that blocking $\alpha_2\beta_1$ reduces α SMA expression of human lung and dermal fibroblasts in a collagen gel model of interstitial flow [58]. These integrins have also been associated with increased contractility, pathological remodeling, and resistance to apoptosis of fibroblasts [60, 61]. To determine the role and production of these integrins in response to non-homogeneous stretch, the expression of $\alpha_1\beta_1$, $\alpha_2\beta_1$, and $\alpha_5\beta_1$ integrins could be alternatively measured and blocked.

In the future, our model system will be utilized in combination with relevant cytokines in three-dimensional studies to assess gradient affects on cell-mediated remodeling as seen during fibrocontractive disease. It has also been established that fibroblasts under mechanical stimulation respond differently to growth factor and cytokine stimulation than statically grown fibroblasts [3, 62, 63]. This is supported by findings of synergy between stretch and profibrotic factors such as TGF- β 1 on the regulation of synthetic activity [64]. TGF- β 1, a fibroblast chemoattractant [65] and profibrotic cytokine, is a potent stimulus of myofibroblast activation and fibrosis onset.[66-71] TGF- β 1 is a direct inducer of the myofibroblast phenotype; exposure to TGF- β 1 induces the expression of the myofibroblast marker α -SMA in both growing and quiescent cultured fibroblastic populations [66], while blocking TGF- β 1 results in a dramatic reduction of α -SMA expression [66]. TGF- β 1 also stimulates fibroblast contractility [67] and the production of ECM compounds associated with fibrosis [72-74].

Future studies could also include the investigation of active versus passive stretch-induced fiber alignment; whether fiber alignment guides cell behavior through contact guidance or if cell mediated activity guides dictates fiber alignment. To test if cells are actively remodeling and reorienting the fibers in response to mechanical conditioning,

Chapter 6: Conclusions and future work

protein degradation could be blocked by treating the fibrin gels with a proteolytic inhibitor (e.g., Aprotinin) and the orientation of cells (e.g., via microscopy), fibers (e.g., PLM), and the amount of matrix synthesis could be measured. To ascertain the passive contribution of fiber alignment in response to mechanical conditioning, acellular fibrin gels could be compared to cellularized fibrin gels, and the fiber orientation measured.

6.5.1. Final Conclusions

This thesis describes the investigation of cellular response in complex biaxial loading conditions, as seen in connective tissues during the process of wound healing. First, a novel model system was developed using equibiaxial stretch that enabled the investigation of mechanical effects on functional cell-mediated matrix remodeling. Using this methodology, we were able to demonstrate that cyclic stretch stimulates fibroblasts to produce a stronger matrix by dramatically increasing compaction, matrix fiber reorganization, and collagen content without in-plane alignment.

We then further developed dose-response curves for multiple aspects of tissue remodeling as a function of stretch magnitude and duration. Allowing a long rest period each day, rather than cycling continuously, enhanced the effects of stretch on structural but not intrinsic properties of the model tissue. Specifically, cycling intermittently rather than continuously did not alter the level of tissue compaction, UTS, or tissue retraction between these groups. Conversely, stretch magnitude-dependent increases in cell number, extensibility, and net collagen accumulation were contingent upon this rest period. Our results indicate that both the magnitude and the duration per day of stretch are critical parameters in modulating fibroblast remodeling of the extracellular matrix, and that these two factors can be used independently or in concert to regulate specific aspects of remodeling.

Finally, we developed a model system that enables the investigation of the impact of strain gradients, strain anisotropy, and strain magnitude in two and three dimensional

systems. Establishing the effects of complex strain distributions not only allows for more relevant modeling of the mechanical conditions in connective tissue, but also allows for the investigation of cellular adaptations to changing mechanical environment over time.

References

- [1] Altman, G. H., Horan, R. L., Martin, I., Farhadi, J., Stark, P. R., Volloch, V., Richmond, J. C., Vunjak-Novakovic, G., and Kaplan, D. L., 2002, "Cell differentiation by mechanical stress," *FASEB J*, 16(2), pp. 270-272.
- [2] Balestrini, J. L., and Billiar, K. L., 2006, "Equibiaxial cyclic stretch stimulates fibroblasts to rapidly remodel fibrin," *J Biomech*, 39(16), pp. 2983-2990.
- [3] Bishop, J. E., Mitchell, J. J., Absher, P. M., Baldor, L., Geller, H. A., Woodcock-Mitchell, J., Hamblin, M. J., Vacek, P., and Low, R. B., 1993, "Cyclic mechanical deformation stimulates human lung fibroblast proliferation and autocrine growth factor activity," *Am J Respir Cell Mol Biol*, 9(2), pp. 126-133.
- [4] Boerboom, R. A., Rubbens, M. P., Driessen, N. J., Bouten, C. V., and Baaijens, F. P., 2008, "Effect of strain magnitude on the tissue properties of engineered cardiovascular constructs," *Ann Biomed Eng*, 36(2), pp. 244-253.
- [5] Boublik, J., Park, H., Radisic, M., Tognana, E., Chen, F., Pei, M., Vunjak-Novakovic, G., and Freed, L. E., 2005, "Mechanical properties and remodeling of hybrid cardiac constructs made from heart cells, fibrin, and biodegradable, elastomeric knitted fabric," *Tissue Eng*, 11(7-8), pp. 1122-1132.
- [6] Chun, J., Tuan, T. L., Han, B., Vangness, C. T., and Nimni, M. E., 2003, "Cultures of ligament fibroblasts in fibrin matrix gel," *Connect Tissue Res*, 44(2), pp. 81-87.
- [7] Isenberg, B. C., and Tranquillo, R. T., 2003, "Long-term cyclic distention enhances the mechanical properties of collagen-based media-equivalents," *Ann Biomed Eng*, 31(8), pp. 937-949.
- [8] Kim, B. S., Nikolovski, J., Bonadio, J., and Mooney, D. J., 1999, "Cyclic mechanical strain regulates the development of engineered smooth muscle tissue," *Nat Biotechnol*, 17(10), pp. 979-983.
- [9] Seliktar, D., Black, R. A., Vito, R. P., and Nerem, R. M., 2000, "Dynamic mechanical conditioning of collagen-gel blood vessel constructs induces remodeling in vitro," *Ann Biomed Eng*, 28(4), pp. 351-362.
- [10] Seliktar, D., Nerem, R. M., and Galis, Z. S., 2003, "Mechanical strain-stimulated remodeling of tissue-engineered blood vessel constructs," *Tissue Eng*, 9(4), pp. 657-666.
- [11] Swartz, D. D., Russell, J. A., and Andreadis, S. T., 2005, "Engineering of fibrin-based functional and implantable small-diameter blood vessels," *Am J Physiol Heart Circ Physiol*, 288(3), pp. H1451-1460.
- [12] Wille, J. J., Elson, E. L., and Okamoto, R. J., 2006, "Cellular and matrix mechanics of bioartificial tissues during continuous cyclic stretch," *Ann Biomed Eng*, 34(11), pp. 1678-1690.

- [13] Ye, Q., Zund, G., Benedikt, P., Jockenhoevel, S., Hoerstrup, S. P., Sakyama, S., Hubbell, J. A., and Turina, M., 2000, "Fibrin gel as a three dimensional matrix in cardiovascular tissue engineering," *Eur J Cardiothorac Surg*, 17(5), pp. 587-591.
- [14] Syedain, Z. H., Weinberg, J. S., and Tranquillo, R. T., 2008, "Cyclic distension of fibrin-based tissue constructs: evidence of adaptation during growth of engineered connective tissue," *Proc Natl Acad Sci U S A*, 105(18), pp. 6537-6542. .
- [15] Tranquillo, R. T., 2002, "The tissue-engineered small-diameter artery," *Ann N Y Acad Sci*, 961, pp. 251-254.
- [16] Seliktar, D., Nerem, R. M., and Galis, Z. S., 2001, "The role of matrix metalloproteinase-2 in the remodeling of cell-seeded vascular constructs subjected to cyclic strain," *Annals of Biomedical Engineering*, 29(11), pp. 923-934.
- [17] Cummings, C. L., Gawlitta, D., Nerem, R. M., and Stegemann, J. P., 2004, "Properties of engineered vascular constructs made from collagen, fibrin, and collagen-fibrin mixtures," *Biomaterials*, 25(17), pp. 3699-3706.
- [18] Clark, R. A. F., 1996, *The molecular and cellular biology of wound repair*, Plenum Press, New York.
- [19] Neidert, M. R., Lee, E. S., Oegema, T. R., and Tranquillo, R. T., 2002, "Enhanced fibrin remodeling in vitro with TGF-beta1, insulin and plasmin for improved tissue-equivalents," *Biomaterials*, 23(17), pp. 3717-3731.
- [20] Li, Y. S., Haga, J. H., and Chien, S., 2005, "Molecular basis of the effects of shear stress on vascular endothelial cells," *J Biomech*, 38(10), pp. 1949-1971.
- [21] Schriefer, J. L., Warden, S. J., Saxon, L. K., Robling, A. G., and Turner, C. H., 2005, "Cellular accommodation and the response of bone to mechanical loading," *J Biomech*, 38(9), pp. 1838-1845.
- [22] Turner, C. H., Robling, A. G., Duncan, R. L., and Burr, D. B., 2002, "Do bone cells behave like a neuronal network?," *Calcif Tissue Int*, 70(6), pp. 435-442.
- [23] Chapman, G. B., Durante, W., Hellums, J. D., and Schafer, A. I., 2000, "Physiological cyclic stretch causes cell cycle arrest in cultured vascular smooth muscle cells," *Am J Physiol Heart Circ Physiol*, 278(3), pp. H748-754.
- [24] Wilson, E., Sudhir, K., and Ives, H. E., 1995, "Mechanical strain of rat vascular smooth muscle cells is sensed by specific extracellular matrix/integrin interactions," *J Clin Invest*, 96(5), pp. 2364-2372.
- [25] Nishimura, K., Blume, P., Ohgi, S., and Sumpio, B. E., 2007, "Effect of different frequencies of tensile strain on human dermal fibroblast proliferation and survival," *Wound Repair Regen*, 15(5), pp. 646-656.
- [26] Hu, Y., Bock, G., Wick, G., and Xu, Q., 1998, "Activation of PDGF receptor alpha in vascular smooth muscle cells by mechanical stress," *FASEB J*, 12(12), pp. 1135-1142.
- [27] Balestrini, J., Lopez, V., and Billiar, K., 2004, "Biaxial stretch-induced changes in fibrin gel failure properties," *Biomedical Engineering Society Annual Meeting Philadelphia, Pa.*
- [28] Robinson, P. S., Johnson, S. L., Evans, M. C., Barocas, V. H., and Tranquillo, R. T., 2006, "Functional Tissue-Engineered Valves from Cell-Remodeled Fibrin with Commissural Alignment of Cell-Produced Collagen." *Tissue Eng*, 12(12), pp. 3285-3303

- [29] Crouch, E., 1990, "Pathobiology of pulmonary fibrosis," *Am J Physiol*, 259(4 Pt 1), pp. L159-184.
- [30] Olman, M. A., Mackman, N., Gladson, C. L., Moser, K. M., and Loskutoff, D. J., 1995, "Changes in procoagulant and fibrinolytic gene expression during bleomycin-induced lung injury in the mouse," *J Clin Invest*, 96(3), pp. 1621-1630.
- [31] Drew, A. F., Liu, H., Davidson, J. M., Daugherty, C. C., and Degen, J. L., 2001, "Wound-healing defects in mice lacking fibrinogen," *Blood*, 97(12), pp. 3691-3698.
- [32] Tuan, T. L., Song, A., Chang, S., Younai, S., and Nimni, M. E., 1996, "In vitro fibroplasia: matrix contraction, cell growth, and collagen production of fibroblasts cultured in fibrin gels," *Exp Cell Res*, 223(1), pp. 127-134.
- [33] Abercrombie, M., Flint, M.H., and James, D.W., 1956, "Wound Contraction in relation to collagen formation in scorbutic guinea pigs," *J. Embryol. Exp. Morph*, 4, pp. 167-175.
- [34] Berry, C. C., Cacou, C., Lee, D. A., Bader, D. L., and Shelton, J. C., 2003, "Dermal fibroblasts respond to mechanical conditioning in a strain profile dependent manner," *Biorheology*, 40(1-3), pp. 337-345.
- [35] Brown, R. A., Prajapati, R., McGrouther, D. A., Yannas, I. V., and Eastwood, M., 1998, "Tensional homeostasis in dermal fibroblasts: mechanical responses to mechanical loading in three-dimensional substrates," *J Cell Physiol*, 175(3), pp. 323-332.
- [36] Clark, R. A., Nielsen, L. D., Welch, M. P., and McPherson, J. M., 1995, "Collagen matrices attenuate the collagen-synthetic response of cultured fibroblasts to TGF-beta," *J Cell Sci*, 108(Pt 3), pp. 1251-1261.
- [37] Gailit, J., Clarke, C., Newman, D., Tonnesen, M. G., Mosesson, M. W., and Clark, R. A., 1997, "Human fibroblasts bind directly to fibrinogen at RGD sites through integrin alpha(v)beta3," *Exp Cell Res*, 232(1), pp. 118-126.
- [38] Grouf, J. L., Throm, A. M., Balestrini, J. L., Bush, K. A., and Billiar, K. L., 2007, "Differential effects of EGF and TGF-beta1 on fibroblast activity in fibrin-based tissue equivalents," *Tissue Eng*, 13(4), pp. 799-807.
- [39] Parsons, M., Kessler, E., Laurent, G. J., Brown, R. A., and Bishop, J. E., 1999, "Mechanical load enhances procollagen processing in dermal fibroblasts by regulating levels of procollagen C-proteinase," *Exp Cell Res*, 252(2), pp. 319-331.
- [40] Merryman, W. D., Lukoff, H. D., Long, R. A., Engelmayr, G. C., Jr., Hopkins, R. A., and Sacks, M. S., 2007, "Synergistic effects of cyclic tension and transforming growth factor-beta1 on the aortic valve myofibroblast," *Cardiovasc Pathol*, 16(5), pp. 268-276.
- [41] Mudera, V. C., Pleass, R., Eastwood, M., Tarnuzzer, R., Schultz, G., Khaw, P., McGrouther, D. A., and Brown, R. A., 2000, "Molecular responses of human dermal fibroblasts to dual cues: contact guidance and mechanical load," *Cell Motil Cytoskeleton*, 45(1), pp. 1-9.
- [42] Lee, A. A., Delhaas, T., McCulloch, A. D., and Villarreal, F. J., 1999, "Differential responses of adult cardiac fibroblasts to in vitro biaxial strain patterns," *J Mol Cell Cardiol*, 31(10), pp. 1833-1843.
- [43] Hashima, A. R., Young, A. A., McCulloch, A. D., and Waldman, L. K., 1993, "Nonhomogeneous analysis of epicardial strain distributions during acute myocardial ischemia in the dog," *J Biomech*, 26(1), pp. 19-35.

- [44] Oomens, C. W., van Ratingen, M. R., Janssen, J. D., Kok, J. J., and Hendriks, M. A., 1993, "A numerical-experimental method for a mechanical characterization of biological materials," *J Biomech*, 26(4-5), pp. 617-621.
- [45] Wang, J. H., Goldschmidt-Clermont, P., Moldovan, N., and Yin, F. C., 2000, "Leukotrienes and tyrosine phosphorylation mediate stretching-induced actin cytoskeletal remodeling in endothelial cells," *Cell Motil Cytoskeleton*, 46(2), pp. 137-145.
- [46] Grassl, E. D., Oegema, T. R., and Tranquillo, R. T., 2002, "Fibrin as an alternative biopolymer to type-I collagen for the fabrication of a media equivalent," *J Biomed Mater Res*, 60(4), pp. 607-612.
- [47] Freed, L. E., Guilak, F., Guo, X. E., Gray, M. L., Tranquillo, R., Holmes, J. W., Radisic, M., Sefton, M. V., Kaplan, D., and Vunjak-Novakovic, G., 2006, "Advanced tools for tissue engineering: scaffolds, bioreactors, and signaling," *Tissue Eng*, 12(12), pp. 3285-3305.
- [48] Selman, M., Ruiz, V., Cabrera, S., Segura, L., Ramirez, R., Barrios, R., and Pardo, A., 2000, "TIMP-1, -2, -3, and -4 in idiopathic pulmonary fibrosis. A prevailing nondegradative lung microenvironment?," *Am J Physiol Lung Cell Mol Physiol*, 279(3), pp. L562-574.
- [49] Tower, T. T., Neidert, M. R., and Tranquillo, R. T., 2002, "Fiber alignment imaging during mechanical testing of soft tissues," *Ann Biomed Eng*, 30(10), pp. 1221-1233.
- [50] Broekelmann, T. J., Limper, A. H., Colby, T. V., and McDonald, J. A., 1991, "Transforming growth factor beta 1 is present at sites of extracellular matrix gene expression in human pulmonary fibrosis," *Proc Natl Acad Sci U S A*, 88(15), pp. 6642-6646.
- [51] Kelly, M., Kolb, M., Bonniaud, P., and Gauldie, J., "Re-evaluation of fibrogenic cytokines in lung fibrosis," pp. 39-49.
- [52] Archambault, J., Tsuzaki, M., Herzog, W., and Banes, A. J., 2002, "Stretch and interleukin-1beta induce matrix metalloproteinases in rabbit tendon cells in vitro," *Journal of Orthopedic Research*, 20(1), pp. 36-39.
- [53] Zhang, H. Y., and Phan, S. H., 1999, "Inhibition of myofibroblast apoptosis by transforming growth factor beta(1)," *Am J Respir Cell Mol Biol*, 21(6), pp. 658-665.
- [54] Edwards, D. R., Murphy, G., Reynolds, J. J., Whitham, S. E., Docherty, A. J., Angel, P., and Heath, J. K., 1987, "Transforming growth factor beta modulates the expression of collagenase and metalloproteinase inhibitor," *EMBO J*, 6(7), pp. 1899-1904.
- [55] Swartz, M. A., Tschumperlin, D. J., Kamm, R. D., and Drazen, J. M., 2001, "Mechanical stress is communicated between different cell types to elicit matrix remodeling," *Proc Natl Acad Sci U S A*, 98(11), pp. 6180-6185.
- [56] Selvaggi, G., Monstrey, S., Van Landuyt, K., Hamdi, M., and Blondeel, P., 2005, "Rehabilitation of burn injured patients following lightning and electrical trauma," *NeuroRehabilitation*, 20, pp. 35-42.
- [57] Arnaout, M. A., Goodman, S. L., and Xiong, J. P., 2002, "Coming to grips with integrin binding to ligands," *Curr Opin Cell Biol*, 14(5), pp. 641-651.

Chapter 6: Conclusions and future work

- [58] Ng, C. P., Hinz, B., and Swartz, M. A., 2005, "Interstitial fluid flow induces myofibroblast differentiation and collagen alignment in vitro," *J Cell Sci*, 118(Pt 20), pp. 4731-4739.
- [59] Racine-Samson, L., Rockey, D. C., and Bissell, D. M., 1997, "The role of alpha1beta1 integrin in wound contraction. A quantitative analysis of liver myofibroblasts in vivo and in primary culture," *J Biol Chem*, 272(49), pp. 30911-30917.
- [60] Chiquet, M., Renedo, A. S., Huber, F., and Fluck, M., 2003, "How do fibroblasts translate mechanical signals into changes in extracellular matrix production?," *Matrix Biol*, 22(1), pp. 73-80.
- [61] Eckes, B., Zigrino, P., Kessler, D., Holtkotter, O., Shephard, P., Mauch, C., and Krieg, T., 2000, "Fibroblast-matrix interactions in wound healing and fibrosis," *Matrix Biol*, 19(4), pp. 325-332.
- [62] Grinnell, F., and Ho, C. H., 2002, "Transforming growth factor beta stimulates fibroblast-collagen matrix contraction by different mechanisms in mechanically loaded and unloaded matrices," *Exp Cell Res*, 273(2), pp. 248-255.
- [63] Grinnell, F., 2003, "Fibroblast biology in three-dimensional collagen matrices," *Trends Cell Biol*, 13(5), pp. 264-269.
- [64] Butt, R. P., and Bishop, J. E., 1997, "Mechanical load enhances the stimulatory effect of serum growth factors on cardiac fibroblast procollagen synthesis," *J Mol Cell Cardiol*, 29(4), pp. 1141-1151.
- [65] Dhainaut, J. F., Charpentier, J., and Chiche, J. D., 2003, "Transforming growth factor-beta: a mediator of cell regulation in acute respiratory distress syndrome," *Crit Care Med*, 31(4 Suppl), pp. S258-264.
- [66] Desmouliere, A., Geinoz, A., Gabbiani, F., and Gabbiani, G., 1993, "Transforming growth factor-beta 1 induces alpha-smooth muscle actin expression in granulation tissue myofibroblasts and in quiescent and growing cultured fibroblasts," *J Cell Biol*, 122(1), pp. 103-111.
- [67] Arora, P. D., Narani, N., and McCulloch, C. A., 1999, "The compliance of collagen gels regulates transforming growth factor-beta induction of alpha-smooth muscle actin in fibroblasts," *Am J Pathol*, 154(3), pp. 871-882.
- [68] Thannickal, V. J., Lee, D. Y., White, E. S., Cui, Z., Larios, J. M., Chacon, R., Horowitz, J. C., Day, R. M., and Thomas, P. E., 2003, "Myofibroblast differentiation by transforming growth factor-beta1 is dependent on cell adhesion and integrin signaling via focal adhesion kinase," *J Biol Chem*, 278(14), pp. 12384-12389.
- [69] Zhang, H. Y., Gharaee-Kermani, M., Zhang, K., Karmiol, S., and Phan, S. H., 1996, "Lung fibroblast alpha-smooth muscle actin expression and contractile phenotype in bleomycin-induced pulmonary fibrosis," *Am J Pathol*, 148(2), pp. 527-537.
- [70] Desmouliere, A., 1995, "Factors influencing myofibroblast differentiation during wound healing and fibrosis," *Cell Biol Int*, 19(5), pp. 471-476.
- [71] Desmouliere, A., and Gabbiani, G., 1996, "The role of the myofibroblast in wound healing and fibrocontractive diseases," *The molecular and cellular biology of wound repair*, R. A. F. Clark, ed., Plenum Press, New York, pp. 391-423.
- [72] Khalil, N., O'Connor, R., Unruh, H., Warren, P., Kemp, A., and Greenberg, A., 1991, "Enhanced expression and immunohistochemical distribution of transforming

Chapter 6: Conclusions and future work

growth factor-beta in idiopathic pulmonary fibrosis," *Chest*, 99(3 Suppl), pp. 65S-66S.

- [73] Igotz, R. A., and Massague, J., 1986, "Transforming growth factor-beta stimulates the expression of fibronectin and collagen and their incorporation into the extracellular matrix," *J Biol Chem*, 261(9), pp. 4337-4345.
- [74] Border, W. A., and Ruoslahti, E., 1992, "Transforming growth factor-beta in disease: the dark side of tissue repair," *J Clin Invest*, 90(1), pp. 1-7.

APPENDIX A

Membrane inflation device

A.1. Introduction

The quantification of the mechanical properties of tissue equivalents is a primary method of assessing feasibility for use in tissue engineering and for determining changes in cell-mediated tissue remodeling, yet the delicate nature of these equivalents makes traditional methods of failure testing difficult. In Chapters 3 and 4, the strength of the samples was determined using a custom equibiaxial tissue inflation system described below and in detail in Billiar *et al.* [1].

A.2. Membrane inflation device set up

The membrane inflation system consists of a circular tissue clamp, a fluid reservoir (saline), an infusion pump, an integrated pressure transducer, and a laser displacement measurement device.

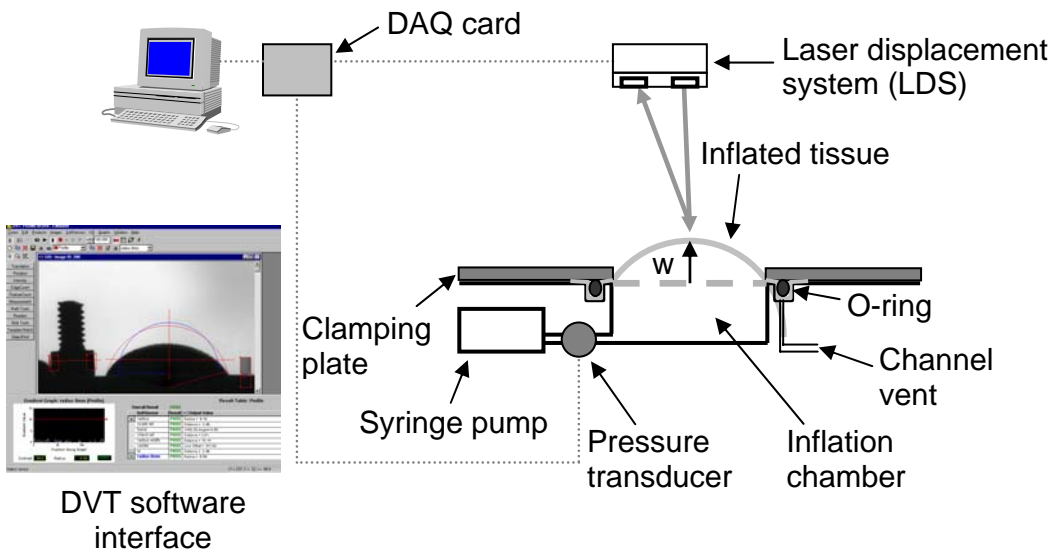


Figure A1: Schematic of the membrane inflation system set up. A circularly-clamped sample is inflated using a syringe pump as the pressure, central displacement (w), and radius of curvature are measured in real time and recorded in LabVIEW via a data acquisition (DAQ) card and a serial port. Diagram not to scale.

Before clamping, samples are treated for 4 hours with cytochalasin D, removed from their substrates and floated over the lower horizontal clamp surface on a layer of PBS to minimize handling. When the sample is centered over the orifice, the channel vent is

Appendix A: Membrane inflation device

opened (drawing the tissue into the channel) and an O-ring is positioned directly over the groove to keep the tissue in place. An even clamping force is produced around the circumference of the tissue by placing a clamping plate on the surface of the O-ring and adjusting the top down onto the clamping plate. The clamping plate is kept stationary relative to the tissue by guide pins.

To apply a load to the tissue, the clamped sample is inflated with room temperature isotonic PBS using a syringe pump (model 200, KD Scientific, New Hope, PA) at 1 mL/min. The pressure is measured by a transducer (PM/4, Living Systems Instrumentation, Burlington, VT). The displacement and radius of curvature of the central region (~80%) of the inflated sample are measured using a laser displacement sensor (LDS, LK-081, Keyence Corporation, Woodcliff Lake, NJ). The displacement in the exact center of the sample was measured. During inflation, simultaneous pressure, curvature, and displacement data are acquired using a data acquisition board (PCI 20428W DAQ, Intelligent Instrumentation, Tucson, AZ) and a serial port (for the DVT data) and recorded by LabVIEW (National Instruments, Austin, TX).

A.3. Determination of mechanical properties of the tissue

In static equilibrium the differential pressure of the inflated membrane, P , is related to the tension, T_i , and local radius of curvature, R_i , along orthogonal axes ($i = 1,2$) by the following equation (i.e., Law of Laplace):

$$P = T_1/R_1 + T_2/R_2 \quad (1)$$

If the inflated shape of a portion of the membrane is a cap, then $R_1=R_2$ and $T_1=T_2$. Therefore, the equibiaxial tension in the membrane is given by:

$$T = 1/2PR \quad (2)$$

For samples that inflate into a spherical-cap geometry (i.e., as is done using this device), the radius can also be estimated from the center displacement, w , by the following equation:

$$R = (w^2 + a^2)/2w, \quad (3)$$

where a is the radius of the clamp (5 mm in this device).

The ultimate tensile strength was calculated from the membrane tension at failure (Eqn. 2) by dividing by the undeformed thickness, t , of each sample. The maximum membrane tension represents the load per unit length that the tissue can withstand before rupture and is thus a “structural” property of the tissue substitutes, whereas the ultimate tensile strength (UTS) is a “material” property.

In addition, samples the average stretch ratio along a given meridian can also be estimated from the radius of curvature using the following geometric relationship:

Appendix A: Membrane inflation device

$$\lambda = \frac{\pi R \arcsin\left(\frac{a}{R}\right)}{a}. \quad (4)$$

The extensibility, E , is defined as Green's tensile strain at failure:

$$E = \frac{1}{2}(\lambda_{failure}^2 - 1). \quad (5)$$

A.4. Labview interface

Labview was used control the membrane inflation device. The program was designed in two parts: calibration of the device and data acquisition (thickness and burst pressure data). This program allows the user to manually manipulate flow rate of saline and the sampling rate of data acquisition. These experimental parameters enable measurements of the pressure (using the pressure transducer) and height (using the laser displacement system) of the sample at burst.

A.5. References

Billiar, K. L., A. M. Throm, et al. (2005). "Biaxial failure properties of planar living tissue equivalents." Journal of Biomedical Materials Research A **73A**(2): 182-91.

APPENDIX B

Validation of equibiaxial strain in Flexcell system and assessment of strain and in-plane tissue alignment

B.1. Introduction

As discussed in Chapter 3, in order to demonstrate that the strain distribution of our Flexcell system was equibiaxial, the two-dimensional distribution of strain in the center of stretched samples was validated by image analysis (HDM) [1]. To demonstrate that there was minimal fiber alignment in our tissue samples resulting from applying this equibiaxial stretch, polarize light microscopy was performed on 9 day old cyclically conditioned fibroblast-populated fibrin gels.

B.2. Measurement of strain distribution across the fibrin gel

Fibroblast-populated fibrin gels were cast into Flexcell plates cyclically stretched for 8 days at 16% equibiaxial strain at a frequency of 0.2 Hz. After 8 days, the culture media was removed, and the surface of each fibrin gels was texturized by dispersing black sand (as discussed in Chapter 3). The fibrin gels were then sequentially stretched using vacuum pressure levels that corresponded to 0, 5, and 10% equibiaxial (engineering) strain according to the manufacturer's instructions.

The resulting strain distribution was equibiaxial in the circumferential and radial directions ($10 \pm 1\%$). Figure B1 depicts fibrin gels prepared for testing, and the resulting strain in the radial direction.

Appendix B: Validation of equibiaxial strain in Flexcell system and assessment of strain and in-plane tissue alignment

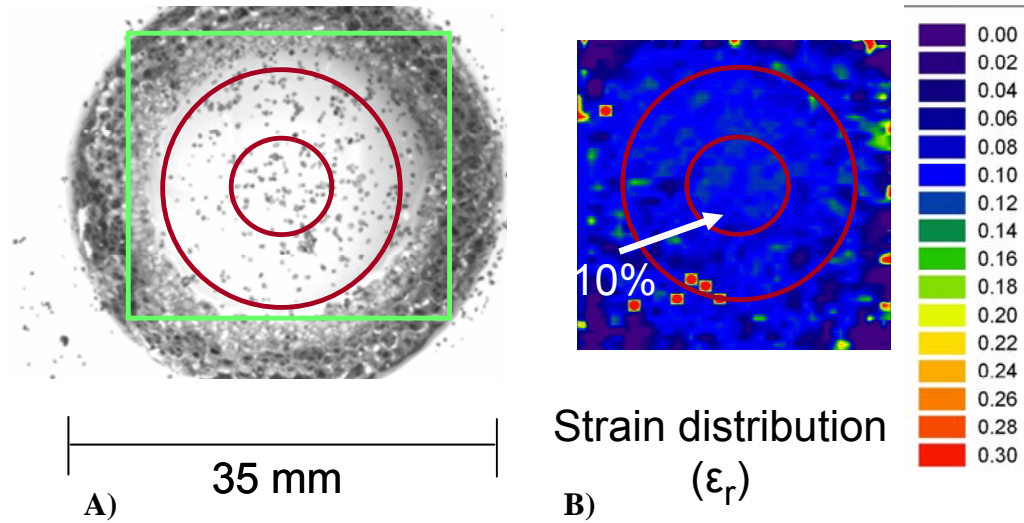


Fig. B.1. A) Fibroblast populated fibrin gel with black sand across the surface (surface markers). The green box represents the area of analysis, the outer red circle represents the circular platen underneath the fibrin gel (corresponding to 25mm), and the inner circle (corresponding to 10mm) represents the area used in mechanical testing. B) When cycled to 10% equibiaxial strain, the distribution of strain corresponded to $10\% \pm 1\%$.

B.3. Polarized light microscopy methods

The determination of birefringence due to fibrin fibril alignment was based on elliptically polarized light and image analysis using an Olympus IX-70 inverted light microscope by Tranquillo and his colleagues [2]. Briefly, after selecting fields spanning the compression axis of the fibrin gel a $1/4$ wave plate was rotated from 0 to 180° in increments of 10° between crossed polars, and ISee software measured the intensity of the transmitted light. Values of the angle of extinction, χ , and retardation, d , which measure the direction and magnitude of alignment of the fibrillar network, respectively, were obtained from regression of these data based on a Mueller matrix representation of the optical train $\sim d$ is the product of the birefringence and sample thickness. Below is representative mapping of birefringence data (Fig B2), demonstrating no preferred direction within the planar field.

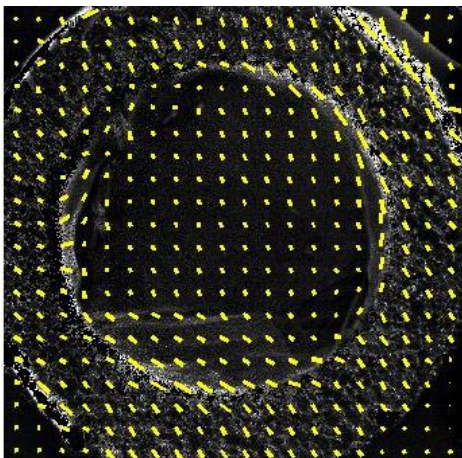


Fig. B.2. Representative data of birefringence data of a fibroblast-populated fibrin gel cycled for 8 days at 16% strain at a frequency of 0.2 Hz. The direction of the yellow markers indicates directionality of the fibrin fibers. After 8 days of cycling equibiaxially, there is no apparent fiber alignment in the fibrin gels.

B.4. References

- [1] Kelly, D. J., Azeloglu, E. U., Kochupura, P. V., Sharma, G. S., and Gaudette, G. R., 2007, "Accuracy and reproducibility of a subpixel extended phase correlation method to determine micron level displacements in the heart," *Med Eng Phys*, 29(1), pp. 154-162.
- [2] Tower, T. T., and Tranquillo, R. T., 2001, "Alignment maps of tissues: I. Microscopic elliptical polarimetry," *Biophys J*, 81(5), pp. 2954-2963.

APPENDIX C

Assessment of ring inserts

C.1. Introduction

As discussed briefly in Ch 5, to assess the feasibility of using Delrin ring inserts to control the strain magnitude of individual wells within our Flexcell system, the resulting strain magnitude of wells as a function of inserts thickness was assessed. In the following section, we investigated the impact of increasing applied pressure on wells with ring inserts to alter the ultimate strain magnitude of strain across the wells.

C.2. Determination of strain magnitude as a function of ring insert thickness

First, delrin rings with thicknesses of 6 and 7.5mm (the range found to be effective in manipulating strain magnitude in this system) were placed on the perimeter of the loading posts, and silicone lubrication was placed across both the loading post and ring inserts. Unaltered 6-well Bioflex plates were placed onto the baseplate and markers composed of 4 ink dots placed across the membrane (Figure C.1).

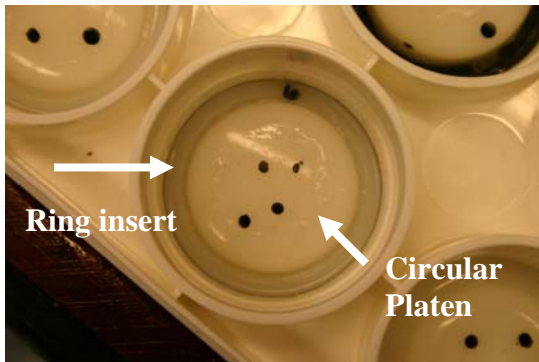


Fig. C.1. Photo of a 6mm ring insert surrounding the edge of the circular platen with markers.

After the Indian ink was allowed to dry, vacuum pressures corresponding to ‘10%’ and ‘20%’ (52 and 89kPa) were applied strain to an unmodified system, and images were taken using a digital SLR camera (6 megapixel, Cannon EOS). The displacement of the markers was then measured using Image J (version 1.38, NIH), and the displacements were converted to principle strains.

Table C.1. The corresponding insert-dependent strain magnitudes as a function of increasing applied pressure.

<u>Applied strain</u>	<u>Measured strain</u>	<u>6mm insert</u>	<u>7.5mm insert</u>
10%	E11	10.0%	1.4%
	E12	1.0%	1.8%
	E22	10.8%	1.0%
20%	E11	10.5%	1.4%
	E12	1.0%	1.8%
	E22	10.2%	1.0%

Conclusions

Increasing the applied pressure from 10% to 20% does not increase the final strain across the membranes within the range of insert thicknesses used in our studies. Therefore, all future analysis was performed using pressures that corresponded to 10% equibiaxial strain. In addition, principle strains in the x and y (1 and 2) directions were approximately equal, indicating that the ring inserts did not impact the homogeneity of the strain field.

APPENDIX D

MATLAB Code

D.1. Matlab code for determining material constants

This matlab code was utilized to determine material constants (matrix stiffness) from experimental data acquired using the low force biaxial characterization device (Ch 4) by fitting the data to a linear elastic model. The primary code (below) includes two functions that determine the experimental stress values and compare them with predicted stress values.

```
% Calculate Stresses using 4 parameters
% isotropic material
%  $S_{11} = ((E*(1-\nu)*E_{11})/((1+\nu)*(1-2*\nu)) + (E*\nu*E_{22})/((1+\nu)*(1-2*\nu)))$ 
%  $S_{22} = ((E*(1-\nu)*E_{22})/((1+\nu)*(1-2*\nu)) + (E*\nu*E_{11})/((1+\nu)*(1-2*\nu)))$ 
% where E11,E22= infinitesimal
%% Preliminary settings

clear all; close all;
clc
startPoint=[.49, 30];
close
%%%%%%%% Reading the Data from the Excel File ---- Each File is arranged
in
%%%%%%%% the following manner
%%%%%%%% Time      %Strain X   %Strain Y   Stress X (psi)  Stress Y (psi)
%%%%%%%% Stress X (Pa)   Stress Y (Pa)

%a=xlsread('Gell_Bi5_10_d.xls','Cycle_10','a2:m500');
%b=xlsread('Gell_Bi10_5_c.xls','Cycle_10','a2:m500');
%c=xlsread('Gell_equi5_e.xls','Cycle_10','a2:m500');
%d=xlsread('Gell_equi10_g.xls','Cycle_10','a2:m500');

%% a = protocol 1 (5:10), b= protocol 2(10:5), c= protocol 3 (5:5) d=
%% predicted (equibiaxial 10%)
%% now converting the strains from percentages (the stresses are in
Pa)

thickness=.048
width=1.265
area=(thickness*width)
```

Appendix D: Matlab Code

```
ratio=[5 10; 10 5; 5 5; 10 10];

ex3=c(:,2)'/100;
ey3=c(:,3)'/100;
ox3=c(:,4) '*6.894;
oy3=c(:,5) '*6.894;

p= polyfit(ex3, ox3, 1);
ox3=ox3-p(2);
p= polyfit(ey3, oy3, 1);
oy3=oy3-p(2);

lambdax3=ex3+1;
lambday3=ey3+1;
forcex3=ox3*area;
forcey3=oy3*area;

%%%%%% Creating one variable by combining the same parameter from
%%%%%% different Protocols
%%%%%% For e.g. ex = sum of the strains in the X axis from all
protocols
global S11 S22 E11 E22
S11=[ox3];
S22=[ox3];
E11=[ex3];
E22=[ex3];

%% Estimate the material constant by minimizing the sse
% sse= sum of squared errors

model = @sseStressequi;
[estimate, sse, flag, output] = fminsearch(model, startPoint);

[sse, S11_Fit, S22_Fit] = model(estimate);%evaluate the function
[m,n]=size(S11); noDataPoints=m*n;
rmsError=sqrt(sse)/noDataPoints; % a global measure of the fit goodness
errorS11=S11_Fit-S11; % residuals
errorS22=S22_Fit-S22; % residuals
sst=S11-mean(S11);
Es=estimate(1);

stS11=S11-mean(S11);
stS22=S22-mean(S22);

sstS11=stS11.^2;
sstS22=stS11.^2;
sst=sstS11+sstS22;

srerrorS11=sum(sum(S11_Fit-mean(S11)).^2);
srerrorS22=sum(sum(S22_Fit-mean(S22)).^2);
srerror=srerrorS11+srerrorS22;
```


Appendix D: Matlab Code

```
rsquared=srerror/sst;

%% Plot Fitting Results
figure;

subplot(2,2,1);
h1=plot(lambdax3,forcex3,'c. '); hold on;
legend(h1,'Original data: P3(5:5)', 'Location', 'NorthWest');
xlabel('Lambda 1'); ylabel('Force X (N)');hold on;
%AXIS TIGHT

subplot(2,2,2);
h2=plot(lambday3,forcey3,'c. '); hold on;
xlabel('Lambda 2'); ylabel('Force Y (N)');hold on

subplot(2,2,3);
h3=plot(lambdax3,lambday3,'c. '); hold on;
xlabel('Lambda 1'); ylabel('Lambda 2'); hold on;
legend (h3,'Gel 1');
figure;

subplot(2,2,1);

h4=plot(ex3,ox3,'c. '); hold on;
legend(h4, 'Original data: P3(5:5)', 'Location', 'NorthWest');
xlabel('E11'); ylabel('Stress S11 (Pa)');

[S11, S22, e11, e22]=predictSequi(ratio(3,1), ratio(3,2), Es);
plot(e11, S11, '-c', 'Marker','*', 'MarkerEdgeColor',[0 0
0], 'MarkerFaceColor',[0 0 0])

subplot(2,2,2);

h5=plot(ey3,oy3,'c. '); hold on;

[S11, S22, e11, e22]=predictSequi(ratio(3,1), ratio(3,2), Es);
plot(e22, S22, '-c', 'Marker','*', 'MarkerEdgeColor',[0 0
0], 'MarkerFaceColor',[0 0 0])

legend(h5, 'Fitting data:P3', 'Location', 'NorthWest');
xlabel('E22'); ylabel('Stress S22 (Pa)');
title(strcat('Estimate=', num2str(round(estimate))));

%% Plot Estimation Errors
subplot(2,2,3);
h6=plot(E11,errorS11, 'b. '); hold on;
legend(h6,'P1, P2, P3', 'Location', 'NorthWest');
xlabel('E11'); ylabel('S11 measured-S11 fit');

subplot(2,2,4);
h7=plot(E22,errorS22, 'b. '); hold on;
legend(h7, 'P1, P2, P3', 'Location', 'NorthWest');
```

Appendix D: Matlab Code

```
xlabel('E22'); ylabel('S22 measured-S22 fit');
titleLabel=strcat('rms=', num2str(round(rmsError)));
title(titleLabel)

%% Save estimation results into a text file
fileNameEst='estResults.txt';

data2save=[estimates,rmsError];
dlmwrite(fileNameEst, data2save, 'delimiter', '\t', '-append');
```

D.1.1 Function to determine predicted stress values

```
function [S11_p S22_p, e11, e22]=predictSequi5(rx, ry, Es);

rx=rx/100;
ry=ry/100;
% rx=10/100;
% ry=10/100;
N=10;

v = 0.25

e11=0:rx/N:rx;
e22=0:ry/N:ry;

S11_p=((Es*(1-v)*e11))/((1+v)*(1-2*v))+((Es*v*e22))/((1+v)*(1-2*v)); %
stress in the x direction
S22_p=((Es*(1-v)*e22))/((1+v)*(1-2*v))+((Es*v*e11))/((1+v)*(1-2*v)); %
stress in the y direction

% figure
% subplot(2,1,1)
% plot(e11, S11_Fit, 'k*')
% subplot(2,1,2)
% plot(e22, S22_Fit, 'g*')
```

D.1.2 Function to determine experimental stress values

```
function [sse, S11_Fit, S22_Fit]=sseStressequi5(params)

v = 0.25
Es=params(1);

global S11 S22 E11 E22

S11_Fit=((Es*(1-v)*E11))/((1+v)*(1-2*v))+((Es*v*E22))/((1+v)*(1-
2*v)); % stress in the x direction
```

Appendix D: Matlab Code

```
S22_Fit=((Es*(1-v)*E22))/((1+v)*(1-2*v))+((Es*v*E11))/((1+v)*(1-2*v)); % stress in the y direction
size(S11_Fit);
errorS11=S11_Fit-S11; % fitting errors for S11
errorS22=S22_Fit-S22;
sseS11=sum(sum(errorS11.^2)); % sum square errors for S11
sseS22=sum(sum(errorS22.^2));
sse=sseS11+sseS22; % over
```

D2. Matlab code for determining radial and circumferential strain

D.2.1. Code that enables multiple tests to be analyzed simultaneously

```
ss
clear all; close all; clc;

N=input('No of files=');
for i=1:N
    inputFile=['name of file', num2str(i), '.xls'];
    HDM_analysis_to_polar_master_loop(inputFile);
end
```

D.2.2. Determination of radial and circumferential strains from u and v displacements, and conversion to polar coordinates

```
function HDM_analysis(inputFile)

% %% Determination of the radial and circumferential strains from
% displacement data determined using HDM
% data will be filtered using the gaussian filtration method
% Equations used:
%  $err=(exx*\cos^2(\theta))+(\text{eyy}*\sin^2(\theta))+(\text{exy}*\sin^2(\theta))$ 
%  $e_{\theta}=(exx*\sin^2(\theta))+(\text{eyy}*\cos^2(\theta))-(\text{exy}*\sin^2(\theta))$ 
%  $er(\theta)=0.5*((du/dy)+(dv/dx))$ , where  $du$ ,  $dy$ , and  $dx$  represent
% partials
%  $\theta = \text{atan2}(v_{dis}-v_{center}, u_{dis}-u_{center})$ 
%  $\rho=\text{sqrt}((v_{dis}-v_{center}).^2+(u_{dis}-u_{center}).^2)$ 
% note: the pixel shift is identical in the x and y direction, and is
% a value designated by the user before processing

% clear all; close all;
% clc
% close
% % % % % Reading the Data from the Excel File
% num_exp = input('Enter number of runs:', 's'); % This should be the
% number of experiments you wish to analyze
% experimentName =input('Enter the Experiment Name:', 's'); % This
% should be whatever you call your input file do not use spaces.
```

Appendix D: Matlab Code

```
%inputFile=strcat(experimentName, '.xls'); % if using excel2007, use the
extension ".xlsx"

%read in input file 2 ways, numerical and text.
%Convenient to do this so specimen # can be a string (i.e. the samples
can have any ID, not just numerical).
%Also can read in sample descriptions (non-numerical).
%Note: sample_info_num ignores the text row (header) and inintial text
columns, so rows and columns do not correspond between these three
files.
%The first row/column are not ignored when reading in text.

[sample_info_num, sample_info_txt, sample_info_raw
]=xlsread(inputFile);
DataFile = strcat(char(sample_info_txt(2,1)), '.xls'); % if using
excel2007, use the extension ".xlsx", note datafile is a cell, need to
convert to character (char) for string
NumFrames=length(sample_info_txt(:,2))-1; %Finds the number of
specimens/runs to be analyzed by finding the length of the second
column on the input sheet - 1 for header.
worksheet=sample_info_txt(2:(NumFrames+1),2); %(*vector) start on row 2
to account for header, since reading in text data.
Usection = char(sample_info_txt(2,3)); % need to convert to character
(char) for string
Vsection = char(sample_info_txt(3,3)); % need to convert to character
(char) for string
u_center = sample_info_num(1,1);%num
v_center = sample_info_num(1,2);%num
PixPerMM = sample_info_num(1,3);%num
FilterWindow =sample_info_num(1,4);%num
FilterSigma = sample_info_num(1,5);%num
Run_number = char(sample_info_txt(2,9)); %start on row 2 to account for
header
%jpgname=strcat(char(Datafile),char(Run_number),'.jpg'); %can create a
jpg

disp('input file read, data reading...');

udis = xlsread(DataFile, 'Udis', Usection);
vdis = xlsread(DataFile, 'Vdis', Usection); %Note - Vdis is in same
location as Udis

disp('udis and vdis read, data reading...');
for i = 1:NumFrames
    frameName = char(worksheet(i)); %worksheet number is a cell, need
to convert to character (char) for string
    u(:, :, i)=xlsread(DataFile, frameName, Usection);
    v(:, :, i)=xlsread(DataFile, frameName, Vsection);
end

disp('data read, filtering started...');
%% 2D Filtering
hsize=[FilterWindow, FilterWindow]; %default value
```

Appendix D: Matlab Code

```
sigma = FilterSigma; %default value
h = fspecial('gaussian', hsize, sigma);

clear utotal vttotal
[NumRows NumColumns NumFrames]= size (u);

utotal=zeros(NumRows, NumColumns); %creating an empty matrix
vttotal=zeros(NumRows, NumColumns); %creating an empty matrix

for i = 1:NumFrames;
    u(:,:,i) = filter2(h,u(:,:,i));
    v(:,:,i) = filter2(h,v(:,:,i));
    utotal = utotal + u(:,:,i);
    vttotal = vttotal + v(:,:,i);
end

%% The average slope
disp('filtered, calculating strain and transforming...');

exx = xSlopeFinder(udis,utotal);
eyy = ySlopeFinder(vdis,vttotal);
dxy = ySlopeFinder(vdis,utotal);
dyx = xSlopeFinder(udis,vttotal);
exy = 0.5*(dxy+dyx);

%% Cylindrical to Polar

% find angle and radius
theta = atan2(vdis-v_center,udis-u_center);
rho=sqrt((vdis-v_center).^2+(udis-u_center).^2);

thetaV=reshape(theta, size(theta,1)*size(theta,2),1);
rhoR=reshape(rho, size(theta,1)*size(theta,2),1);
[rhoSort, rhoIndex]=sort(rhoR);

for i = 1 : NumRows
    for j = 1 : NumColumns

err(i,j)=(exx(i,j)*(cos(theta(i,j))*cos(theta(i,j))))+(eyy(i,j)*(sin(theta(i,j))*sin(theta(i,j))))+(exy(i,j)*(sin(2*theta(i,j))));

etheta(i,j)=(exx(i,j)*sin(theta(i,j))*sin(theta(i,j)))+(eyy(i,j)*(cos(theta(i,j))*cos(theta(i,j))))-(exy(i,j)*(sin(2*theta(i,j))));
        end
    end

clear rhoBins binflag errBin errBinAvg errBinSD ettBin ettBinAvg
ettBinSD numInBin

sizeBin=16; %% the step size is 16 (pixel shift), so the binning was
based on this
m1=1;
```

Appendix D: Matlab Code

```
i=1;
numBins = floor(max(rho(:)))/sizeBin; %to include all radius values,
note this may lose the last few points
for bin=1:numBins
    rhoBins(bin,1)=bin*sizeBin-sizeBin/2;
    numInBin(bin)=0;
    binflag(bin)=0;
    while rhoSort(i)< sizeBin*bin
        i=i+1;
        binflag(bin)=1;
        numInBin(bin)=numInBin(bin)+1;
    end %while
    if binflag(bin)==1
        m2=i-1; %subtract 1 since i was incremented in while loop
        errBin=err(rhoIndex(m1:m2));
        errBinAvg(bin,1)=mean(errBin);
        errBinSD(bin,1)=std(errBin);
        ettBin=etheta(rhoIndex(m1:m2));
        ettBinAvg(bin,1)=mean(ettBin);
        ettBinSD(bin,1)=std(ettBin);
        m1= i;
    elseif bin==1 % to avoid the 0 index
        errBinAvg(1)=0;
        errBinSD(1)=0;
        ettBinAvg(1)=0;
        ettBinSD(1)=0;
    else
        errBinAvg(bin)=errBinAvg(bin-1);
        errBinSD(bin)=0;
    end % if binflag = 1
end % bin for loop

radius = (rhoBins/PixPerMM);
% radiust=radius';
% errBinAvgt=errBinAvg';
% ettBinAvgt=errBinAvg';

r_max = 10;
errBinMax=max(errBinAvg(:));
ettBinMax=max(ettBinAvg(:));
disp('Rendering plots');

%% Plot the results
xmin = 0;
xmax = r_max;
ymin= -0.1;
ymax = 0.2;
figname=strcat('results_',char(sample_info_txt(2,1)),Run_number)
titlename1= strcat('experiment name:
',char(sample_info_txt(2,1)),'_ ',Run_number);
titlename2= strcat('errBinmax: ',errBinMax,'
ethetaBinmax:',ettBinMax);

m =figure;
subplot(2,2,1);char
```

Appendix D: Matlab Code

```
h1 = contourf(err); hold on;
colorbar('location','eastoutside');
ylabel('y step (16pix ea)','FontWeight','Bold');xlabel('x step
(16px)','FontWeight','Bold');hold on;

subplot(2,2,2);
h2 = contourf(etheta);hold on;
colorbar('location','eastoutside'); hold on;
ylabel('y step (16px)','FontWeight','Bold');xlabel('x step
(16px)','FontWeight','Bold'); hold on;
title(titlename1);

subplot(2,2,3);
h3=errorbar(radius, errBinAvg, errBinSD,'k'); hold on;
axis([xmin xmax ymin ymax]);hold on;
xlabel('Distance from center (mm)','FontWeight','Bold');
ylabel('errBin','FontWeight','Bold');hold on;
%axis([xmin xmax min(errBinAvg-errBinSD)*1.1
max(errBinAvg+errBinSD)*1.1]);hold on;
subplot(2,2,4);
h4=errorbar(radius, ettBinAvg, ettBinSD,'k'); hold on;
axis([xmin xmax ymin ymax]); hold on;
xlabel('Distance from center (mm)','FontWeight','Bold');
ylabel('ettBin','FontWeight','Bold');
title(titlename2);

%% Write to excel file, save jpg
Filename = strcat(figname, '.xls');
Filename2 = strcat('angiemethod',figname, '.xls');
data2save=[radius,errBinAvg,errBinSD,ettBinAvg,ettBinSD];% Makes a
matrix of values
dlmwrite(Filename, data2save,'delimiter','\t', '-append' );%Writes all
values to excel file named: experiment number_Results
saveas(m, figname, 'jpg') %saves figure
```

D.2.3. Function to determine strain in the y-direction

```
function [output] = ySlopeFinder(xdata,ydata)
```

```
%% Constants
```

```
avgSize = 2;
```

```
%% Find the size of input data
```

```
[inputR inputC] = size(xdata);
```

```
%% For loop to find the average
```

```
for i = 1 : inputC
    for j = 1 : inputR
        unitCnt = 1; %counter
```

Appendix D: Matlab Code

```
    for k = -avgSize : avgSize
        if (j+k > 0 && j+k <= inputR)
            temp_xData(unitCnt,1) = xdata(j+k,i);
            temp_yData(unitCnt,1) = ydata(j+k,i);
            unitCnt = unitCnt + 1;
        end
    end
    [avgSlope avgConstant] = getLineEq(temp_xData,temp_yData);
    output(j,i) = avgSlope;
end
end
```

D.2.4 Function to determine the slope of the displacement/distance (strain)

```
function [slopeOfLine,constantOfLine] = getLineEq(xdata,ydata)

%% Calculations

x_bar = mean(xdata);
y_bar = mean(ydata);
x_xbar = xdata - x_bar;
y_ybar = ydata - y_bar;
x_xbar_sq = x_xbar .* x_xbar;
y_ybar_sq = y_ybar .* y_ybar;
x_xbar_y_ybar = x_xbar .* y_ybar;
N = length(xdata);

total_x_xbar_sq = sum(x_xbar_sq);
total_y_ybar_sq = sum(y_ybar_sq);
total_x_xbar_y_ybar = sum(x_xbar_y_ybar);

R_sq = total_x_xbar_y_ybar / sqrt(total_x_xbar_sq * total_y_ybar_sq); %
Calculate the R-square
slope_of_line = total_x_xbar_y_ybar / total_x_xbar_sq; % Calculate the
slope
c = y_bar - slope_of_line*x_bar; % Calculate the intercept

%% Final Values

% numberOfDataPoints = N;
% rValue = R_sq;
slopeOfLine = slope_of_line;
constantOfLine = c;
```

B3. Function to determine the strain in the x-direction

```
function [output] = xSlopeFinder(xdata,ydata)

%% Constants
```


Appendix D: Matlab Code

```
avgSize = 2;

%% Find the size of input data
[inputR inputC] = size(xdata);

%% For loop to find the average
for i = 1 : inputR
    for j = 1 : inputC
        unitCnt = 1; %counter
        for k = -avgSize : avgSize
            if (j+k > 0 && j+k <= inputC)
                temp_xData(unitCnt,1) = xdata(i,j+k);
                temp_yData(unitCnt,1) = ydata(i,j+k);
                unitCnt = unitCnt + 1;
            end
        end
        [avgSlope avgConstant] = getLineEq(temp_xData,temp_yData);
        output(i,j) = avgSlope;
    end
end
```

APPENDIX E


Experimental protocols

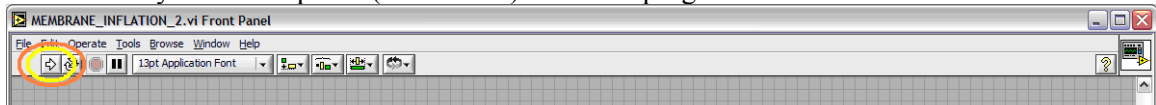
E.1. Mechanical testing protocol (membrane inflation device)

This LabVIEW program is to be used in for experimental calibration and data acquisition with the membrane inflation testing setup.

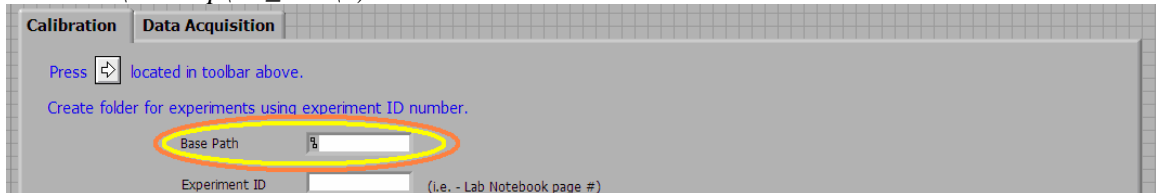
Instructions for use:

Program Initiation

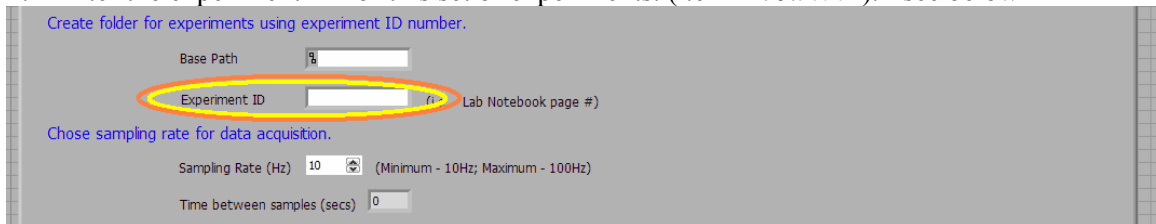
1. Open “Membrane Inflation” folder from All Users directory (if access is given to all users). Open “Membrane Inflation.vi.”
2. Press  button located in toolbar. This will begin execution of the program, though there may be a brief pause (~ 5-10 sec) while the program is loaded into RAM.



3. Enter the base path that you want the current set of experimental data to be saved in. (i.e. – “C:\Desktop\MI_tests\”) <see below>



4. Enter the experiment ID for this set of experiments. (i.e – “17Jun06”). <see below>



5. Determine sampling rate (Hz) by either entering number or scrolling to desired rate. The resultant sampling period is displayed in the numeric indicator below the sampling rate control. <see below>

Appendix E: Experimental protocols

Create folder for experiments using experiment ID number.

Base Path

Experiment ID (i.e. - Lab Notebook page #)

Chose sampling rate for data acquisition.

Sampling Rate (Hz) (Minimum - 10Hz; Maximum - 100Hz)

Time between samples (secs)

Calibration Procedures

1. Position displacement laser at whatever height represents zero (this can be arbitrary because displacement is measured relative to this position).
2. Press “Measure voltage” which will acquire the voltage representing zero displacement and display it as “Offset voltage.”

Calibration procedures:

Displacement (mm)	Pressure (mmHg)
Zero system and measure voltage: <input type="button" value="Measure voltage"/> Offset voltage: <input type="text" value="0"/>	Zero system and measure voltage: <input type="button" value="Measure voltage"/> Offset voltage: <input type="text" value="0"/>

3. Modify laser position by a known positive quantity (in mm) and enter manual displacement.

Apply known displacement (mm): Enter value of known quantity: <input type="text" value="0"/> <input type="button" value="Measure voltage"/> Measured voltage: <input type="text" value="0"/>	Apply known pressure (mmHg): Enter value of known quantity: <input type="text" value="0"/> <input type="button" value="Measure voltage"/> Measured voltage: <input type="text" value="0"/>
---	---

4. Press second “Measure voltage” button.

Apply known displacement (mm): Enter value of known quantity: <input type="text" value="0"/> <input type="button" value="Measure voltage"/> Measured voltage: <input type="text" value="0"/>	Apply known pressure (mmHg): Enter value of known quantity: <input type="text" value="0"/> <input type="button" value="Measure voltage"/> Measured voltage: <input type="text" value="0"/>
---	---

5. Check displacement calibration displayed on the screen for accuracy.

Apply known displacement (mm): Enter value of known quantity: <input type="text" value="0"/> <input type="button" value="Measure voltage"/> Measured voltage: <input type="text" value="0"/> Calibration Factor (mm/V): <input type="text" value="0"/>	Apply known pressure (mmHg): Enter value of known quantity: <input type="text" value="0"/> <input type="button" value="Measure voltage"/> Measured voltage: <input type="text" value="0"/> Calibration Factor (mmHg/V): <input type="text" value="0"/>
--	--

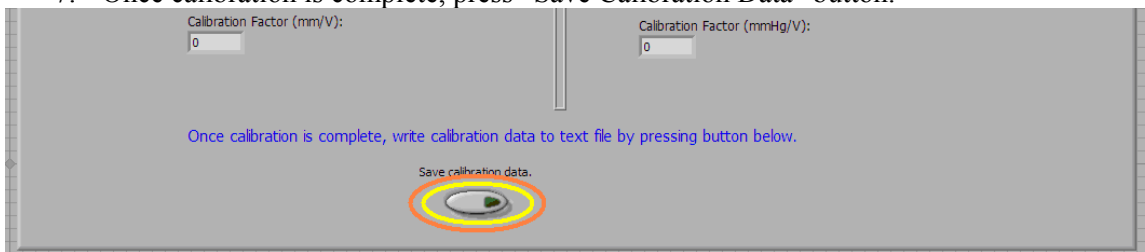
6. Repeat steps 1-5 for pressure calibration.

Calibration procedures:

Displacement (mm)	Pressure (mmHg)
Zero system and measure voltage: <input type="button" value="Measure voltage"/> Offset voltage: <input type="text" value="0"/>	Zero system and measure voltage: <input type="button" value="Measure voltage"/> Offset voltage: <input type="text" value="0"/>
Apply known displacement (mm): Enter value of known quantity: <input type="text" value="0"/> <input type="button" value="Measure voltage"/> Measured voltage: <input type="text" value="0"/>	Apply known pressure (mmHg): Enter value of known quantity: <input type="text" value="0"/> <input type="button" value="Measure voltage"/> Measured voltage: <input type="text" value="0"/>
Calibration Factor (mm/V): <input type="text" value="0"/>	Calibration Factor (mmHg/V): <input type="text" value="0"/>

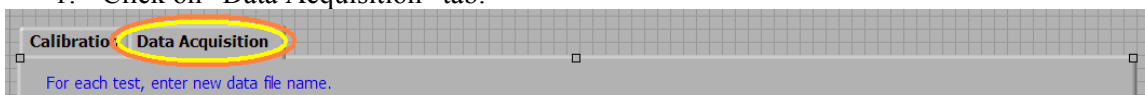
Appendix E: Experimental protocols

7. Once calibration is complete, press “Save Calibration Data” button.

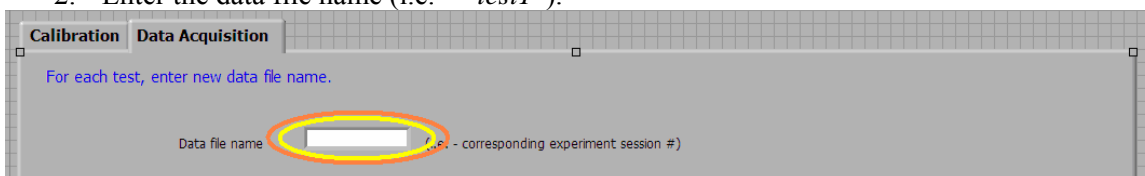


Data Acquisition Procedures

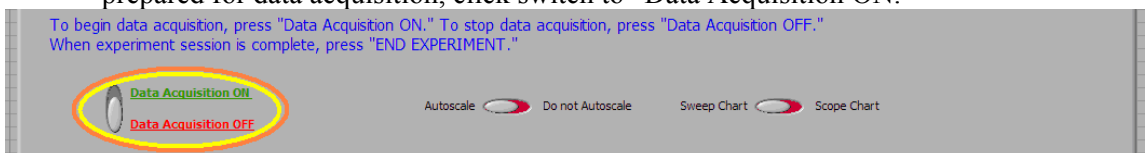
1. Click on “Data Acquisition” tab.



2. Enter the data file name (i.e. – “test1”).

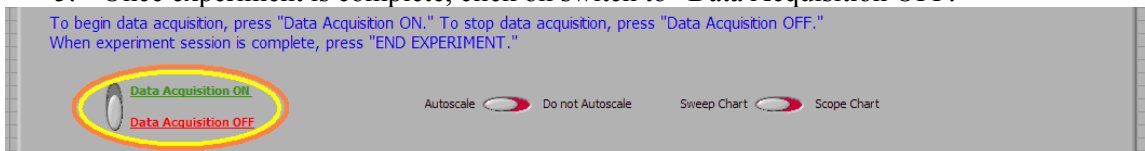


3. Once syringe pump is programmed as desired and all experiment components are prepared for data acquisition, click switch to “Data Acquisition ON.”

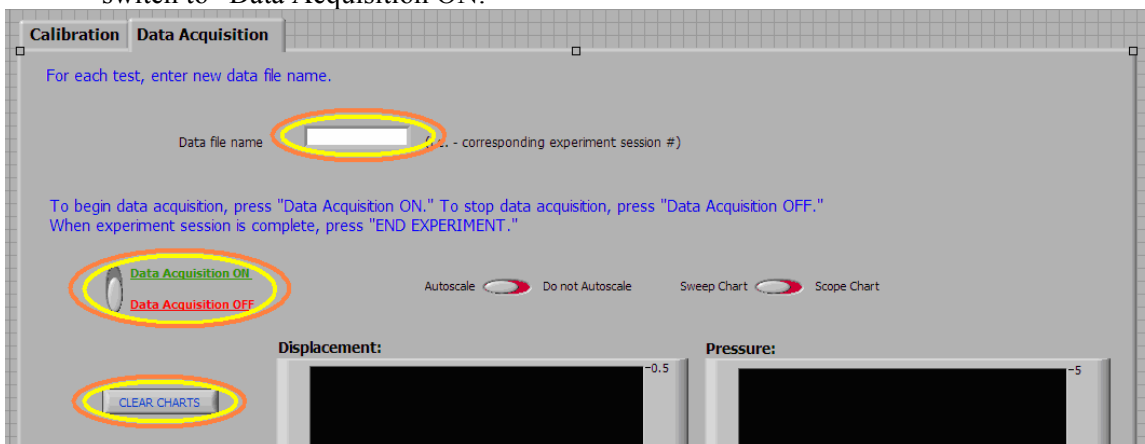


4. Once data acquisition is active, turn on syringe pump.

5. Once experiment is complete, click on switch to “Data Acquisition OFF.”

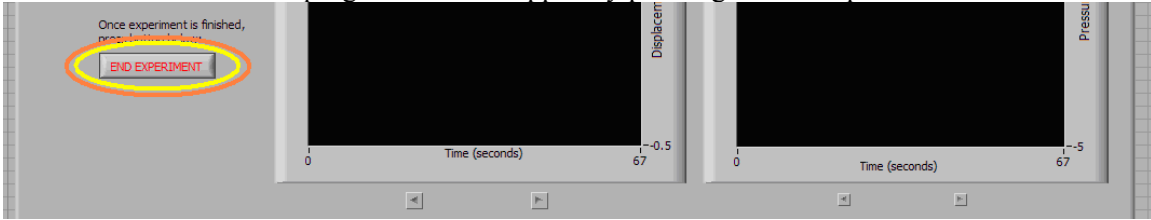


6. If another data set is desired, prepare all experimental apparatus for next test, change data file name (i.e. – “test2”), clear charts using the “Clear Charts” button, and click on switch to “Data Acquisition ON.”



Appendix E: Experimental protocols

7. Repeat step 5 until all data sets for that experiment ID are complete. Once finished, the entire LabVIEW program can be stopped by pressing “END Experiment.”



E.2. Fabrication of fibrin gels

Materials:

- Thrombin aliquot (see E.3.)
- Fibrinogen aliquot (see E.3.)
- 20 mM HEPES in 0.9% NaCl saline solution (HBSS)
- DMEM 1x
- 2 N Ca⁺⁺ (see E.3.)
- Cell Culture Media (FBS+1% P/S+1x DMEM)
- Fibroblasts
- Growth media
- Flexcell Tissue Train 6 well plates

Procedure:

The final solution to make fibrin gels (25 mm diameter) consists of 2/3 fibrinogen solution, 1/6 cell solution, and 1/6 thrombin solution, with the thrombin always being added last. The final concentrations should be calculated based on using 1.5mL of combined solution if you are making hemisphere gels.

Fibrinogen:

- Add fibrinogen aliquot (1.5mL) to 7.5mL of HBSS. The concentration is now 5mg/mL.
- Separate fibrinogen aliquots into desired amount of containers
- For one aliquot it is easiest to divide the 9mL of this solution into 3 containers each having 3mL.

Cell Suspension:

- Spin down cells in centrifuge for 10 minutes @ 1200 rpm.
- Resuspend cells in enough cell culture media (DMEM + 10% FBS) to give desired final concentration.
- Once desired concentration is achieved, add amount of cell suspension to each fibrinogen container
- Place containers on ice.
- For one aliquot of fibrinogen and thrombin 0.67mL of cells should be added to each container. (To keep 4:1:1 ratio)

Appendix E: Experimental protocols

Thrombin:

- Add 2mL of DMEM w/o FBS or BCS (just use 1x here) and 7.5 μ L of 2 N Ca⁺⁺ to 100 μ L aliquot of thrombin. Put on ice.

Gel Preparation:

- Take the container of the fibrinogen and cell suspension and add amount of thrombin needed (0.67mL for one aliquot of each). Mix the suspension.
- Quickly place 3 ml of the total solution in the center of the Flexcell plate.
- 4 gels can be made with the amount of volume of one container. (If only one aliquot of each is used.
- Repeat steps 3-5 in Gel Preparation until all of the containers are used.

E.2. Fabrication of stock solutions for the preparation of fibrin gels

E.2.1 Fibrinogen Stock Solution

Materials:

- Bovine Fibrinogen Sigma F4753 Type IV
- HEPES Buffered Saline Solution (HBSS)
20mM HEPES in 0.9% NaCl saline solution

Procedure:

- Dissolve 5g of fibrinogen in 150mL of HBSS. Warm to 37 °C in H₂O bath to aide in dissolution. Shake every 10 minutes or so. This will take at least an hour to dissolve.
- Once dissolved, filter solution through 0.45µm or 0.2µm bottle top filter using a glass prefilter to minimize clogging.
- Aliquot into 1.5mL volumes and freeze. Final concentration is 30mg/mL.

E.2.2. Preparation of 2N Ca²⁺ or 2M solution

Materials:

- Calcium Chloride
- Sterile H₂O

Procedure:

- Take 0.44g of CaCl₂
- Place into 2mL of H₂O
- Filter sterilize
- Place into sterile container
- Store in fridge at 4°C

E.2.3. Thrombin Stock Solution

Materials:

- Bovine Thrombin Sigma T7513
- HEPES Buffered Saline Solution (HBSS)
20 mM HEPES in 0.9% NaCl saline solution

Appendix E: Experimental protocols

- Sterile H₂O

Procedure:

- Dissolve 500 units of thrombin in 2mL of H₂O and 18mL of HBSS.
- Filter using 0.2µm syringe filter.
- Divide solution into 125µL aliquots and freeze. Aliquot concentration is 25U/µL.

Appendix E: Experimental protocols

E.3. Hoechst Stain Assay

Materials:

- Hoechst Stock Solution
- Sterile H₂O

Procedure:

- Combine 1.5mL of sterile H₂O and 5μL of stock solution
- Add desired concentration of staining solution to the gel. (For fibrin gels of 1.5mL initial volume 200μL was sufficient for staining final concentration of stain is 5.7×10^{-6} M)
- Let staining solution + gel sit for 30-45 minutes in the incubator.
- After time elapses gather samples for microscopy.
- Fluorescence filter UV2A is used which excites at 380 and absorbs at 420.
- Turn on spot camera and Mercury Lamp and use Spot Imaging program to image gels.

Appendix E: Experimental protocols

E.4. Histology Fixation

Materials:

- 10% buffered formalin
- 70% EtOH

Procedure:

- Place lattice in conical tube with enough formalin to cover the sample
- Refrigerate for 18-24hrs at 4°C
- Replace formalin with 70% ethanol
- Refrigerate until testing begins

E.5. Operation of Biorad Flour-S MultiImager and Quantity-One Software for Retraction Studies

Materials:

- Circular tissue equivalent samples
- Scoopula or Pasteur pipet (whichever is preferred)
- Stopwatch
- BIO-RAD Flour-S MultiImager
- Quantity-One software

Procedure:

- Turn on Biorad one hour prior to use
- Log on to TE Biorad.wpi.edu computer as Administrator
- Retract gels using a scoopula in the hood if sterility is important
 - **NOTE:** A scoopula was found to be more advantageous than a Pasteur pipet because of the greater area that can be retracted in less time with the scoopula
 - If the gels are in a #-well plate, and sterility is not an issue, the gels should be retracted near Biorad to prevent loss of time by going from the hood to the Biorad machine
- Place specimen in Biorad
 - **NOTE:** Most importantly, if sterility is not an issue, leave the cover off when scanning the gels in the multiimager. If the cover has to stay on, be aware of the fact that both condensation and/or EtOH bubbles from spraying in the laminar flow hood that form/remain on the cover may interfere with the retraction analysis
- Open Quantity One software
- Click on 'file' and go to 'Flour-S'
- In the Flour-S MultiImager setup screen, make sure that 'Step III – Set Exposure Time (sec)' is set to an optimal exposure time for the experiment
 - For retraction studies, 6.1 seconds was determined to be optimal
 - To determine what exposure time is optimal for your experiment, vary the exposure times and click on 'preview' to decide if the results are acceptable
- Click on 'Acquire' to save the image
 - **NOTE:** This takes about 13-14 seconds to save the scan so be sure to click 'acquire' 13-14 seconds prior to the desired time interval.
- Click on 'Acquire' at every time interval as needed
 - E.g., for studies in Chapter 4, time intervals were as follows: pre-retraction, 5min, 10 min, 15min, 20min, 25min, 30 min, 24hrs

To analyze scans:

- Click on 'zoom in' tool and zoom into one well

Appendix E: Experimental protocols

- Click on 'Volume'
 - If your specimen is a perfect circle, you may want to try the 'volume circle tool.'
 - If your specimen is not a perfect circle or rectangle, use the 'volume free hand tool.'
 - You may need to determine for yourself which tool produces the more accurate parameter determinations
- Trace the specimen using the mouse
- Click on 'Volume' again
- Click on 'Volume Analysis Report'
- Print scans